EVALUATION OF MECHANICAL BEHAVIOR OF NUCLEAR COMPONENT MATERIALS USING AUTOMATED BALL INDENTATION APPROACH

A thesis submitted in partial fulfillment of the requirement for the award of degree of

MASTER OF ENGINEERING
IN
PRODUCTION & INDUSTRIAL ENGINEERING

Submitted By
Harshit Kumar Khandelwal
Roll No. 800982005

Under the guidance of

Dr. Rahul Chhibber
Assistant Professor
Mechanical Engineering Department
Thapar University
Patiala – 147004

Mr. Kamal Sharma
Scientific Officer 'E'
Reactor Safety Division
Bhabha Atomic Reaserch Centre
Mumbai – 400085

DEPARTMENT OF MECHANICAL ENGINEERING
THAPAR UNIVERSITY
PATIALA -147001, INDIA
July, 2011

CERTIFICATE

This is to certify that the thesis titled, **'Evaluation of Mechanical Behavior of Nuclear Component Materials using Automated Ball Indentation Approach'** being submitted by **Mr. Harshit Kumar Khandelwal**, in partial fullfillment of the requirement for the award of **Master of Engineering (Production & Industrial Engineering)** at **Thapar University, Patiala** is an authantic record of the work carried out by him under the guidance of Dr. Rahul Chhibber, Assistant Professor, Mechanical Engineering Department, Thapar University, Patiala and Mr. Kamal Sharma, Scientific Officer 'E', Reactor Safety Division, Bhabha Atomic Reseach Centre, Mumbai.

The matter embodied in this report has not been submitted in part or full to any other university or institute for the award of any other degree.

Dr. Rahul Chhibber
Assistant Professor
Mechanical Engineering Department
Thapar University
Patiala – 147004

Mr. Kamal Sharma
Scientific Officer 'E'
Reactor Safety Division
Bhabha Atomic Reaserch Centre
Mumbai – 400085

18/7/11

Dr. Ajay Batish
Professor & Head
Mechanical Engineering Department
Thapar University
Patiala – 147004

Dr. S.K. Mohapatra
Dean
Academic Affairs
Thapar University
Patiala – 147004

ACKNOWLEDGEMENT

Words are often less to revels one's deep regards. With an understanding that work like this can never be the outcome of a single person, I take this opportunity to express my profound sense of gratitude and respect to all those who directly or indirectly helped me through the duration of this work.

I take the opportunity to express my heartfelt adulation and gratitude to my supervisors, ***Dr. Rahul Chhibber****, and* ***Mr. Kamal Sharma*** *for their unreserved guidance, constructive suggestions, thought provoking discussions and unabashed inspiration in the nurturing work. It has been a benediction for me to spend many opportune moments under the guidance of the perfectionist at the acme of professionalism. The present work is testimony to their activity, inspiration and ardent personal interest, taken by them during the course of this work in its present form. I am grateful to* ***Dr. Ajay Batish****, Prof. & Head, Mechanical Engineering Department and* ***Dr. S. K. Mohapatra,*** *Dean of Academics Affairs for providing the constant support for the completion of the work.*

I offer special regards to ***Mr. K. K. Vaze****, Head, Reactor Safety Division, Bhabha Atomic Reaserch Centre, Mumbai for providing his immense support in performing the practical work in Reactor Safety Division. No words acknowledge the support I received from my friends for their valorous help and co-operation.*

I take pride of myself being son of ideal parents for their everlasting desire, sacrifice, affectionate blessings, and help, without which it would not have been possible for me to complete my studies.

I would like to thank to all the members and employees of Mechanical Engineering Department, Thapar University Patiala for their everlasting support. Above all, I express my indebtedness to the "ALMIGHTY" for all his blessing and kindness. Last but not least, I would like to express my gratitude to my God, without the help of who's this work was not performed.

Harsh

Harshit Kumar Khandelwal
Registration Number: 800982005

ABSTRACT

Automatic ball indentation (ABI) is a non-destructive methodology to determine the mechanical properties of materials. Moreover, it is a promising method for in-situ assessment of mechanical properties. For in-situ application it is almost non-destructive since almost no material is removed from the test surface. Hence, it could prove valuable in the evaluation of mechanical properties of different materials of nuclear applications at different environmental conditions.

In the present work, mechanical behavior of nuclear component materials (bimetallic weld joint, similar weld joint, reactor pressure vessel material, and pressure tube material) at different conditions was studied using Automated Ball Indentation approach. In this respect, material properties (yield strength, ultimate tensile strength, strength coefficient, and strain hardening exponent) of nuclear component materials were studied using ABI approach. Characterization of bimetallic weld joint and similar weld joint shows how mechanical properties vary from zone to zone, and from point to point in each zone of weld joint used in nuclear application using Automated Ball Indentation approach. The present work is also an attempt to characterize the mechanical behavior degradation of reactor pressure vessel materials during their operation in typical radiation environmental conditions (radiations of neutrons, alpha, beta, gamma rays and fission products) existing inside the nuclear reactor. The present work is also an attempt to show the modified fabricating procedure of zirconium alloy (Zr-2.5-Nb) pressure tube of a pressurized heavy water reactor. For this purpose, mechanical behavior examination of Zr-2.5- Nb alloy at different environmental condition was performed with the help of ABI methodology.

Finally, analytical investigation of ABI approach was performed. For this purpose, 2D axis symmetric finite element model was prepared and simulated using ANSYS software.

TABLE OF CONTENTS

LIST OF FIGURES

LIST OF TABLES

ABBREVIATIONS

S. No.	Name/Symbol	Explanation
1	ABI	Automated Ball Indentation
2	AGR	Advanced Gas Cooled Reactor
3	ASME	American Society of Mechanical Engineers
4	ASTM	American Society of Testing and Materials
5	BIT	Ball Indentation Technique
6	BWR	Boiling Water Reactor
7	CANDU	Canada Deuterium-Uranium reactor
8	CW	Cold Work
9	FEM	Finite Element Method
10	HAZ	Heat Affected Zone
11	NDT	Nil Ductility Temperature
12	PHWR	Pressurized Heavy Water Reactor
13	PTS	Pressurized Thermal Shock
14	PWR	Pressurized Water Reactor
15	SD	Standard Deviation
16	SRS	Strain Rate Senstivity
17	SSM	Stress Strain Microprobe
18	YS	Yield Strength
19	UTS	Ultimate Tensile Strength
20	2D	Two Dimensional
21	U	Uranium
22	Th	Thorium
23	Pu	Plutonium
24	n	Neutron
25	Xe	Xenon
26	Γ	Gamma Ray
27	p	Proton
28	σ	True Stress
29	ε_p	True Plastic Strain
30	h_t	Total Depth
31	h_p	Plastic Depth
32	D	Ball Diameter

33	P	Maximum Applied Load
34	S_m	Normal Pressure on Work Surface
35	K	Strength Coefficient
36	n	Strain Hardening Exponent
37	σ_y	Yield Strength
38	σ_{UTS}	Ultimate Tensile Strength
39	SS	Stainless Steel
40	Sn	Chemical Symbol of Tin
41	Sb	Chemical Symbol of Antimony
42	Zr	Chemical Symbol of Zirconium
43	Nb	Chemical Symbol of Niobium
44	MPa	Chemical Symbol of Mega Pascal
45	KeV	Kilo Electron Volt (1 Kev= 1.6×10^{-16} Joule)
46	Mev	Mega Electron Volt (1 MeV = 1.6×10^{-13} Joule)
47	(n,γ)	Reaction in which an element absorbs a neutron and releases gamma ray
48	(n,p)	Reaction in which an element absorbs a neutron and releases a proton
49	(n,2n)	Reaction in which an element absorbs a neutron and releases two neutron

CHAPTER 1

INTRODUCTION

1.1 History of Nuclear Energy

Nuclear energy is considered as one of the incredible sources of the world's energy needs in the present and future scenario. It is an emission-free alternative, given the hue and cry about global temperature rise from excessive carbon emissions these days.

Nuclear energy is the energy generated from nucleus of atom. Ancient Greek philosophers first developed the idea that all matter is composed of invisible particles called atoms. The word 'ATOM' comes from the Greek word, 'atomos', means indivisible. Scientists in the 18th and 19th centuries revised the concept based on their experiments. By 1900, physicists knew that the atom contains large quantities of energy. British physicist Ernest Rutherford was called the father of nuclear science because of his contribution to the theory of atomic structure. In 1904 he wrote:

"If it were ever possible to control the rate of disintegration of the radioactive elements, an enormous amount of energy could be obtained from a small amount of matter".

Albert Einstein developed his theory of the relationship between mass and energy one year later. The mathematical formula given by Einstein is $E= mc^2$, which means "energy equals mass times the speed of light squared." The fundamental theory behind nuclear energy is based on Einstein's theory.

1.2 Fundamentals of Nuclear Energy

Nuclear energy is produced by nuclear reactions. There are two such types of nuclear reactions:

i. Nuclear Fission Reaction
ii. Nuclear Fusion Reaction

i. Nuclear Fission Reaction: Reactions, in which an atom's nucleus splits into smaller parts, releasing a large amount of energy in the process. Most commonly this is done by "firing" a neutron at the nucleus of an atom. The energy of the neutron causes the target element to split into two (or more) elements that are lighter than the parent atom. [23]

The splitting of an atom's nucleus releases an incredible amount of heat and gamma radiation, or radiation made of high-energy photons. The two atoms that result from the fission later release beta radiation (super fast electrons) and gamma radiation of their own as well. The energy released by a single fission comes from the fact that the fission products and the neutrons, together, weigh less than the original U-235 atom. The difference in weight is converted directly to energy at a rate governed by the equation $\mathbf{E = mc^2}$ [24].

During the fission of U-235, three neutrons and gamma rays are released in addition to the two daughter atoms and energy (approx. 200 Mev) (Fig. 1.1) . If these released neutrons collide with nearby U-235 nuclei, they can stimulate the fission of these atoms and start a self-sustaining nuclear chain reaction. This chain reaction is the basis of nuclear power. As uranium atoms continue to split, a significant amount of energy is released from the reaction. The heat released during this reaction is harvested and used to generate electrical energy.

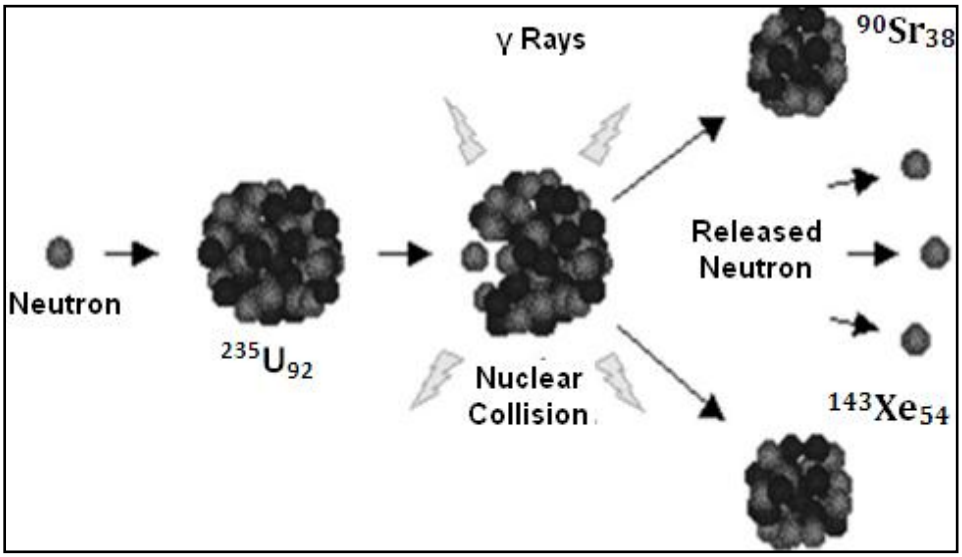

Fig 1.1: Nuclear Fission Reaction of U-235 [27]

Fission fragments, after fission process, are in excited state, and they de-excite generally by beta, gamma and neutron emissions. The neutrons emitted during fission are called 'Prompt Neutrons', and those emitted by the fragments after a delay are called 'Delayed Neutrons'. Similarly, prompt and delayed gammas are also emitted [24].

Fission products (i.e. fission fragments, released neutrons, gamma radiation, etc.) contain different amount of energy. The approximate distribution of fission energy through various emissions is given in Table 1.1.

Table: 1.1: Distribution of Fission Energy through various emissions [27]

Type of Fission Product	Occupied Energy (MeV)
Kinetic energy of fission fragments	170
Prompt Radiations (Gammas and Neutrons)	12
Delayed Radiations (Neutrons and Gammas)	12
Total	**194**

ii. Nuclear Fusion Reaction: Reactions in which two or more elements "fuse" together to form one larger element, releasing energy in the process. A good example is the fusion of two "heavy" isotopes of hydrogen (deuterium: H_2 and tritium: H_3) into the element helium.

Fusion reactions release tremendous amounts of energy and are commonly referred to as thermonuclear reactions [23]. Although many people think of the sun as a large fireball, the sun (and all stars) is actually enormous fusion reactors. Stars are primarily gigantic balls of hydrogen gas under tremendous pressure due to gravitational forces. Hydrogen molecules are fused into helium and heavier elements inside of stars, releasing energy that we receive as light and heat [23].

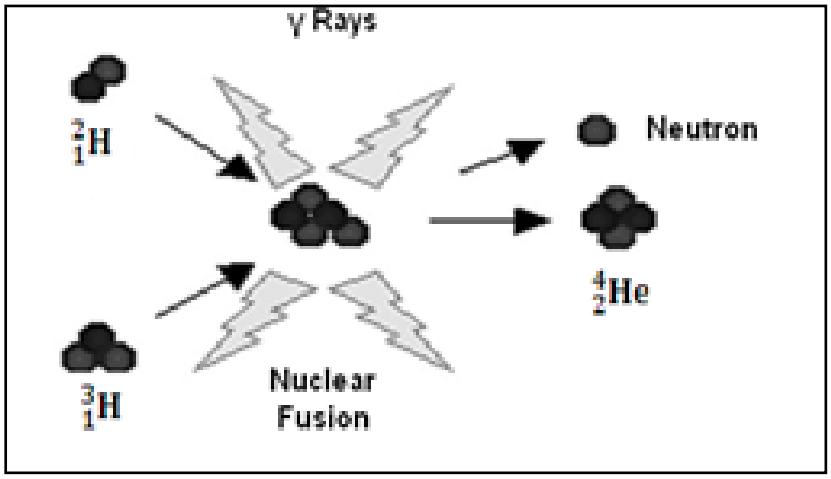

Fig. 1.2: Nuclear Fusion of Two Hydrogen Isotopes [29]

1.3 Introduction to Nuclear Power Plants

Nuclear power plant is nothing but another thermal power plant in its working. In this plant, the heat required for conversion of water into steam is obtained through heat released in the nuclear reaction. On the basis of types of nuclear reactions, the nuclear power plants are of two types. These are as follows:

a. Nuclear Fission Power Plant
b. Nuclear Fusion Power Plant

1.3.1 Nuclear Fission Power Plant

A nuclear fission power plant uses the heat generated by a nuclear fission reaction to drive a steam turbine which generates usable electricity. When an atom of nuclear fuel (uranium) absorbs a neutron, the uranium will fission into two smaller atoms (waste) and release one to three neutrons. The kinetic energy of the waste is used to heat the water for the steam turbine. And the steam turbine is coupled with electricity generator to produce the electric energy.

The neutrons are used to fission the next lot of uranium atoms and the process continues. If none of these neutrons are absorbed by another uranium atom then the reaction dies out. If too many neutrons are absorbed then the reaction grows extremely quickly and could explode.

1.3.2 Nuclear Fusion Power Plant

Fusion power is the power generated by nuclear fusion reactions. In this kind of reaction, two light atomic nuclei fuse together to form a heavier nucleus and in doing so, release a large amount of energy. The studies for fusion power plants involve using the fusion reactions to create heat, which is then used to operate a steam turbine, which drives generators to produce electricity [23]. But these power plants are only an idea till now. Except for the use of a thermonuclear heat source, this is similar to most coal, oil, and gas-fired power stations as well as fission-driven nuclear power stations.

1.3.1.1 Principal Components of Nuclear Fission Power Plant

Following are the principal components, which are common to any nuclear power plant[24]:

1. Reactor core

Reactor core is the heart of any nuclear reactor. Inside the core, where the nuclear reactions take place are the fuel rods and assemblies, the control rods, the moderator, and the coolant. Outside the core are the turbines, the heat exchanger, and part of the cooling system. Nuclear fission reaction, which is required for energy production is taking place inside the reactor core. Inside reactor core, kinetic energy of produced due to fission is converted into heat energy. The reactor core consists of following sub parts;

a. Fuel rods and Fuel Assembly: The fuel assemblies are collections of fuel rods. These rods are each about 3.5 meters (11.48 feet) long. They are each about a centimeter in diameter. These are grouped into large bundles of a couple hundred rods called fuel assemblies, which are then placed in the reactor core. Inside each fuel rod are hundreds of pellets of uranium fuel stacked end to end.

b. Control Rods: Also in the core are control rods. These rods have pellets inside that are made of very efficient neutron capturers. An example of such a material is cadmium. These control rods are connected to machines that can raise or lower them in the core. When they are fully lowered into the core, fission cannot occur because they absorb free neutrons. However, when they are pulled out of the reactor, fission can start again anytime a stray neutron strikes a U-235 atom, thus releasing more neutrons, and starting a chain reaction.

c. Moderator: Another component of the reactor is the moderator. The moderator serves to slow down the high speed neutrons flying all around the reactor core. If a neutron is moving too fast, and thus is at a high-energy state, it passes right through the U-235 nucleus. It must be slowed down to be captured by the nucleus and to induce fission. The most common moderator is water, but sometimes it can be another material.

d. Thermal Shielding: It surrounds the entire reactor core and absorbs some of the radiations in the form of alpha rays, beta rays and escaping neutrons produced by fissioning. In this manner it gets heated and prevents the reactor wall from getting heated. Coolant flows over the shielding to take away the heat. The shielding is usually constructed from iron.

2. Coolant

The job of the coolant is to absorb the heat from the reaction. The most common coolant used in nuclear power plants today is water. In actuality, in many reactor designs the coolant and the moderator are one and the same. The coolant water is heated by the nuclear reactions going on inside the core. However, this heated water does not boil because it is kept at an extremely intense pressure, thus raising its boiling point above the normal 100°C.

3. Reactor Pressure Vessel

The reactor vessel is a pressure vessel containing the coolant and reactor core. It is a device for containing and controlling a chemical reaction. The chemical process enables the conversion of raw material into a final product under given pressure and temperature. During the reaction it becomes necessary to remove excess heat in the process to order to keep the process under control. Vessels are built to withstand high pressure in the system.

4. Steam Generator or Heat Exchanger

Steam generators are heat exchangers used to convert water into steam from heat produced in a nuclear reactor core. They are used in pressurized water reactors between the primary and secondary coolant loops. Boiling water reactors do not use steam generators, as steam is produced in the pressure vessel. Various high-performance alloys and super alloys have been used for steam generator tubing, including type 316 stainless steel,

5. Containment Building

The containment building itself is typically an airtight steel structure enclosing the reactor normally sealed off from the outside atmosphere. The steel is either free-standing or attached to the concrete missile shield. The containment is the final barrier to radioactive release (part of a nuclear reactor's defense in depth strategy), the first being the fuel ceramic itself, the second being the metal fuel cladding tubes, the third being the reactor vessel and coolant system For a pressurized water reactor, the containment also encloses the steam generators and the pressurizes, and is the entire reactor building.

6. Turbine Hall

The turbine hall, generating hall or turbine building is a building that is a part of any steam cycle power plant which houses a number of components vital to the generation of electricity from the steam that comes from the boiler. The components in the turbine hall typically comprise of the turbines, moisture separators, repeaters, electric generator, and/or exciter.

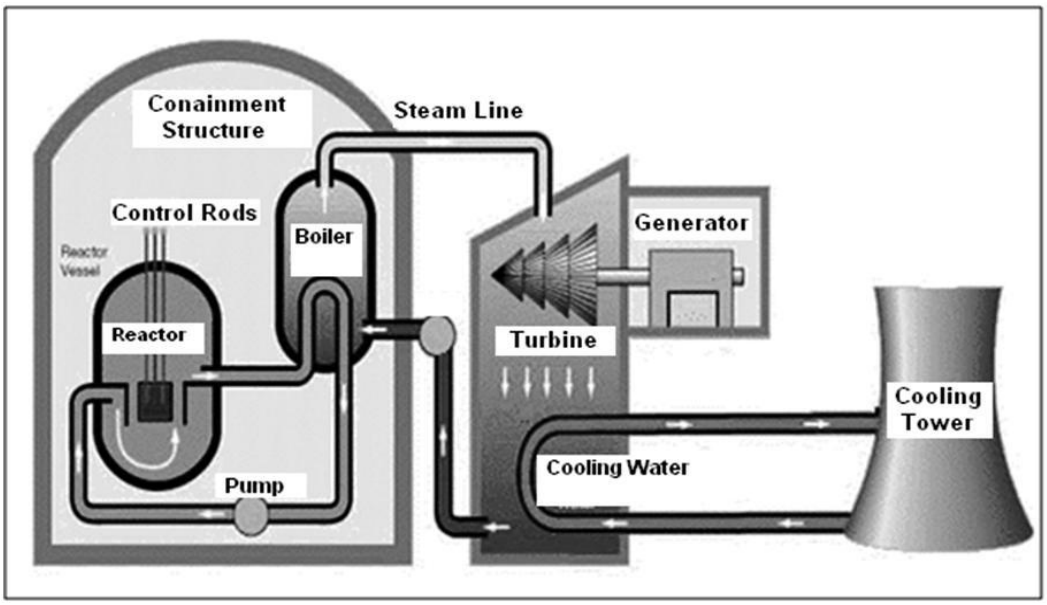

Fig.1.3: Nuclear Power Plant General Layout [32]

1.4 Classification of Nuclear Reactor

The speed of the neutrons in the chain reaction determines the reactor type. On the basis of the speed of neutrons, the nuclear reactors can be classified as in following ways:

A. Thermal Reactor
B. Fast Reactor

1.4.1 Thermal Reactor

Thermal reactors use slow neutrons to maintain the reaction. These reactors require a moderator to reduce the speed of neutrons produced by fission.

1.4.1.1 Types of Thermal Reactor

i. Graphite Moderate Reactor
ii. Advanced Gas Cooled Reactor
iii. Heavy Water Reactor
iv. Light Water Reactor

i. Graphite Moderate Reactor[29]

Of the four main commercial reactor types, two (Mango and AGR) owe much to the very earliest reactor designs in that they are graphite moderated and gas cooled. Magnox reactors (Fig 1.4) were built in the UK from 1956 to 1971 but have now been superseded. The Magnox reactor is named after the magnesium alloy used to encase the fuel, which is natural uranium metal. Fuel elements consisting of fuel rods encased in Magnox cans are

loaded into vertical channels in a core constructed of graphite blocks. Further vertical channels contain control rods (strong neutron absorbers) which can be inserted or withdrawn from the core to adjust the rate of the fission process and, therefore, the heat output. The whole assembly is cooled by blowing carbon dioxide gas past the fuel cans, which are specially designed to enhance heat transfer. The hot gas then converts water to steam in a steam generator.

Early designs used a steel pressure vessel, which was surrounded by a thick concrete radiation shield. In later designs, a dual-purpose concrete pressure vessel and radiation shield was used.

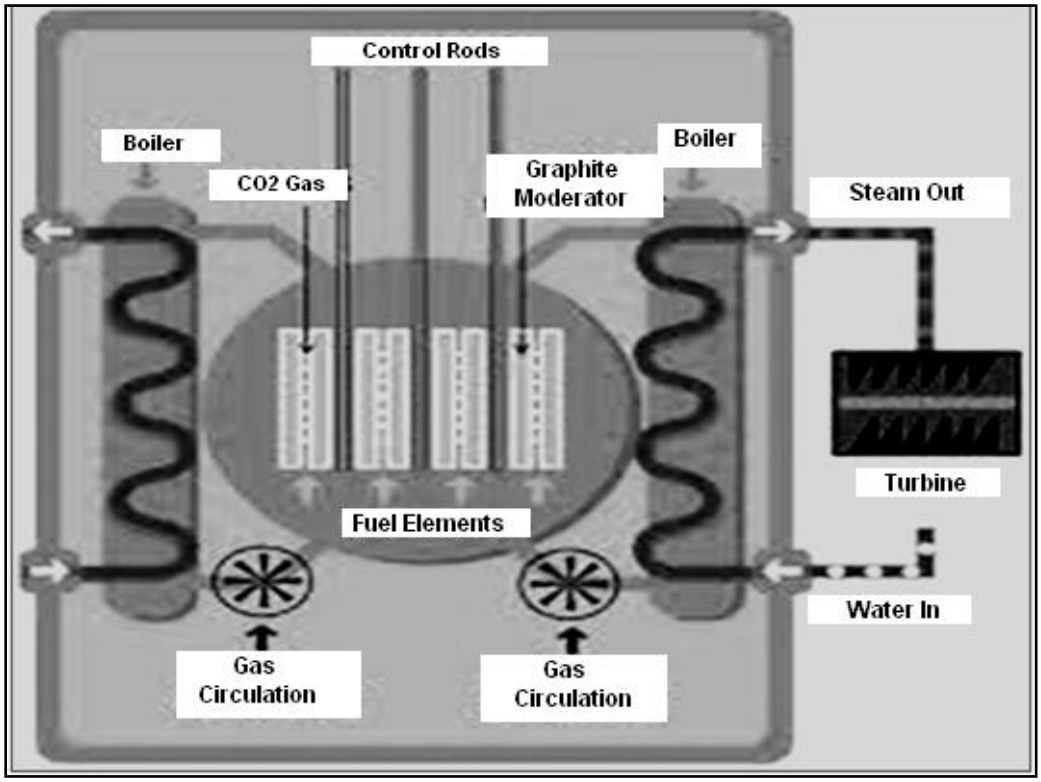

Fig. 1.4: Basic Gas-Cooled Reactor (MAGNOX) [29]

ii. Advanced Gas Cooled Reactor[30]

In order to improve the cost effectiveness of this type of reactor, it was necessary to go to higher temperatures to achieve higher thermal efficiencies and higher power densities to reduce capital costs. This entailed increases in cooling gas pressure and changing from Magnox to stainless steel cladding and from uranium metal to uranium dioxide fuel. This in turn led to the need for an increase in the proportion of U-235 in the fuel. The resulting design, known as the Advanced Gas-Cooled Reactor, or AGR (Fig 1.5), still uses graphite

as the moderator and, as in the later Magnox designs, the steam generators and gas circulators are placed within a combined concrete pressure-vessel/radiation shield.

iii. Heavy Water Cooled and Moderated (CANDU) Reactor [31]

The only design of heavy water moderated reactor in commercial use is the CANDU**,** designed in Canada and subsequently exported to several countries. In the CANDU reactor, (Fig 1.6) unenriched uranium dioxide is held in zirconium alloy cans loaded into horizontal zirconium alloy tubes. The fuel is cooled by pumping heavy water through the tubes (under high pressure to prevent boiling) and then to a steam generator to raise steam from ordinary water (also known as natural or light water) in the normal way. The necessary additional moderation is achieved by immersing the zirconium alloy tubes in an unpressurised container (called a 'Callandria') containing more heavy water. Control is effected by inserting or withdrawing cadmium rods from the callandria. The whole assembly is contained inside the concrete shield and containment vessel.

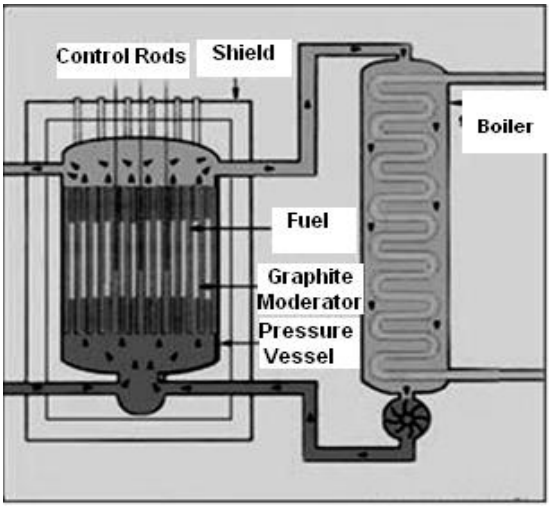

Fig. 1.5: Advanced Gas-Cooled Reactor (AGR) [30]

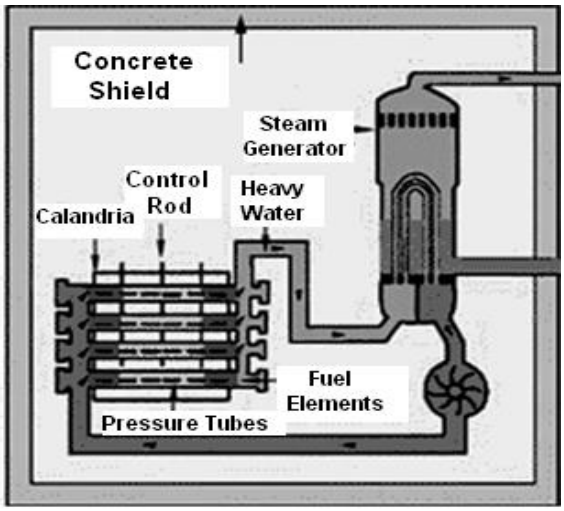

Fig. 1.6: Pressurized Heavy Water Reactor (CANDU) [31]

iv. Light Water cooled and moderated

By moving to greater levels of enrichment of U-235, it is possible to tolerate a greater level of neutron absorption in the core (that is, absorption by non-fissile, non-fertile materials) and thus use ordinary water as both a moderator and a coolant. The two commercial reactor types based on this principle are both American designs, but are widely used in over 20 countries.

a. Pressurized Water Reactor (PWR)

b. Boiling Water Reactor (BWR)

a. Pressurized Water Reactor (PWR)

The most widely used reactor type in the world is the Pressurized Water Reactor (PWR) (Fig 1.7) which uses enriched (about 3.2% U-235) uranium dioxide as a fuel in zirconium alloy cans. The fuel, which is arranged in arrays of fuel "pins" and interspersed with the movable control rods, is held in a steel vessel through which water at high pressure (to suppress boiling) is pumped to act as both a coolant and a moderator. The high-pressure water is then passed through a steam generator, which raises steam in the usual way. As in the CANDU design, the whole assembly is contained inside the concrete shield and containment vessel. [33]

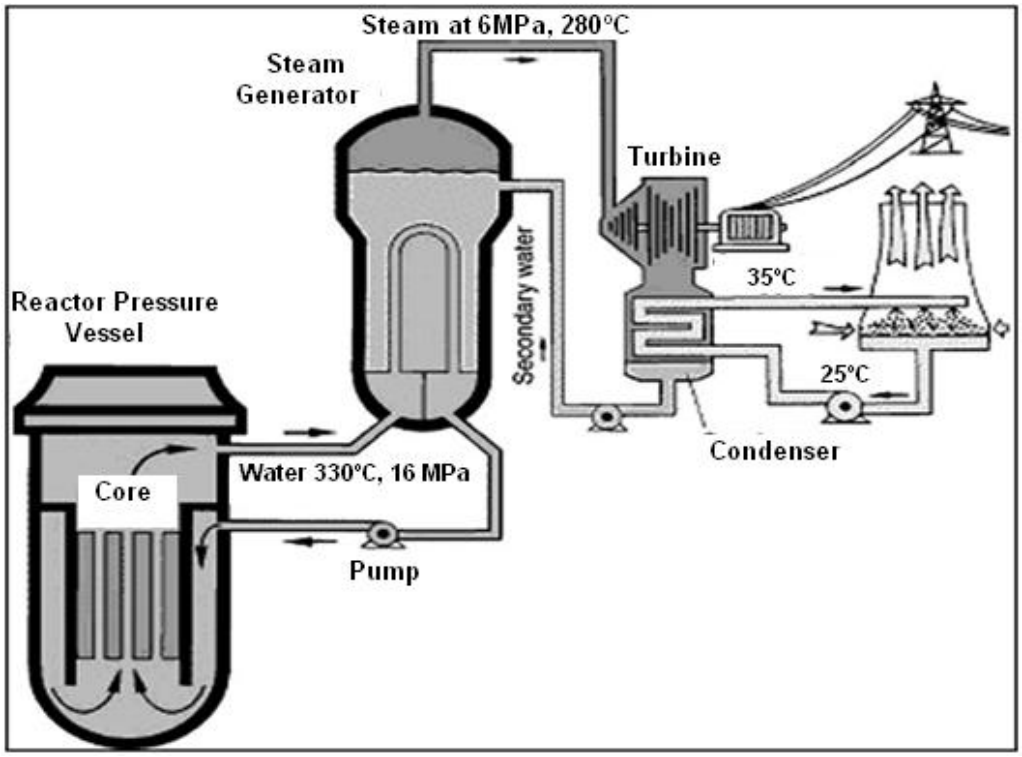

Fig 1.7: Nuclear power plant with pressurized water reactor [33]

b. Boiling Water Reactor (BWR)

The second type of water cooled and moderated reactor does away with the steam generator and, by allowing the water within the reactor circuit to boil, it raises steam directly for electrical power generation. This, however, leads to some radioactive contamination of the steam circuit and turbine, which then requires shielding of these components in addition to that surrounding the reactor.

Such reactors, known as Boiling Water Reactors (BWRs), (Fig.1.8) are in use in some ten countries throughout the world. [34]

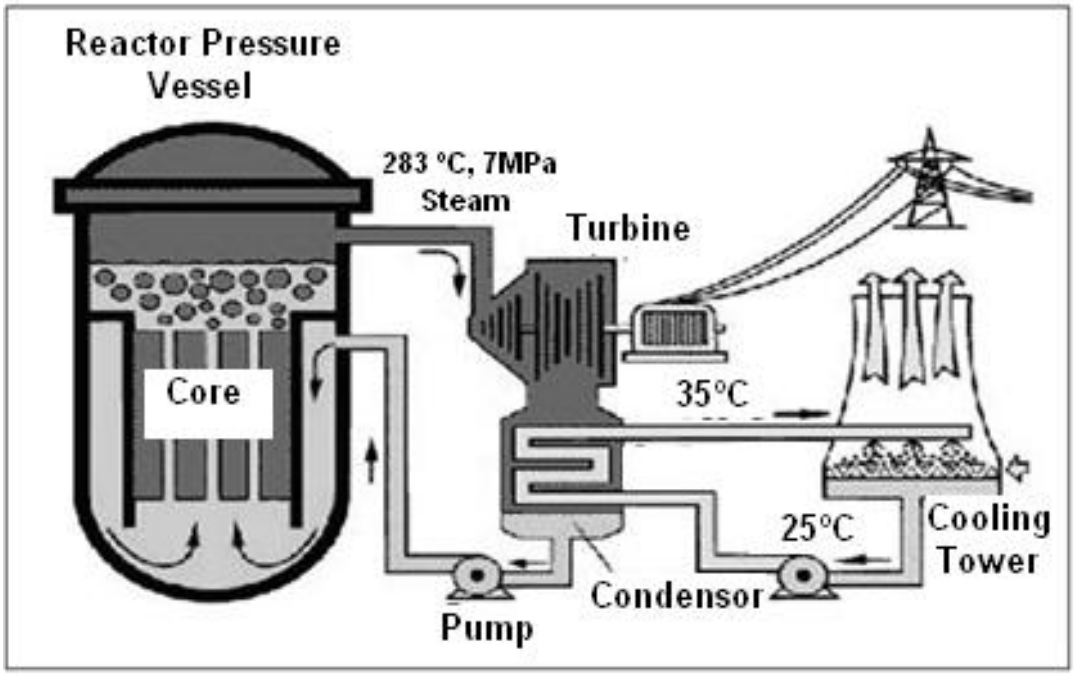

Fig 1.8: Nuclear power plant with Boiling Water Reactor [34]

1.4.2 Fast Reactor or Fast Breeder Reactor

All of today's commercially successful reactor systems are thermal reactors, using slow or thermal neutrons to maintain the fission chain reaction in the U-235 fuel. Even with the enrichment levels used in the fuel for such reactors, however, by far the largest numbers of atoms present are U-238, which are not fissile. Consequently, when these atoms absorb an extra neutron, their nuclei do not split but are converted into another element, Plutonium. Plutonium is fissile and some of it is consumed in situ, while some remains in the spent fuel together with unused U-235. These fissile components can be separated from the fission product wastes and recycled to reduce the consumption of uranium in thermal reactors by up to 40%, although clearly thermal reactors still require a substantial net feed of natural uranium. [35].

It is possible, however, to design a reactor which overall produces more fissile material in the form of Plutonium than it consumes. This is the fast reactor in which the neutrons are unmoderated, hence the term "fast". The physics of this type of reactor dictates a core with a high fissile concentration, typically around 20%, and made of Plutonium. In order to make it breed, the active core is surrounded by material (largely U-238) left over from the thermal reactor enrichment process. This material is referred to as 'fertile', because it converts to fissile material when irradiated during operation of the reactor.

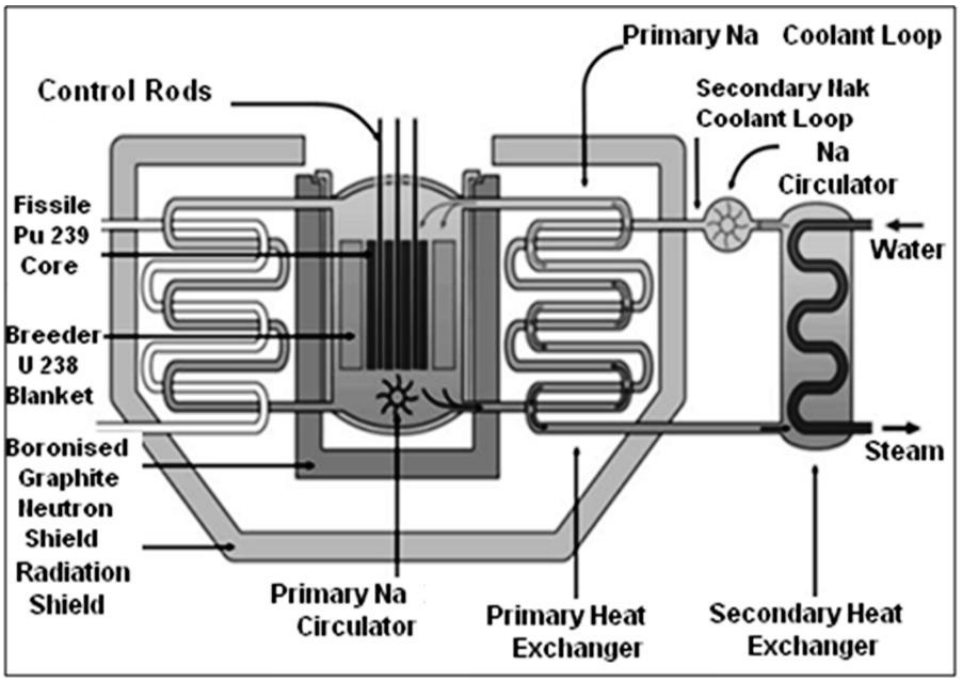

Figure 1.9: Sodium-Cooled Fast Reactor [35]

Due to the absence of a moderator, and the high fissile content of the core, heat removal requires the use of a high conductivity coolant, such as liquid sodium. Sodium circulated through the core heats a secondary loop of sodium coolant, which then heats water in a steam generator to raise steam. Otherwise, design practice follows established lines, with fuel assemblies clad in cans and arranged together in the core, interspersed with movable control rods. The core is either immersed in a pool of coolant, or coolant is pumped through the core and thence to a heat exchanger. The reactor is largely unpressurised since sodium does not boil at the temperatures experienced, and is contained within steel and concrete shields (Fig. 1.9).[35]

The successful development of fast reactors has considerable appeal in principle. This is because they have the potential to increase the energy available from a given quantity of uranium by a factor of fifty or more, and can utilize the existing stocks of depleted uranium, which would otherwise have no value. Fast reactors, however, are still currently at the prototype or demonstration stage.

1.5 Summary of Nuclear Reactors

Table 1.2: Summary of Nuclear Reactors

Reactor Type	Coolant	Moderator	Chemical Form of Fuel	Fuel Enrichment Level
Thermal Reactor				
Graphite Moderated Reactor	Carbon Dioxide or Helium	Graphite	Uranium Dicarbide or Uranium Metal	Slightly Enriched or Natural Uranium
Advanced Gas Cooled Reactor	Carbon Dioxide or Helium	Graphite	Uranium Di oxide	More Enriched
Heavy Water Reactor	Heavy water	Heavy Water	Uranium Dioxide or Uranium Metal	Natural, Unenriched Uranium
Boiling Water Reactor	Light Water	Light Water	Uranium Dioxide	Low Enriched Uranium
Pressurized Water Reactor	Light Water	Light Water	Uranium Dioxide	Low Enriched Uranium
Fast Breeder Reactor	Molten Sodium or Lead	None Required	Various mixtures of Plutonium Dioxide and Uranium Dioxide	various mixtures of Plutonium Dioxide and Uranium Dioxide

1.6 Principal Environmental Conditions inside a Nuclear Reactor

1.6.1 Radiations in Nuclear Reactor

a. Radioactive Radiation

The naturally occurring forms of the great majority of elements are stable, but a few of high atomic weight, from plutonium (atomic number 84) onward, e.g. radium (88), thorium (90), uranium (92), consist entirely of unstable, radioactive isotopes. The unstable substances undergo spontaneous change, i.e. radioactive disintegration or radioactive decay, at definite rates. This decay is associated with the emission from the atomic nucleus of an electronically charged particle, either an alpha particle i.e. a helium nucleus, or a beta particle, i.e. an electron (Reaction (1.1) and Reaction (1.2)). In many cases gamma radiation accompanies the particle emission [23].

Example: $^{238}U_{92} \longrightarrow {}^{234}Th_{90} + \alpha$ particle (Reaction 1.1)

$^{239}Pu_{94} \longrightarrow {}^{235}U_{92} + \alpha$ particle (Reaction 1.2)

Frequently the products of radioactive decay are themselves radioactive, expelling either an alpha or a beta particle. After a number of disintegrations, an atomic species with a stable nucleus is formed.

b. Radiations Produced by Nuclear Fission Reaction

Nuclear fission products are the atomic fragments left after a large atomic nucleus fissions. Typically, a large nucleus like that of uranium fissions by splitting into two smaller nuclei, along with a few neutrons and a large release of energy in the form of heat (kinetic energy of the nuclei), gamma rays and neutrinos. The two smaller nuclei are the fission products. More over in most of the cases, the fission products are also radioactive in nature [24]. The nuclear fission reaction equation of U-235 is as shown as follows:

$$^{235}U_{92} + {}^{1}n_{0} \longrightarrow {}^{90}Sr_{30} + {}^{143}Xe_{54} \qquad \text{(Reaction 1.3)}$$

Reaction (1.3) produces a large amount of energy (average energy of 2 MeV) and emits gamma rays apart from the fission products and neutrons. Figure 1.10 shows a typical nuclear fission reaction and its products. When nucleus absorbs a neutron, it will get converted into excited nucleus. This excited nucleus is unstable and it will break into two segments (fission fragments). During this reaction, gamma rays, neutrons and fission fragments are released. These products carry huge amount of energy.

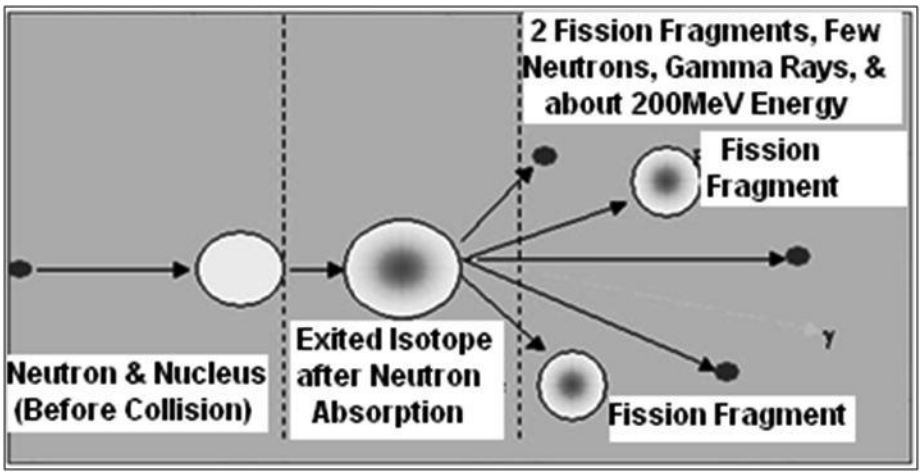

Fig. 1.10: Radiation produced during Nuclear Fission Reaction [27]

Note: In Fig. 1.10, shaded circles represent unstable atoms.

c. Artificial or Induced Radioactivity

Besides the radioactive substances, there have been produced in recent years a total of about 800 so called 'artificial' radioisotopes of all known elements. These have been obtained either by one of the following reasons:

i) Bombardment of stable elements with charged particles,
ii) By the capture of neutrons or
iii) Most nuclear fission products (nuclei) are radioactive in nature

A few of them induced alpha particles, but large proportions, including most of the fission products, are negative beta emitters. Fission fragments, after fission process, themselves are in excited state, and they de-excite generally by beta, gamma and neutron emissions. The neutrons emitted during fission are called 'prompt neutrons', and those emitted by the fragments after a delay are called 'delayed neutrons'. Similarly, prompt and delayed gammas are also emitted [24].

A number of artificial radioactive species emit positive beta particles, i.e. positrons or positively charged electrons, but such substances play essentially no part in nuclear reactor.

1.6.2 Thermal Environment

In many reactor components there is very considerable internal heating, due to either fission, to the slowing down of fast neutrons, or to the absorption of various radiations. The removal of the heat from exterior results in high temperature gradients within the material. Such materials, therefore, face thermal stress.

1.7 Radiation Interaction with Nuclear Component Material

Intense nuclear radiations of various types that occur in a typical reactor environment are capable of changing the microstructure of many materials. Often, these changes have an unfavorable effect on physical and mechanical properties. Since the materials are in a sense 'damaged', the term *radiation damage* is often used. This deleterious change in properties is an important design consideration and is unique in nuclear engineering [24].

The radiations in a nuclear reactor consist mainly of alpha, or beta particles (from radioactive decay), gamma rays, neutrons, and fission products. Although fission products are not strictly nuclear radiations, their behavior is generally similar to that of alpha particles, except that they are more massive and carry more energy.

As far as non fuel materials, which are mainly metals, are concerned, neutrons are the most important in producing radiation effects. High energy fission products and alpha particles from radioactive sources are restricted to the fuel because of their short range; hence they have little effects on other materials. However alpha particles produced by (n,α) reactions in non fuel materials can be significant. Beta particles and gamma rays can cause ionizations and electronic excitation, but these do not produce substantial permanent changes except in non metallic substances, such as water and organic compounds. Ionization and electronic excitation cause very little permanent change in metals. The reason is that in a metal, the electrons in the conduction band are able to accept very small amounts (quanta) of excitation energy, and so a considerable portion of the energy of the radiation is absorbed in causing electronic excitation. Because of the large number of empty energy states available, the excited electrons rapidly lose their excess energy; this is taken up by the atoms of the metals and appears in the form of heat i.e. vibration energy of the nuclei [23].

Heavier particles, however such as neutrons, alpha particles and fission segments, do produce significant changes in properties of metals. The effects of neutrons on materials arise in following ways:

a. Atomic Displacements
b. Neutron capture

a. Atomic Displacements [24]

As a result of elastic collisions, these particles (neutrons) may transfer appreciable amount of energy to the nuclei of a solid. If the amount of energy transferred is sufficient to cause

the nuclei to be displaced from their normal (or equilibrium) positions in the space lattice, physical changes of an essentially permanent character will be observed in the metals. This effect of nuclear radiations is sometimes referred to as 'radiation damage'.

If, as the result of an elastic collision between the relatively heavy nuclear particle and an atomic nucleus, the energy transferred to the latter exceeds a certain minimum value (usually assumed to be about 25 ev for a metal), the struck ('Knocked on') atom may be displaced from normal or equilibrium position in the solid lattice. As a general rule, the primary knock on atom acquires sufficiently energy to cause displacement of another atom by collision, and latter becomes secondary knock on. The process will continue until the displaced atom does not have sufficient energy to eject another atom from the crystal lattice. Thus a cascade of knock on atoms will develop from the initial interaction of a high energy radiation particle with an atom in a solid.

This effect is especially important when the knock on atom (or nucleus) is produced as the result of an elastic collision with a fast neutron (or other energetic particle); the energy of primary knock on can then be quite high and the cascade may be extensive. Thus the net result is thus a more or less permanent defect in the solid, which, if sufficiently common, may be accompanied by a change in physical properties of materials.

b. Neutron Capture [24]

The capture of neutron by the nuclei in a solid can produce two effects under suitable conditions; these are:

i) Introduction of impurity atoms
ii) Indirect atomic displacements

i) Introduction of impurity atoms

When exposed to thermal neutrons, most elements undergo (n,γ) reactions to some extent. In (n, γ) reactions the excited compound nucleus emits its excess energy as gamma radiation, referred to as *captured gamma rays,* eventually leaving the compound nucleus in its lowest energy (or ground) state. The process may be represented symbolically by the Reaction (1.4).

$$^{A}X_{Z} + {}^{1}n_{0} \longrightarrow {}^{A+1}X_{Z} + \gamma \text{ ray} \qquad \text{(Reaction 1.4)}$$

Where $^{A}X_{Z}$ is the target nucleus having an atomic number Z and a mass number A. The product of the radioactive capture reaction ($^{A+1}X_{Z}$ **)** is seen to be an isotope of X since it has the same atomic number but has a mass number one unit grater.

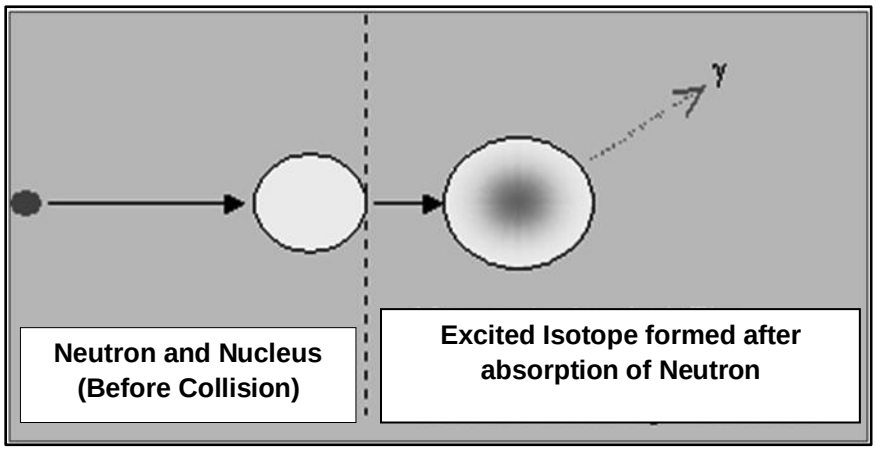

Fig.1.11: Radioactive capture reaction (n, γ) [27]

According to the circumstances, the nuclide $^{A+1}X_Z$ may or may not be radioactive. If it is radioactive, then it will most likely be a negative beta emitter, since the capture of a neutron will have produced a nucleus in which the neutron/ proton ratio is too large for stability for given atomic number. In that case it will emit beta particles and be thereby converted into a different element. In addition, fast neutrons can produce new elements directly by (n,p) and (n, 2n) reactions. As a result of these nuclear reactions, impurity atoms are introduced into the original crystal lattice.

After long exposure to the fast and thermal neutrons in a reactor, a sufficient number of such atoms may accumulate to affect the physical properties of the material.

Essentially all the elements, from hydrogen to uranium, exhibit radiative capture to a greater or a lesser extent. However, as may be expected, nuclei having magic numbers of neutrons like 2, 8, 20, 50, 82, or 82 neutrons, show little tendency to capture neutrons.

ii) Indirect atomic displacements

In addition to the production of impurity atoms, there is another consequence of (n,γ) reactions which may be more significant. This is the displacement produced by the recoil following the emission of a gamma ray photon.

The total energy of gamma ray accompanying an (n,γ) reaction is roughly 6 to 8 MeV, and so for an element of low atomic weight e.g., about 10, the recoil energy would be 2 or 3 Kev. This is probably an overestimate because it does not take into account the effect of cascade emission of gamma ray photons, which occurs frequently. Nevertheless, since it requires only 25 ev to displace an atom, the recoil energy should be capable of causing an appreciable number of atomic displacements [24].

In a thermal reactor, in which the thermal neutron flux may greatly exceed that of fast neutrons, the radiation damage caused by recoil from (n,y) reactions may be of the same order as (or greater) than that due to the fast neutrons in a material having an appreciable radiative capture cross section for thermal neutrons. It should be noted, however, that if the cross section were large, the effect of (n, γ) reactions would be mainly near the surface of the material where most of the captures would occur. The damaged produced by fast neutrons would extend more deeply into the interior.

1.8 Mechanics of Radiation Damage

Theoretical predictions, computer simulations and experimental observations indicate that three situations can be arising due to collision between any heavy particle and target atom. These are as follows:

i) Temperature Spike
ii) Thermal Spike
iii) Displacement Spike

i) Temperature Spike

If a struck atom produced directly by the particle or by an energetic knock on, has sufficient energy to cause it to undergo vibrations of large amplitude without leaving its lattice position entirely. Some of this excess vibration energy will be rapidly transferred to its immediate neighbors who will, in turn, transfer some energy to their neighbors. The result will be formation of a limited region in which the atoms have vibration energies in excess of the normal value corresponding to bulk temperature of the solid [24]. The situation is then similar to that which would exist if the small volume were suddenly heated to a high temperature. Consequently, the region in which the atoms are in vibration excited states is referred to as a 'Temperature Spike.

ii) Thermal Spike

If the excitation is relatively small, so that few (if any) of the vibration atoms leave their equilibrium sites, the disturbance is called 'Thermal Spike'. It has been estimated that in such a situation a region containing on the order of a thousand atoms is heated to a temperature of around 1000 °C (1800 F) for a period of about 10^{10} sec. at the high temperature of the thermal spike, distortion of the lattice, due to expansion, is to be expected. In the very rapid cooling, resulting from the conduction of heat to the surrounding atoms, a certain amount of lattice distortion will be 'frozen', since there will

not be sufficient time for all the atoms to be relocated in equilibrium positions Consequently stress may be develop in the material[24].

iii) Displacement Spike

If the vibration excitation may be sufficient to permit a large number of atoms to leave their lattice sites and move about. As a result of collisions with other atoms a displacement spike will be produced. Several thousands of atoms in a small volume would thus acquire sufficient vibration energy to permit them to move through the lattice colliding with, and displacing, other atoms. As a consequence, there would be formed a spike, containing a large number of interstitials and vacancies and other disoriented regions.

When an atom is ejected from a crystal lattice, it leaves a vacant normal site, known as 'vacancy'. Some of the knock-on atoms produced by neutrons (or other radiations) will eventually fill vacancies left by the removal of other atoms. But not all knock-on atoms can find nearby vacancies although vacancies are present in the material[24]. These knock ones will then occupy non equilibrium interstitial sites that lie between equilibrium sites. An atom occupying interstitial position is called an interstitial atom or, in brief, an Interstitial. For each interstitial produced by the action of radiation, there is vacancy somewhere in the lattice. A lattice vacancy and interstitial when considered as a unit are referred to as a frenkel pair (Frenkel defect). Solids commonly contain some frenkel defects, but the number increases markedly as a result of exposure to the fast neutrons.

Both vacancies and interstitials migrate at random through the solids at the rates that increase with temperature. An interstitial migrates by moving to another non equilibrium site, whereas a vacancy efficiently migrates when neighbor atom (from an equilibrium site) moves into the vacancy leaving another vacancy behind. During the course of migration, an interstitial and vacancy occasionally suffer mutual annihilation when an interstitial atom enters the vacancy and remains there. Interstitial and vacancies are lost most at 'skins', such as radiation induced or preexisting dislocations and grain boundaries, within the solid.

Provided the temperature is high enough to permit the interstitials and vacancies to be fairly mobile but not so high that they are moved by recombination and by migration to the skins, a relatively large (supersaturated) concentration of defects can be maintained under irradiation. In these circumstances, the interstitials tend to agglomerate or cluster to form roughly circular 2-diminsional disks or platelets, commonly called 'interstitial

loops'. These loops can then grow to the point where they transform to network dislocations. Vacancies on the other hand, can agglomerate to form either 2 dimensional vacancy loops, which collapse into dislocation loops, or 3 dimensional clusters called 'voids'. Substantial void growth following a prolonged incubation results in swelling, primarily under the fast fluence and temperature conditions found in fast reactors.

1.9 General Irradiation Effects in Metals

The general physical and mechanical effects of the irradiation of metals by fast neutrons and other high energy particles are summarized in following way [24]:

i. Both yield strength and ultimate tensile strength of a metal are increased by irradiation, but the increase in yield strength is generally greater than the increase in ultimate tensile strength.

ii. Irradiation usually increases the brittleness of material.

iii. Plastic flow range of a metal, which is representative of the behavior of many metals including steels and zircaloy, is decreased due to irradiation. Hence, irradiation results in a decrease in ductility of a material.

iv. The increase in the yield strength also results in a corresponding increase in the Nil Ductility Transition (NDT) temperature, characterizing the transformation from ductile to brittle fracture.

v. Since the pressure vessel steel is subjected to cyclic changes in temperature, the possibility of fatigue failure must be considered. Since irradiation tends to decreases the ductility, it would be expected to facilitate fatigue failure. However, preliminary indications, suggest that irradiation has only a minor effect on fatigue failure.

vi. Irradiation frequently decreases the density of a metal over a certain temperature range, so that a specimen exhibits an increases in volume, i.e. it swells. This swelling can cause changes in dimensions of coolant channels and also interfere with the free movement of control elements.

As measured by the relative increase in volume, swelling increases with the fluence and in some stainless steels it may amount to as much as 15% after exposure to a fast neutron fluence of 10^{27} neutrons/m^2.irradiation induced swelling usually significant only in temperature range of very roughly 0.3 to 0.5 Tm, where, Tm is the melting point of the metal. At lower and higher temperatures swelling is small.

vii. The absorption of neutrons frequently results in the production of radioactive nuclei. This phenomenon called 'Induced Radioactivity'. The radioactivity induced in this manner can present a problem because maintenance and repair of equipment exposed to neutrons becomes difficult. Furthermore, corrosion and erosion products, which are unavoidable in the primary coolant system of a water cooled reactor, may become radioactive when they pass through the core. The removal of this activity places an additional load on the radioactive-waste treatment system of a nuclear power plant.

1.10 Degradation in Mechanical Properties of RPV Material

Reactor pressure vessels (RPVs), which contain the nuclear fuel in nuclear power plants, are made of thick steel plates that are welded together. Neutrons from the fuel in the reactor irradiate the vessel as the reactor is operated. This can embrittle the steel, or make it less tough, and less capable of withstanding flaws which may be present. Embrittlement usually occurs at a vessel's "beltline," that section of the vessel wall closest to the reactor fuel.

Other factors also contribute to the degree to which a particular vessel material becomes embrittled. Steels with a higher proportion of copper and nickel will tend to be more susceptible to embrittlement, than are steels with lower proportions of these two elements.

Pressurized water reactors (PWRs) are more susceptible to embrittlement than are boiling water reactors (BWRs), due to following reasons:

a) BWR vessels generally experience less neutron irradiation and therefore less embrittlement. Many utilities owning PWRs use core designs that reduce the number of neutrons that reach the vessel wall. These design features therefore reduce the rate of embrittlement in the reactor vessels.

b) Another reason reactor vessel embrittlement is more of a concern for PWRs is because PWRs may experience pressurized thermal shock (PTS). PTS can occur under some accident scenarios that introduce cold water into the reactor vessel while the vessel is pressurized. Introduction of cold water in this manner can cause the vessel to cool rapidly, resulting in large thermal stresses in the steel. These thermal stresses, along with the high internal pressure and an embrittled vessel, could lead to cracking and even failure of the vessel.

1.11 Non Destructive Evaluation of Mechanical Behavior

Mechanical properties are properties that indicate the elastic and inelastic behavior of a material when it is subjected to a force. Some of the commonly measured mechanical properties include the Young's modulus, yield strength, ultimate tensile strength, work hardening coefficients and hardness numbers. The mechanical properties provide the basic design information on the strength of materials and for the specification of materials. These properties are typically measured by tensile tests, compression tests and the hardness tests. Tensile tests are often time consuming, destructive and need specially prepared specimens. On the other hand, there is no direct theoretical correlation between the hardness number and the mechanical properties of a material although phenomenological relationships do exist.

In this area, Automated Ball Indentation (ABI) is a recent methodology for evaluating the in-situ mechanical properties of a material. The advantages of indentation techniques are that they are non-destructive, quick, and can be applied to small material samples and localized in fashion. Mechanical properties are typically determined from spherical indentation load-depth curves. This process is again a time consuming one and not suitable for situations where a quick assessment is required such as in the sheet metal rolling industry.

1.11.1 Automated Ball Indentation (ABI) Approach

Automatic ball indentation is a non-destructive methodology to determine the mechanical properties of degraded materials. The ABI technique uses a very small volume of test material. Hence, it could prove valuable in new alloy development and when limited amounts of material are available. For this purpose, the specimen undergoes multiple indentations by a spherical indenter. In each cycle, a loading-holding-unloading-reloading sequence is maintained. The multiple load and indentation diameters are then converted into true stress true strain of the material being tested. Finally the useful mechanical properties like yield strength, ultimate tensile strength, strength and hardening co-efficient and fracture toughness can be obtained from ABI technique.

Ball indentation technique is a promising method for in-situ assessment of mechanical properties. For in-situ application it is nearly non-destructive since no material is removed from the test surface. Only a smooth shallow spherical indentation is left at the end of the test. This spherical impression is harmless for the tested structure because it has no sharp

edge and does not introduce any stress concentration site. Furthermore, it can be used to characterize weldments and their HAZ, avoids the need to fabricate test specimen and relatively rapid.

The mechanical properties determined by this innovative approach include elastic modulus, yield strength, strain-hardening exponent, Brinell hardness, and true-stress/true-plastic strain (σ - ε_p) curve up to 20% strain. The fracture toughness is also estimated using the ABI measured flow properties and a modified critical fracture strain model. Furthermore, the shift in the ductile-to-brittle transition temperature for steel plates and welds, for example, due to neutron irradiation embrittlement, can be estimated from the ABI measured changes in the material's yield strength and flow properties [4].

1.11.1.1 Methodology of ABI Testing

The field indentation microprobe is utilized in the following manner. After the testing head is properly secured to the structure to be tested so that the load cell is perpendicular to the surface of the region where testing is to be performed, this surface is prepared using the polishing tool. Thereafter, the computer, through use of the capability of the head, causes the indenter tip to be brought into contact with the polished surface. The total and plastic indentation depths (h_t and h_p) and the applied indentation load (P) are then measured for the first cycle. Typically the load is increased for each succeeding cycle and the values of P, h_t, and h_p are measured for each cycle [20].

Several load cycles (typically five or more) are conducted at the same indentation location for determining a full true-stress/true-plastic-strain curve at this location (data from each cycle yield a point on this curve). This cyclic loading can be continued; however, the maximum total indentation depth (h_t) should not exceed one half of the diameter, D, of the indenter.

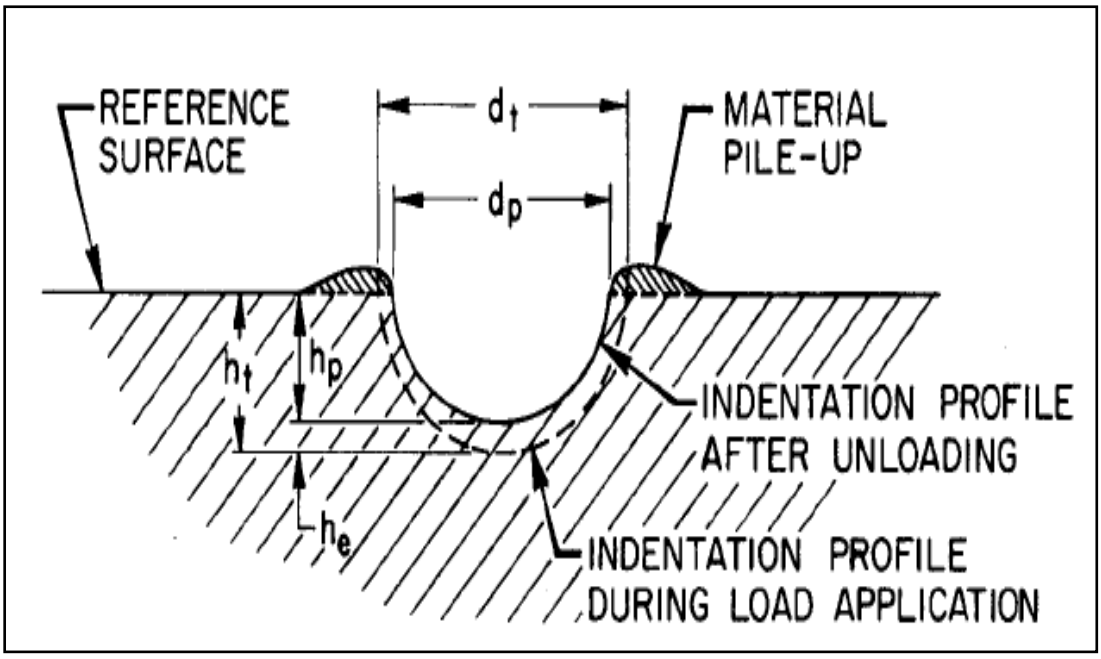

Fig. 1.12: Illustration of indentation geometries before and after load application (the material pileup around the indentation is exaggerated) [22]

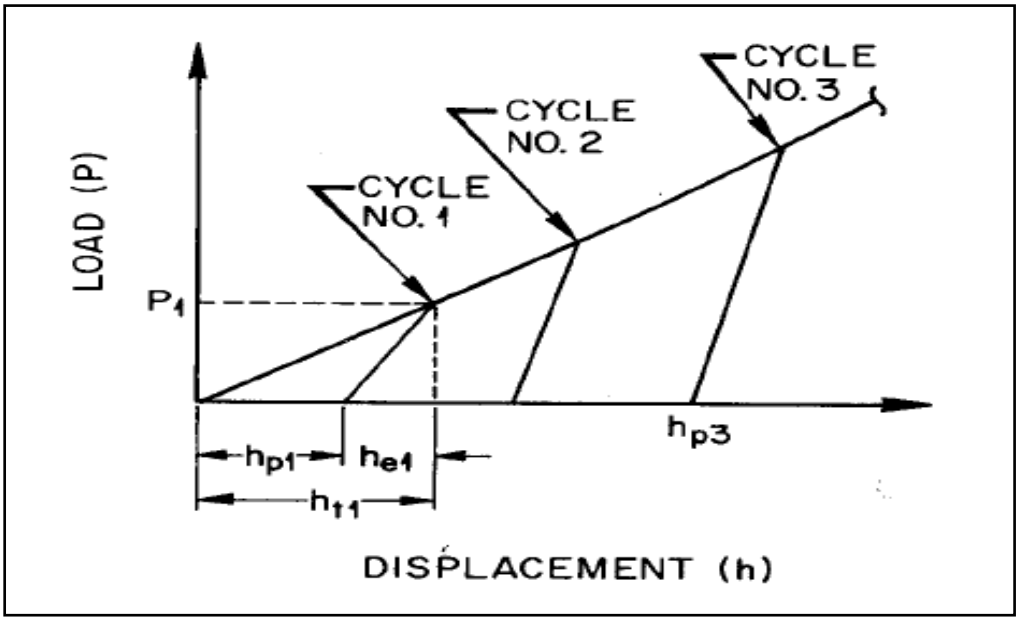

Fig.1.13: Schematic representation of the relationship between load and displacement of the ball indenter [22]

Following the final cycle, the plastic indentation diameter, d_p, can be independently measured using the video camera. If a measure of the amount of material pile-up and existence and orientation of residual stresses overall are required, thickness measurements are performed before and after indentation using the ultrasonic transducers over a traverse

distance of at least one indenter diameter from each side of the indentation and in two nominally perpendicular directions. As stated previously, the ABI operation is typically controlled by a program stored in the computer, and data such as the load, indentation depth, etc., measured using the data acquisition system are stored on magnetic discs in the computer for post-test processing [22].

a) True Plastic Strain

Tabor [1] was the first to correlate indentation hardness and strain associated with a spherical indenter to uniaxial tensile test results.

Tabor established the following correlation (Eq. 1.1) between true plastic strain ($\in_p$) in a uniaxial tensile test and indentation strain (dp /D) from a ball indentation test [1]

$$\in_p = 0.2 \times \frac{dp}{D} \qquad \text{(Eq. 1.1)}$$

Where D is the diameter of the ball indenter, and d_p is plastic indentation diameter.

The plastic depth (h_p) determined from unloading of specimen is converted into plastic indentation diameter d_p, using equation Eq. (1.2).

$$d_p = 2 \times \left(D \times h_p - h_p^2\right) \qquad \text{(Eq. 1.2)}$$

Where P is the measured load, E_{spec} and E_{ind} are the elastic modulai of the specimen and indenter, respectively.

The maximum strain that can be measured in an ABI test is 20% when $d_p = D$.

b) Flow Stress

Under load P, the mean normal pressure (S_m) acting on the material is $4P/\pi d_t^2$ where d_t is total diameter of the impression. The uniaxial flow stress (σ) is related to mean normal pressure by Eq. (1.3) and Eq. (1.4) [25]

$$\sigma = \frac{Sm}{\delta} \qquad \text{(Eq. 1.3)}$$

$$\sigma = \frac{4 \times P}{\pi \times dt^2 \times \delta} \qquad \text{(Eq. 1.4)}$$

Where δ is a constraint factor.

$$\delta = 2.87 \times \alpha_m \qquad \text{(Eq. 1.5)}$$

The parameter α_m depends mainly on the strain rate sensitivity and work hardening characteristics of the material being tested. α_m varies from 0.9 to 1.25 for different materials, typically with a value of 1.0 for low strain rate sensitive materials [13].

c) Flow Curve (True Stress and True Plastic Strain Relationship)

The homogeneous plastic flow portion of the true stress-true plastic strain curves can be represented by power law equation, Eq. (1.6); [22]

$$\sigma = K \times (\in_p)^n \qquad \text{(Eq. 1.6)}$$

Where, n - Strain Hardening Exponent of the material,

K - Strength Coefficient of the material,

σ - True Stress,

$\in_p$ - True Plastic Strain,

Values of Strength Coefficient (K) and Strain Hardening Exponent (n) are determined by linear regression analysis of the data fitted to Eq. (1.6).

d) Ultimate Tensile Strength

For $\in_p = n$, Eq. (1.6) will provide the expression for true ultimate tensile strength [22].

i.e. $$\sigma_{True\ UTS} = K \times n^n \qquad \text{(Eq. 1.7)}$$

The engineering value of ultimate tensile strength is then given by Eq. (1.8),

$$\sigma_{UTS} = K \times \left(\frac{n}{e}\right)^n \qquad \text{(Eq. 1.8)}$$

where e = 2.71

e) Yield Stress

The flow stress corresponding to the initiation of plastic deformation i.e. true yield stress is not determined from Eq. (1.4) because the corresponding strains are too small for direct measurement during the indentation test. The minimum attainable ball indentation strains for a nominal size indenter are about 20 times larger than the yield strain. Therefore, a different approach is used for the estimation of the yield strength [22].

Yield strength is estimated from the relationship between the mean pressure and impression diameter as developed by Meyer [22]. Data points from all loading cycles (maximum value of $d_t/D = 1.0$) are fit by linear regression analysis to the relationship shown by Eq. (1.9).

$$P = \frac{A}{{d_t}^2} \times \left(\frac{d_t}{D}\right)^{m-2} \qquad \text{(Eq. 1.9)}$$

where d_t is the total diameter of the impression,

m is the Meyer's exponent (m generally has a value between 2 and 2.5)

A is a material yield parameter obtained from the regression analysis.

The value of d_t is determined from total depth of penetration (Fig. 2.1) using the Eq. (1.10).

$$d_t = 2 \times (D \times h_t - h_t^2) \quad \text{(Eq. 1.10)}$$

Where h_t is the total depth of the indentation.

The yield strength (σ_y) is proportional to the Meyer hardness ($4P/pd^2$), where d is the final impression diameter, and is given in Eq. (1.11).

$$\sigma_y = \beta_m \times A \quad \text{(Eq. 1.11)}$$

Where β_m is a constant for a given class of materials. The value of β_m for each class of materials is determined from yield strength obtained from standard tensile tests, and the value of A is obtained from ABI tests.

CHAPTER 2
LITERATURE REVIEW

2.1 Review of Work

Fahmy M. Haggag, Randy K. Nanstad, John T. Hutton, David L. Thomas, and Ronald L. Swain [2] investigated the applicability of automated ball indentation (ABI) test, to measure the flow properties of metallic materials (carbon steels, titanium alloys, etc.). The ABI test was based on multiple indentations (at the same penetration location) of a polished metallic surface by a spherical indenter. Automation of the test was done, in which a computer and test controller were used in to control the test as well as to analyze test data, made it simple, rapid, accurate, economical, and reproducible.

F. M. Haggag, R. K. Nanstad, and D. N. Braski [3] performed ABI analysis on the laboratory version ABI apparatus for irradiate and un irradiated pressure vessel material. Results of the laboratory version of the ABI tests on un irradiated and irradiated A212B pressure vessel steel show that excellent agreement was obtained between yield strength and flow properties (true-stress/true-plastic-strain curve) measured by the ABI tests and those of uniaxial tensile tests.

F.M. Haggag [4] uses ABI method for measuring mechanical properties of kerosene pipeline by multiple spherical indentations is developed. A series of indentations are made on the substrate with a spherical indenter with different loads. The diameter of the indentation is related to the load applied to determine the mechanical properties of the material, namely the yield strength and the work hardening parameters.

F. M. Haggag [5] used portable/in-situ stress-strain microprobe successfully to test a circumferentially welded type 347 stainless steel pipe. Four V-blocks were used to mount the testing head of the flow properties microprobe. He describes in detail ABI test results, from several welds and their HAZs, using the patented microprobe system developed recently at Advanced Technology Corporation, Oak Ridge, Tennessee.

Fahmy M. Haggag [6] utilized ABI approach to nondestructively measure flow properties of alloy 718 (a nickel based alloy) base metal and welds. These measurements were integrated with micro structural features to determine fracture toughness of specimens.

stress-strain curves were measured (using its nondestructive and localized automated ball indentation technique) on base and weld samples of alloy.

F. M. Haggag [7] proposed a theoretical model to estimate the fracture toughness of ferritic steels in the transition region from ball indentation test data. The key concept of the model is that the indentation energy to a critical load is related to the fracture energy of the material. By applying the new model, the fracture parameters of reactor pressure vessel steel base and weld metals were estimated from the indentation load-depth curves.

F M Haggag, Larry D. Phillips [8] used ABI system on a short segment of a 356-mm (14-inch) diameter Kerosene pipeline. Although there was no documentation of the pipeline steel grade, the minimum ABI-measured yield strength at four locations was 277 MPa (40.2 ksi) and the minimum ultimate tensile strength was 378 MPa (54.8 ksi). This work proves that the integration of the ABI measurements with the corrosion pitting profile allows calculation of the maximum safe operating pressure in order to make the appropriate decision of replacement or repair of certain pipeline sections.

F. M. Haggag [9] performed nondestructive detection and assessment of damage in aircraft using a novel ABI approach. The properties of aluminum alloys, titanium alloys, and nickel-based super alloys used in aircraft structures and engines might degrade with service conditions associated with the operation of the aircraft. Important aspects of environmental conditions encountered in service cannot be accurately simulated. Thus, it will be a great advantage that the in-situ mechanical properties can be obtained nondestructively.

F. M. Haggag, H. Wong, D. J. Alexander, R. K. Nanstad [10] used ABI approach for evaluating the structural integrity of metallic component (including base metal, welds, and heat-affected zones) in situ in a nondestructive manner. An automated ball indentation (ABI) unit was used for determining the mechanical properties (yield strength, flow properties, estimates of fracture toughness, etc.) and a nondestructive evaluation (NDE) unit (consisting of ultrasonic transducers and a video camera) for determining the physical properties such as crack size, material pile-up around indentation, and residual stress presence and orientation. The laboratory version used in this work performs only ABI testing.

F. M. Haggag and Glenn E. Lucas [11] investigated techniques to characterize flow properties of steels exhibiting strains from ball indentation hardness/ micro hardness tests. A quantitative relationship was found between the amount of pile-up formed during indentation and the magnitude of the strain exhibited during tensile testing in SAE 1015 steel. Moreover, by nonlinear regression analysis, a single set of equations was found which correlated hardness data to the homogeneous true-stress-true-plastic strain relationship of steels in a variety of metallurgical conditions in the strain range of 1 to 10 percent at room temperature.

F. M. Haggag and R. K. Nanstad [12] used the modified model in combination with either tensile or ball indentation data to estimate fracture toughness of A515 grade 70 carbon steel and A533 grade B class 1 pressure vessel steel, respectively. The difference between fracture toughness predictions and measured values, using a computerized single-specimen unloading compliance technique in accordance with ASTM E-813, was less than 11%.

Goutam Das, Sabita Ghosh, S.K. Sahay [14] worked on, ball indentation technique (BIT) to explore the possibilities for revealing the effect of cold rolling on mechanical properties on a SS316L steels. The as-received steel was cold rolled up to 40%. Results are presented for 7%, 15%, 24% and 40% of cold rolling effect on the SS316L steels. For all the specimens tested, the dependence of yield strength (YS), ultimate tensile strength (UTS), strength coefficient (K) and strain hardening component (n) values on cold rolling effect were made available from the ABI results and they were validated with the standard conventional mechanical test results. It was found that, with increase in cold rolling the YS, UTS and K values have increased as revealed by ball indentation test (BIT), while n value has decreased. Overall, it is found that BIT can be effectively used to determine the change of mechanical properties after cold working by using a small amount of test materials and quite rapidly compared to conventional test. An in-house developed BI system was employed to evaluate the mechanical properties.

G. E. C. Bell [15] used portable ABI system to evaluate the integrity of metallic components [including base metal, welds, and heat-affected-zones (HAZs)]. ABI technique was used to determine several key mechanical properties (e.g., yield strength, true-stress/true-plastic-strain curve, strain-hardening exponent, Luders strain, and elastic modulus). Author describes ABI test results, from several welds and their HAZs, using the

patented ABI system developed recently at Advanced Technology Corporation. A special configuration of the ABI system was used successfully to test spot welds in 1020 ferritic steel and 2219 aluminum sheets at various strain rates.

K.L. Murty, M.D. Mathew, Y. Wang, V.N. Shahb, F.M. Haggag [16] investigated the tensile and fracture properties of ASTM grade A36 steel using nondestructive automated ball indentation (ABI) technique. Tests have been carried out on as-received, and cold worked (4, 8 and 12%) materials at several temperatures in the range -150°C to +200°C at a constant strain rate. Tensile properties determined from ABI tests agreed well with the results from conventional tensile tests. As expected, cold working resulted in increase in strength, decrease in fracture toughness and increase in ductile to brittle transition temperature. ABI is a reliable nondestructive technique for determining tensile and fracture properties of materials and has potential applications in the nuclear industry particularly to determine toughness degradation due to aging in service.

K.L. Murty, P.Q. Miraglia, M.D. Mathew, V.N. Shahb, F.M. Haggag [17] studied the gradients in mechanical and fracture properties of SA-533B steel welds using ball indentation technique. The local stress–strain behaviors of different micro structural zones of the weld were determined at various temperatures. Gradients in the strength of the base metal, weld metal and the different positions in the heat affected zone were observed to be consistent with the changes in the microstructure.

K. Linga Murty and Fahmy M. Haggag [18] applied ABI tester to evaluate the mechanical properties of Sn 5%Sb solder material at room temperature by varying the indenter velocity over three orders of magnitude. Constant load creep tests were also performed on the same material which covered the low strain-rate range and were in good agreement with ABI. The tensile test results exhibited slight deviation in reasonable agreement with creep and ABI data.

F. M. Haggag [19] measured mechanical properties of Steel Bridges during service using automated ball indentation (ABI) technique to nondestructively measure yield strength, true- stress versus true plastic-strain curve, strength coefficient, strain-hardening exponent, and to estimate fracture toughness.

M.D. Mathew, K.L. Murty, K.B.S. Rao, S.L. Mannan [20] investigated the effect of aging on mechanical behavior of Alloy 625 using ABI setup. The technique was used for evaluation of mechanical properties such as yield strength, ultimate tensile strength,

strength coefficient and strain hardening exponent. Alloy 625 was aged at six different temperatures in the range of 873–1173 K for 500 hours each. ABI tests were carried out at room temperature and at 473 K. The variation of yield and ultimate tensile strengths with aging temperature exhibited a peak in strength following aging at 973 K. These studies demonstrate that ABI can be used as a non-destructive technique to determine changes in mechanical properties of nickel base alloy components due to aging.

Randy K. Nanstad ,F.M. Haggag, John T. Hutton, David L. Thomas, and Ronald L. Swain [22] checked the accuracy, reliability, and easy field applicability of the ABI technology to test ferritic steels The ABI-measured tensile and fracture toughness values are in excellent agreement with the results from destructive tests over the temperature range from -130°C to 288°C.

Thak Sang Byun Jin Weon Kim, Jun Hwa Hong [26] proposed a theoretical model to estimate the fracture toughness of ferritic steels from ball indentation test data. The key concept of the model is that the indentation energy at a critical load is related to the fracture energy of the material. By applying the new model, the fracture parameters of reactor pressure vessel steel base and weld metals were estimated from the indentation load-depth curves.

2.2 Summary of Work Review

Table: 2.1: Summary of Work Review

S. No.	Material Investigated/ Application	Properties Investigated	Nature of work	Year of Publish	Reference
1	Carbon steels, Titanium alloys, Aluminum alloys	Flow properties and Fracture toughness	Experimental	1988	[2]
2	A212B Pressure Vessel Steel	Flow properties (true-stress/true-plastic-strain curve)	Experimental	1993	[3]
3	Kerosene Pipeline ASME B31G Code	Tensile and Fracture Properties	Experimental	2004	[4]
4	347 Stainless Steel Pipe Weld	Yield strength, true-stress/true-plastic-strain curve, strain-hardening exponent, and elastic modulus	Experimental	1986	[5]
5	Nickel Based Alloy 718 Base Metals and Weld Zone	Tensile and Fracture Properties	Experimental	1998	[6]
6	Alloy Steel 1015	Flow Properties	Experimental	1989	[7]
7	Natural Gas Pipe Line Material	Yield Strength, Ultimate Tensile Strength, Strength Coefficient, Strain Hardening Exponent, Fracture Toughness	Experimental	1986	[8]
8	Aircraft structures	Yield Strength, True-stress versus True-plastic-strain curve, Strength Coefficient, Strain-Hardening Exponent, and Fracture Toughness	Experimental	-	[9]
9	Reactor Pressure Vessel Steel (SA 508 Gr. 3 Steel) weld Metal	Fracture Toughness	Theoretical Model was proposed, Experimental, FEM Modeling by ABAQUS	1992	[10]
10	A515 grade 70 carbon steel and A533 Steel	Facture Toughness	Experimental	1993	[11]

11	1020 Ferritic steel and 2219 aluminum sheets	Yield strength, True-Stress/True Plastic Strain Curve, Strain-Hardening Exponent, and Elastic Modulus	Experimental	1989	[12]
12	ASTM grade A316 steel	Fracture Toughness and Tensile Properties	Experimental	2005	[14]
13	Stainless Steel base metal (type 316L), Heat-affected-zone, and welds (type 308)	Yield strength and Flow Properties (True Stress/ True Plastic Strain Curve	Experimental	1992	[15]
14	SS316 Steel	Yield Strength, Ultimate Tensile Strength, Strength Coefficient, Strain Hardening Component	Experimental	1998	[16]
15	SA-533B steel welds	Gradients in stress-strain Behavior at different positions of HAZ, weld metal and base metal	Experimental	1999	[17]
16	Sn5%Sb solder	Flow Property and Fracture Toughness	Experimental	1989	[18]
17	Steel Bridge material (347 stainless steel (SS)	Flow Properties	Experimental	1998	[19]
18	Alloy 625	Yield Strength, Ultimate Tensile Strength, Strength Coefficient, Strain Hardening Exponent	Experimental	1998	[20]
19	Low Carbon Steel Material	Tensile and Fracture Properties	Experimental	1990	[22]
20	Ferritic steels	Fracture Toughness	Experimental	1998	[26]

CHAPTER 3
PROBLEM DEFINITION

3.1 Aim of Thesis

Automatic ball indentation (ABI) is a non-destructive methodology to determine the mechanical properties of materials. Moreover, this is a promising method for in-situ assessment of mechanical properties. For in-situ application it is nearly non-destructive since almost no material is removed from the test surface. It could prove valuable in the evaluation of mechanical properties of different materials of nuclear applications at different environmental conditions. Moreover, it could be also valuable in gradient characterization of mechanical behavior as a weld joint.

Hence, present work concentrates on the following objectives;

i. A weld joint is a combination of 3 principal zones (i.e. Base Metal, HAZ of Base Metal, and weld). Thus, the gradients in mechanical properties could not only exist from zone to zone, but also from point to point at each zone of a weld joint. In this respect, conventional method of testing cannot be adopted successfully, since it is the destructive methodology. Moreover, it could not be able to characterize the material using small amount of material. In this connection, ABI methodology was considered to be very useful, since it can characterize the mechanical properties using a very small amount of material and in non destructive way.

Hence, the present work is an attempt to show how mechanical properties vary from zone to zone, and from point to point in each zone of a weld joint. For this purpose, following two types of weld joints were studied by ABI technique;

1. Bimetallic weld joint, joining SA 508-Class 2 reactor vessel nozzle with SS 304 LN pipeline using Inconel weld used in pressurized water reactor.

2. Similar weld joint, connecting two SS 304 LN material pipelines.

ii. Reactor Pressure Vessel is a very important structural component of a nuclear reactor. During operation of nuclear reactor, reactor pressure vessel faces irradiation and thermal cycling conditions. Due to this, degradation in its mechanical properties in the form of embrittlement, decrease in ductility, fracture toughness and increase in nil ductility temperature (NDT) take place. Similar effects could be found out with the help of cold

working treatment. The CANDU reactor (PHWR) consists of a horizontal calandria (Vessel) which has tubes for the fuel rods and cooling water (heavy water). The calandria vessel is made up of SS 304 LN austenitic stainless steel. SA 508 is a reactor pressure vessel steel commonly used in pressurized water reactor. Both SS 304 and SA 508 continuously face irradiation environment conditions.

Hence, present work is an attempt to characterize the mechanical behavior degradation of reactor pressure vessel materials (SA 508 and SS 304 LN) at different cold working levels, through Automated Ball Indentation (ABI) technique.

iii. Pressure tube is a critical structural component of pressurized heavy water reactor. The pressure tube is made up of cold worked Zr-2.5-Nb alloy. Highly pressurized heavy water flows inside pressure tubes in order to carryout heat generated from nuclear fission reaction of fuel. The conventional fabricating procedure of the pressure tube used to produce the product having low ultimate tensile strength and yield strength. Thus, this product cannot be successfully used for commercial application. Some modification in the fabricating route is required so as to get higher ultimate tensile strength and yield strength. The present work is an attempt to show the modified fabricating procedure of Zr-2.5 Nb pressure tube of a pressurized heavy water reactor. More over mechanical behavior examination of Zr-2.5- Nb alloy at different environmental condition was performed with the help of ABI methodology.

iv. The validation of the ABI experiments is also required. In this connection, validation of ABI experiments was performed through Finite Element Method (FEM) with the help of ANSYS software. For this purpose, a 2-d axis symmetric FEM model of ball indentation was prepared in ANSYS software. In this model, power law fitted true stress vs. true strain curve (generated through ABI methodology) was taken as input material property and corresponding load vs. displacement curve was generated as output. Finally the comparison between the two load vs. displacement curves (i.e. experimental and FEM simulation) was performed in order to check the validity of ABI experiments.

CHAPTER 4
EXPERIMENTATION AND ANALYTICAL INVESTIGATION

4.1 Characterization of Bimetallic Weld Joint using ABI Approach

4.1.1 Introduction

Bimetallic weld joint is a combination of 5 different zones (i.e. Base Metal 1, HAZ of Base Metal 1, weld, Base Metal 2, and HAZ of Base Metal 2). Main objective was to characterize how mechanical properties vary from zone to zone, and from point to point at each zone of bimetallic weld joint. In this respect, conventional method of testing cannot be adopted, since it is the destructive methodology. Moreover, it could not be able to characterize the material using small amount of material. In this connection, ABI methodology was considered to be very useful, since it can characterize the mechanical properties using a very small amount of material and also in non destructive way.

Hence, the present work is an attempt to show how mechanical properties vary from zone to zone, and from point to point in each zone of bimetallic weld joint (weld joint of SA 508-Class 2 nuclear reactor vessel nozzle with a SS 304 LN pipeline using an Inconel weld).

4.1.2 Introduction to Bimetallic Weld Joint (Weld Joint of SS 304 LN & SA 508 Cl-2)

The most widely used reactor type in the world is the Pressurized Water Reactor (PWR) which uses enriched (about 3.2% U 235) uranium dioxide as a fuel in zirconium alloy cans. The fuel, which is arranged in arrays of fuel "pins" and interspersed with the movable control rods, is held in a steel vessel through which water at high pressure (at 16 MPa, to suppress boiling) is pumped to reactor vessel via. cold lag pipeline to act as both a coolant and a moderator. After taking heat from core of reactor, the high-pressure water is passed to a steam generator, via. hot lag pipeline which raises steam in the usual way (Fig. 4.1).

Both hot lag and cold lag pipe lines are joined by reactor vessel nozzle by a bimetallic weld joint. The hot lag weld is a bimetallic weld joining the SA 508-Class 2 reactor vessel nozzle with a SS 304 LN pipe using an Inconel weld.

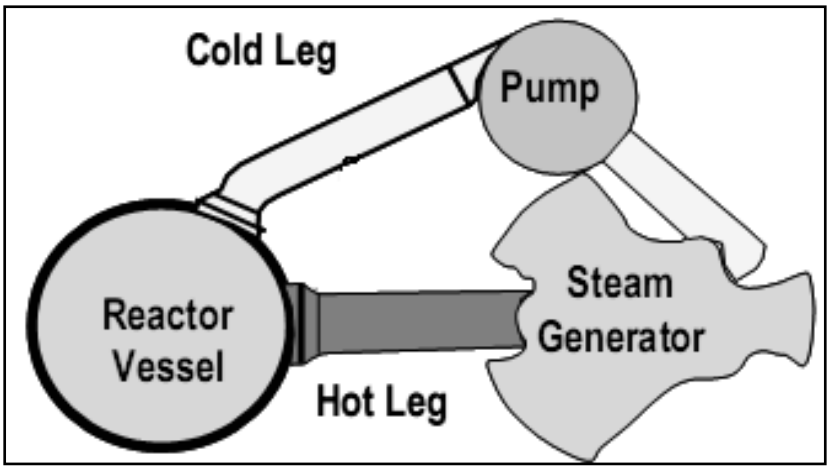

Fig. 4.1: Arrangement of Reactor Pressure Vessel and Piping System

4.1.2.1 Chemical Composition

The chemical composition of 3 zones of bimetallic weld joint i.e., SS 304 LN (Base Metal 1), Inconel 182 (weld), SA 508 Class 2 (Base Metal 2) are shown in Table 4.1.

Table 4.1: Chemical Composition of three zones of bimetallic weld joint

Chemical Element	Symbols	SS 304 LN (wt %)	INCONEL 182 (wt %)	SA 508 LN (wt %)
Carbon	C	0.03 Max	0.10 Max.	0.21
Manganese	Mn	2.0 Max	5.0-9.5	1.36
Nickel	Ni	8-12	59.0 Min. (Ni+Co)	0.64
Silicon	Si	1.0 Max	1.0 Max.	0.29
Sulpher	S	0.03 Max	0.015 Max.	0.004
Phosphorus	P	0.045 Max	0.030 Max.	0.009
Chromium	Cr	18-20	13.0-17.0	0.19
Nitrogen	N	0.10-0.16	-	-
Vanadium	V	-	-	< 0.1
Molybdenum	Mo	-	-	0.52
Copper	Cu	-	0.5 Max.	-
Titanium	Ti	-	1.0 Max.	-
Niobium	Nb	-	1.0-2.5	-
Iron	Fe	Balance	10 Max.	Balance

4.1.3 ABI Specimen Photograph

In order to characterize the bimetallic weld joint, ABI experiments were performed along the weld joint. The specimen of Bimetallic Weld Joint (i.e. weld joint of SS 304-LN and SA-508 Class 2), which was used for ABI experimentation work, is shown in Fig. 4.2. In Fig. 4.2, bottom row and top row of indents are corresponding to loading rates of 0.5 KN/min. and 1.5 KN/min. respectively.

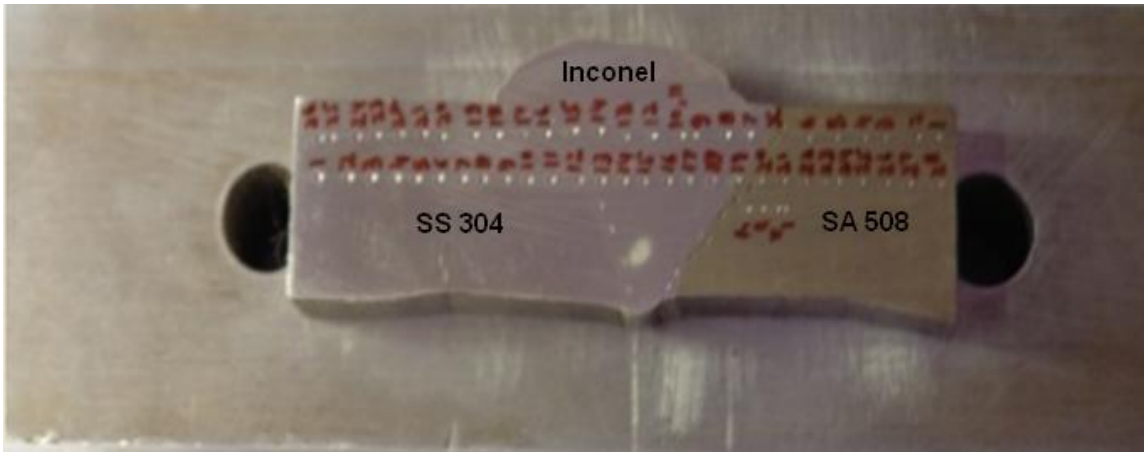

Fig. 4.2: Specimen Bimetallic weld Joint of SS 304-LN and SA-508 Class 2

4.2 Characterization of Similar Weld Joint through ABI Approach

4.2.1 Introduction

A similar weld joint is a combination of 3 different zones (i.e. Base Metal, HAZ of Base Metal, and weld). Main objective was to characterize how mechanical properties vary from zone to zone, and from point to point at each zone of bimetallic weld joint. In this respect, conventional method of testing cannot be adopted, since it is the destructive methodology. Moreover, it could not be able to characterize the material using small amount of material. In this connection, ABI methodology was considered to be very useful, since it can characterize the mechanical properties using a very small amount of material and in non destructive way.

Hence, the present work is an attempt to show how mechanical properties vary from zone to zone, and from point to point in each zone of similar weld joint (weld joint of two SS 304 LN pipelines).

4.2.2 ABI Specimen Photograph

In order to characterize the similar weld joint, ABI experiments were performed along the weld joint of two SS-304 pipelines. ABI machine was installed on the weld jointed pipelines (Fig. 4.3). The indent points after ABI experiments on Similar Weld Joint (i.e. weld joint of SS 304-LN), are shown in Fig. 4.4.

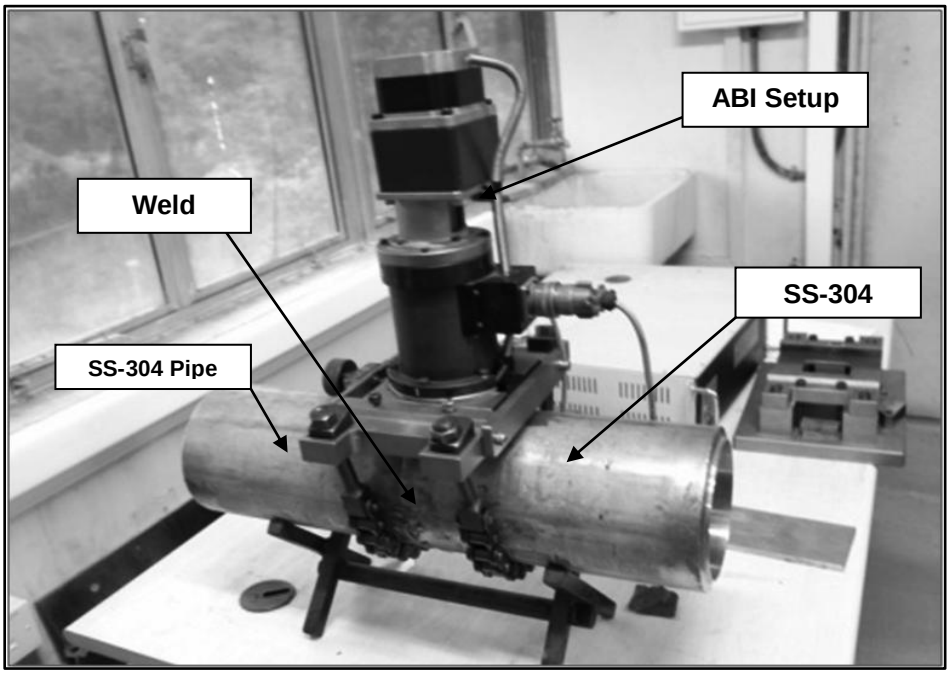

Fig. 4.3: ABI Machine installed on two weld jointed pipes of SS 304 LN material

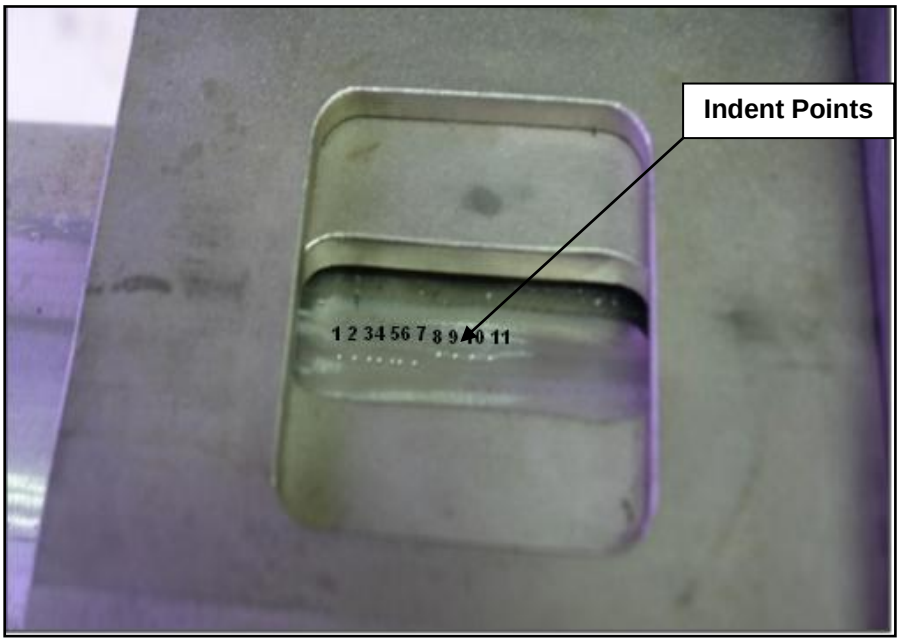

Fig. 4.4: Final indentation points after ABI experiments on similar weld joint

4.3 Mechanical Behavior Characterization of SA 508 Steel at Different Cold Working Conditions through ABI Approach

4.3.1 Introduction to SA 508 Steel

SA 508 steel, commonly used in reactor pressure vessels and supports, exhibit radiation embrittlement and decreased fracture toughness. Similar effects are expected following cold-working also. The work presented here shows the influence of different cold-working conditions on mechanical characteristics of SA 508 steel examined by ABI methodology.

4.3.1.1 Chemical Composition

The chemical composition of SA 508 is shown in Table 4.2.

Table 4.2: Chemical Composition of SA 508 steel

Chemical Element	Symbol	Amount (wt. %)
Carbon	C	0.21
Manganese	Mn	1.36
Nickel	Ni	0.64
Silicon	Si	0.29
Sulpher	S	0.004
Phosphorus	P	0.009
Chromium	Cr	0.19
Nitrogen	N	-
Vanadium	V	< 0.1
Molybdenum	Mo	0.52
Iron	Fe	Balance

4.3.2 ABI Specimen Photographs

The embrittlement effect of reactor pressure vessel steel generated due to radiations can be simulated with the help of cold working process. In this connection, SA 508 steel samples were cold worked at 0, 8, 10, 12, 14, 15% levels. ABI experiments were carried out on these specimens in order to characterize the effect of cold work on mechanical properties. The specimens at 0, 8, 10, 12, 14, and 15 % cold working conditions used for ABI experimentation work are shown in Fig. 4.5 to Fig. 4.10 respectively.

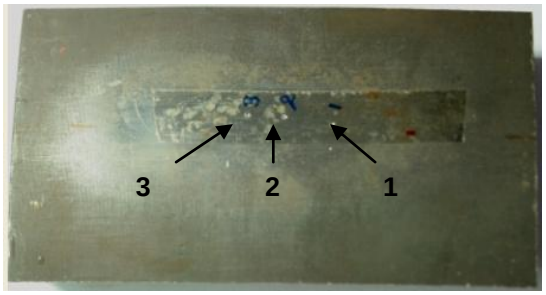

Fig. 4.5: SA 508 Class 2 Specimen at 0% CW Level

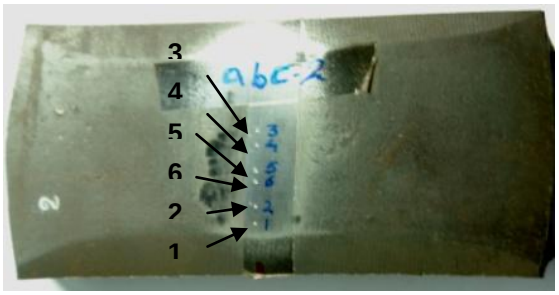

Fig. 4.6: SA 508 Class 2 Specimen at 8% CW Level

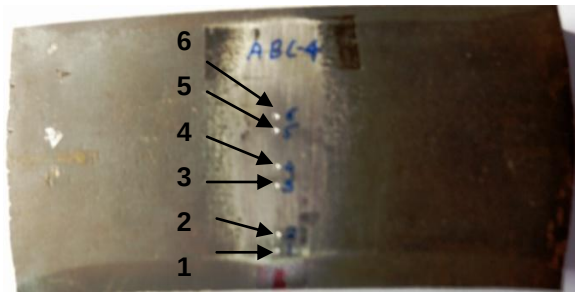

Fig. 4.7: SA 508 Class 2 Specimen at 10% CW Level

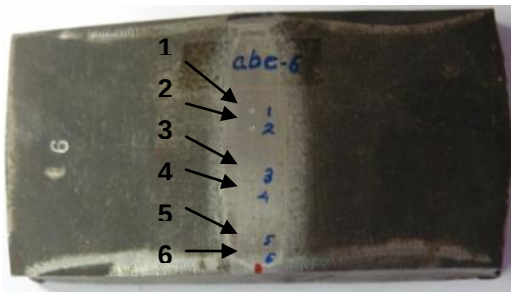

Fig. 4.8: SA 508 Class 2 Specimen at 12% CW Level

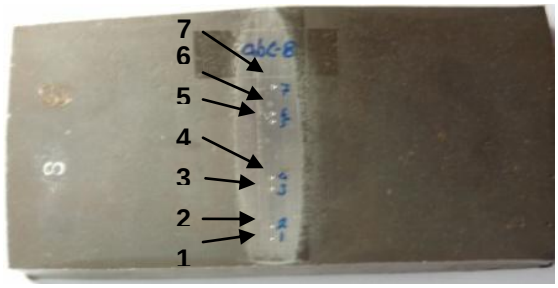

Fig. 4.9: SA 508 Class 2 Specimen at 14% CW Level

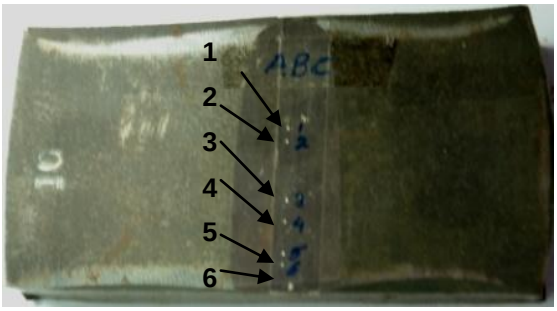

Fig. 4.10: SA 508 Class 2 Specimen at 15% CW Level

4.4 Mechanical Behavior Characterization of SS 304-LN Steel at Different Cold Working Conditions through ABI Approach

4.4.1 Introduction

The CANDU reactor (PHWR) consists of a horizontal calandria (Vessel) which has tubes for the fuel rods and cooling water (heavy water). Around these tubes is heavy water, which acts as the moderator to slow down the neutrons. The calandria vessel is a horizontal, cylindrical, single walled, stepped shell enclosed at each end by tube sheets

and spanned horizontally by calandria tubes. The calandria vessel made up of SS 304 LN austenitic stainless steel.

Researchers have shown that SS 304-LN austenitic stainless steel irradiated by fast neutrons will experience an increase in both the yield and the ultimate tensile strengths with corresponding decrease in flow range (ductility). These effects are expected following cold-working also. The work presented here shows the influence of different cold-working conditions on mechanical characteristics of SS 304 LN steel examined by ABI methodology.

4.4.2 Introduction to SS 304 LN Steel

4.4.2.1 Chemical Composition

The chemical composition of SS 304-LN is shown in Table 4.3.

Table 4.3: Chemical Composition of SS-304 LN

Chemical Element	Symbol	Amount (wt. %)
Carbon	C	0.03 Max
Manganese	Mn	2.0 Max
Nickel	Ni	8-12
Silicon	Si	1.0 Max
Sulpher	S	0.03 Max
Phosphorus	P	0.045 Max
Chromium	Cr	18.20
Nitrogen	N	0.10-0.16
Iron	Fe	Balance

4.4.2.2 Mechanical Properties

Mechanical Properties of SS 304-LN is shown in Table 4.4.

Table 4.4: Mechanical Properties of SS-304 LN

Mechanical Properties	Amount
Density (×1000 kg/m^3)	7.7-8.03
Poisson's Ratio	0.27-0.30
Elastic Modulus (GPa)	190-210
Tensile Strength (Mpa)	515
Yield Strength (Mpa)	205

4.4.3 ABI Specimen Photographs

The embrittlement effect of calandria generated due to radiations can be simulated with the help of cold working process. In this connection, calandria vessel material (SS- 304) samples were cold worked at 0, 10, and 20% levels.

ABI experiments were carried out on these specimens in order to characterize the effect of cold work on mechanical properties. The specimens of SS 304 LN material at 0, 10, and 20% cold working conditions used for ABI experimentation work are shown in Fig. 4.11, Fig. 4.12, & Fig. 4.13 respectively.

Fig. 4.11: SS 304 Specimen at 0% CW Level

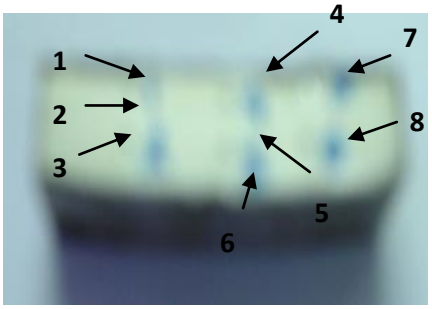

Fig. 4.12: SS 304 Specimen at 10% CW Level

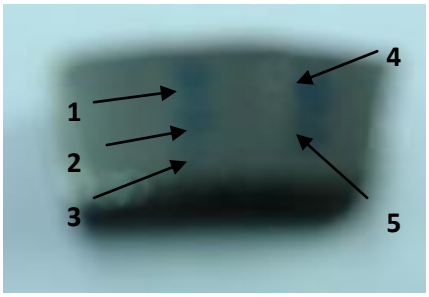

Fig. 4.13: SS 304 Specimen at 20% CW Level

4.5 Characterization of Zr-2.5-Nb alloy under Different Environmental Conditions using ABI Approach

Pressure tube is a critical structural component of pressurized heavy water reactor. It is generally made up of cold worked Zr-2.5-Nb alloy. Highly pressurized heavy water flows inside pressure tubes in order to carryout heat generated from nuclear fission reaction of fuel. The conventional fabricating procedure of the pressure tube used to produce the product having low ultimate tensile strength and yield strength. Thus, this product cannot be successfully used for commercial application. Some modification in the fabricating route is required so as to get higher ultimate tensile strength and yield strength.

The present work is an attempt to show the modified fabricating procedure of Zr-2.5 Nb pressure tube of a pressurized heavy water reactor. In this connection, mechanical behavior examination of Zr-2.5- Nb alloy at different environmental condition was performed with the help of ABI methodology.

4.5.1 Chemical Composition of Zr-2.5-Nb

The chemical composition of Zr-2.5-Nb is shown in Table 4.5.

Table 4.5: Chemical Composition of Zr 2.5 Nb

Chemical Element	Symbol	Amount (wt. %)
Niobium	Nb	2.5
Iron	Fe	0.01
Oxygen	O	0.03
Hafnium	Hf	0.04
Zirconium	Zr	Balance

4.5.2 Conventional Fabrication Procedure

The conventional route of fabrication of Zr 2.5 Nb pressure tubes consists of 4 phases (ingot preparation, ingot to log preparation, log to billet preparation, billet to hollow tube preparation, and cold drawing operation). In the conventional fabrication procedure, first of all Zirconium sponge, which is produced from zirconium silicate ore, is compacted into briquettes along with a master alloy of zirconium, niobium and recycled material. These briquettes are then electron beam welded together to form a long rod that is melted in a consumable electrode arc furnace to form a Zr-2.5%Nb ingot about 0.6 m in diameter.

A portion of an ingot is preheated to close to 1000°C and forged into round logs about 0.2 m in diameter using press and rotary forges. Then the logs are machined to remove their outer surface and to produce hollow billets. The machined billets are then beta quenched from 1000°C in order to get α (HCP) + β Nb microstructure (Fig. 4.14). This structure is then hot extruded at 850°C so that short hollow billets will converted into hollow tube. During hot extrusion process, 850°C temperature used to taken in order to convert α (HCP) + β Nb microstructure into a required elongated (α Zr + β Zr) microstructure. This microstructure is needed because the combination of high strength with a good ductility and toughness of Zr–2.5Nb pressure tubes is essentially derived from the fine (α+β) fibrous microstructure consisting of elongated α-grains containing about 0.5Nb and the β-phase (15-20Nb) stringers primarily located at α-grain boundaries.

The tubes are then cold drawn in a single phase of 25 % reduction in area. The cold drawn tubes are honed with at least 0.06 mm being removed from the inside surface to ensure that any small surface flaws are removed. In order to remove the residual stress and brittleness, caused by cold working step, full annealing treatment was used to given.

Full annealing treatment successfully removed the brittleness and residual stresses caused due to cold working treatment, but it also tends to coarsen the microstructure, which results in a substantial drop in ultimate tensile strength and yield strength.

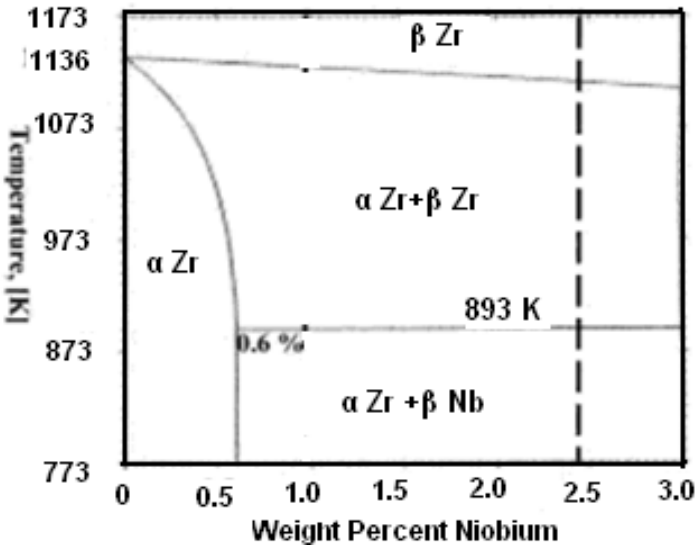

Fig. 4.14: Binary Phase Diagram of Zr-Nb alloy

4.5.3 Modified Fabrication Procedure

Since the conventional route of fabricating the Zr 2.5 Nb pressure tubes, produces the coarse microstructure, which results in a substantial drop in ultimate tensile strength and yield strength. This microstructure cannot be successfully used for commercial application. Thus, there was a need for improvement in the fabrication route.

This has been achieved by incorporating cold working by drawing or pilgering in two steps (instead of one in the conventional process) with an optimized intermediate annealing treatment. The purpose of intermediate annealing treatment prior to second pilgering in the modified route is to annihilate all the cold work introduced in the first pilgering step so as to get a microstructure and flow properties similar to that obtained after extrusion. Retention of this structure is necessary for obtaining optimum tensile properties.

In this investigation, the annealing temperature was varied between 550ºC and 900ºC (as specified in Table 4.6). It was observed that the elongated two-phase structure could be retained if the annealing temperature is kept 550ºC. An annealing treatment at 550C for 6 h caused nearly complete recrystallization of phase without altering the elongated morphology of the α+β microstructure.

If second cold working pass will be given to this elongated α+β microstructure, the final product (pressure tube) will has higher yield strength and ultimate tensile strength as compared to those generated by conventional fabrication route.

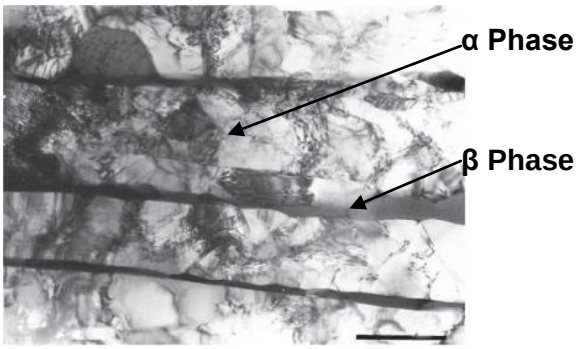

Fig.4.15: TEM microstructure of as extruded Pressure Tube

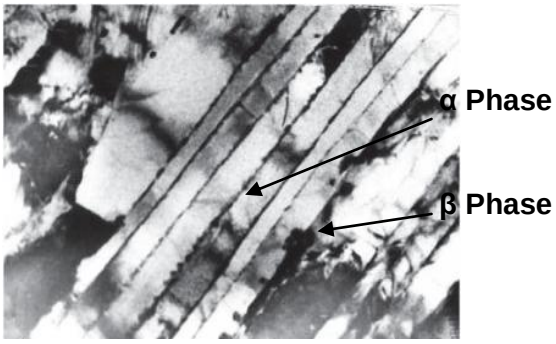

Fig 4.16: TEM microstructure of material annealed at 550ºC for 6 hours

In the present work, mechanical behavior examination of these annealed materials at different conditions was performed through Automated Ball Indentation (ABI) Methodology.

4.5.4 Environment Conditions

The specimens of Zr 2.5 Nb material used for mechanical behavior characterization through ABI methodology were treated in 6 different environment conditions (A, B, C, D, E, and F). These environment conditions are given in Table 4.6.

Table 4.6: Environment Conditions of Zr 2.5 Nb material

Condition Name	Condition Explanation
A	As received (AR) Pressure Tube Material
B	AR + 550ºC for 6 hours and Furnace Cooled
C	AR + 700ºC for 2 hours and Furnace Cooled
D	AR + 800ºC for 0.5 hours and Furnace Cooled
E	AR + 850ºC for 0.5 hours and Furnace Cooled
F	AR + 900ºC for 0.5 hours and Furnace Cooled

4.5.5 ABI Specimen Photographs

The specimens at different conditions used for ABI experimentation work, are shown in Fig. 4.17 to Fig. 4.18.

Fig. 4.17: ABI specimen at condition A

Fig. 4.18: ABI specimen at condition B

Fig. 4.19: ABI specimen at condition C

Fig. 4.20: ABI specimen at condition D

Fig. 4.21: ABI specimen at condition E

Fig. 4.22: ABI specimen at condition F

4.6 Analytical Investigation

4.6.1 Finite Element Model Description

In order to validate the ABI experiments, an axis symmetric 2D FEM model of ball indentation was prepared with the help of ANSYS software. In this model, power fitted true stress vs. true strain curve (generated through ABI methodology) was taken as input material property and corresponding load vs. displacement curve was generated as output. Finally the comparison between both load vs. displacement curves (i.e. experimental and FEM simulation) was performed in order to check the validity of ABI experiments. FEM analysis consists of following three stages;

Phase 1 (Preprocessing Phase)

Preprocessing Phase is the first phase of FEM analysis. During this phase tasks like; model preparation, material property allotment and meshing of model were performed. The detailed description of each of the sub steps in this phase is shown as follows;

i. First of all, an axis symmetric 2D model of ball indentation arrangement was made. In this model, ball has diameter of 1.46 mm. and work piece has 2 mm height and 2 mm length.

ii. After preparation of model, the material properties were allotted in the FEM model. Material input properties for work piece and indenter are as following;

For Indenter: Young's Modulus - 645000 MPa,

Poisson's Ratio - 0.3

For Work Piece: Young's modulus, Poisson's Ratio, and power law fitted True Stress vs. True Strain curve (generated through ABI methodology)

iii. For meshing of the model axis symmetric 8 node Plane 183 element was chosen and both indenter and work piece model were meshed with the help of this element. Curved line of indenter was meshed with contact element (CONTA 175) and top line of work piece was meshed with the help of target element (TARGET 169). Final meshed model is shown in Fig. 4.23. Final meshed model consists of 1650 nodal points and 553 elements.

Phase 2 (Applications of Loading & Boundary conditions)

After prepration of model, material properties allotment and meshing, the loading and boundary conditions were applied in the FEM model. In this phase, pressure of 896.429 N/mm^2 is applied on the top surface of indenter. This pressure is gradually applied on wok piece through indenter. Left side of work piece was constrained to move in x direction and bottom side of work piece was constrained to move in y direction. After applying these loading and boundary conditions on model, the model was analyzed.

Phase 3 (Post Processing Phase)

Post Processing Phase is a result generation phase. In this phase the output of FEM analysis was taken in following forms;

i. Pressure data with varying with respect to time at the top line of work piece.
ii. Displacement of indenter inside work piece was monitored at contact point of indenter and work piece.

Load applied on work piece was calculated by using Eq. (4.1).

$$\text{Load} = \text{Pressure} \times \frac{\pi}{4} \times 1.46^2 \qquad \text{Eq. (4.1)}$$

Finally, load vs. displacement curve were plotted and compare with corresponding experimental ABI generated load vs. displacement curve.

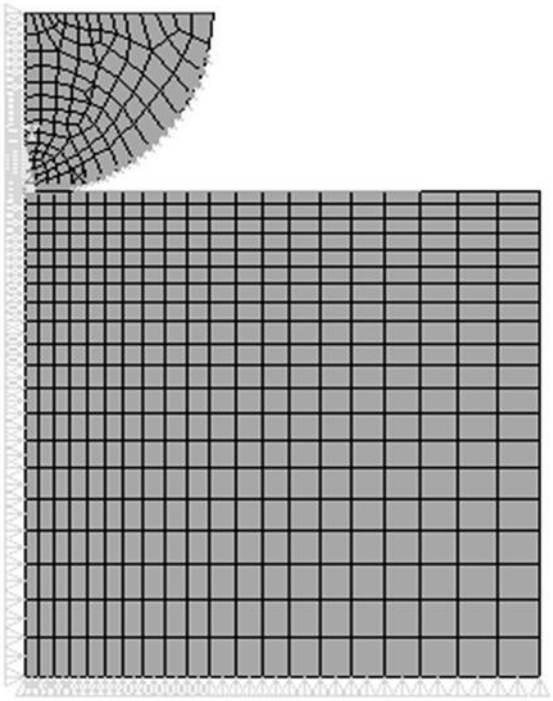

Fig. 4.23: 2D Axis Symmetric FEM model of Ball Indentation (Before Deformation)

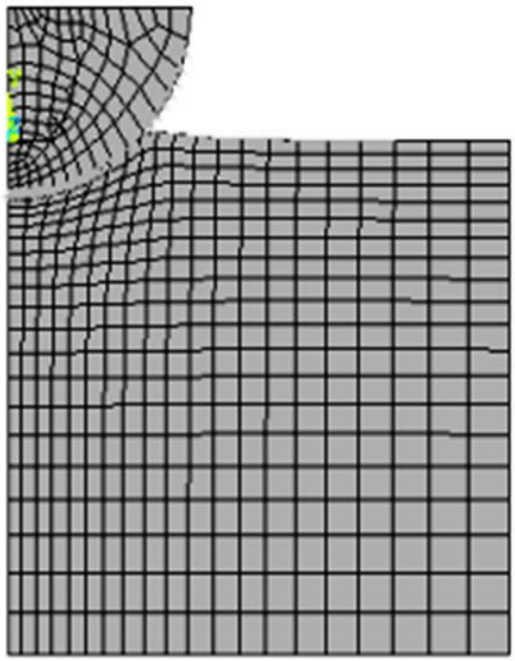

Fig. 4.24: 2D Axis Symmetric FEM model of Ball Indentation (After Deformation)

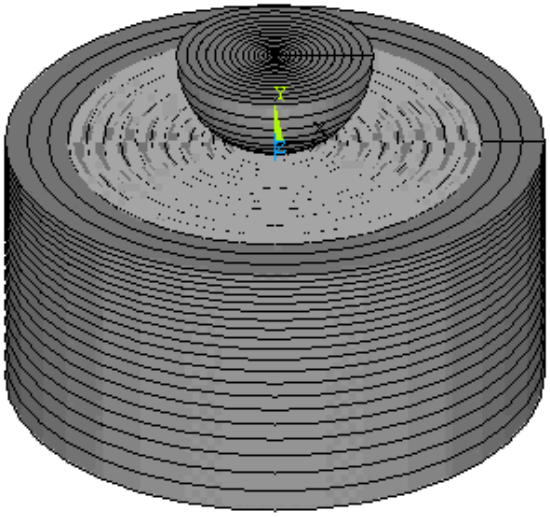

Fig.4.25: Full expansion of 2d axis symmetric FEM model (Before Deformation)

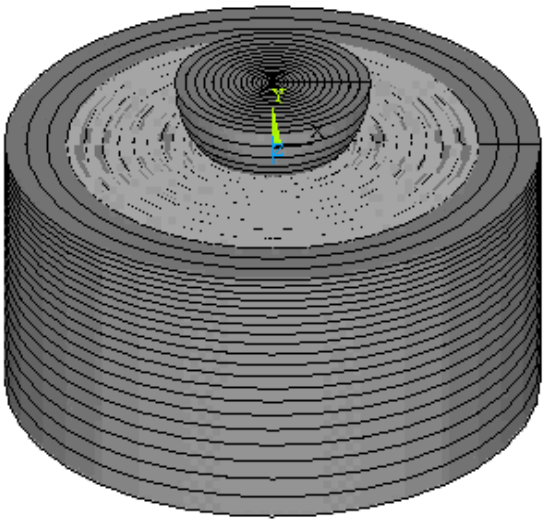

Fig. 4.26: Full expansion of 2d axis symmetric FEM model (Before Deformation)

CHAPTER 5

RESULTS AND DISCUSSIONS

5.1 Characterization of Bimetallic Weld Joint through ABI Methodology

5.1.1 Reproducibility in ABI Load vs. Displacement Curve

In order to characterize the mechanical behavior variation in bimetallic weld joint, ABI experiments were carried out at different points of 3 main zones of bimetallic weld joint (i.e. SS 304 LN, Weld, and SA-508 Class 2). Out of these experiments, the reproducibility in load vs. displacement curves on respective zones is shown in Fig 5.1 to Fig. 5.6.

Reproducibility at 0.5 KN/min. Rate

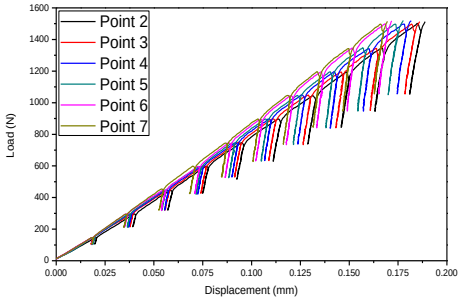

Fig. 5.1: Reproducibility of Load vs. Displacement Curves in weld zone

Reproducibility at 1.5 KN/min. Rate

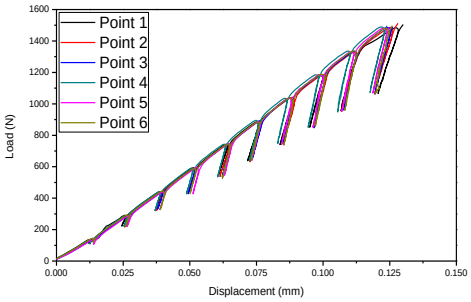

Fig. 5.2: Reproducibility of Load vs. Displacement Curves in SA 508 Zone

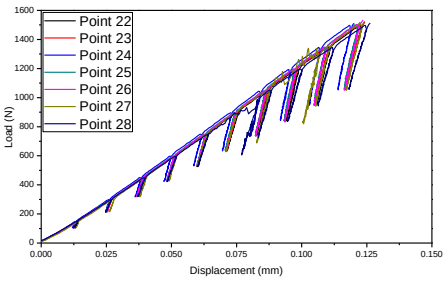

Fig. 5.3: Reproducibility of Load vs. Displacement Curves in SS 304 zone

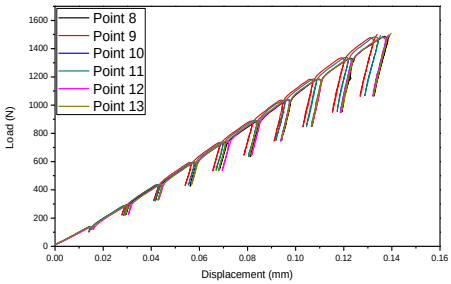

Fig. 5.4: Reproducibility of Load vs. Displacement Curves in weld zone

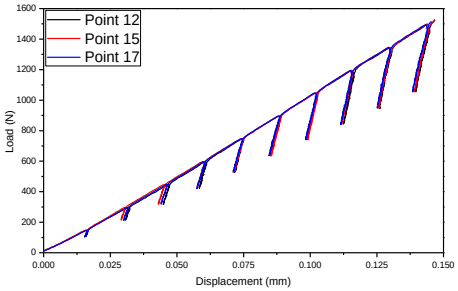

Fig. 5.5: Reproducibility of Load vs. Displacement Curves in SA 508 zone

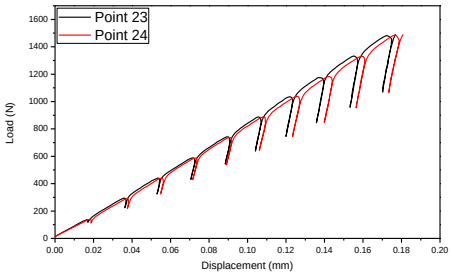

Fig. 5.6: Reproducibility of Load vs. Displacement Curves in SS 304 Zone

5.1.2 Comparison of Load vs. Displacement Curves With Respect to Loading Rate

The comparison of load vs. displacement curves at each of the 5 zones of bimetallic weld joint (i.e. SS 304 LN, HAZ of SS 304 LN, Weld, HAZ of SA-508 Class 2, and SA-508 Class 2) with respect to loading rates of 0.5 KN/min. and 1.5 KN/min. are shown in Fig.5.7to Fig.5.11, which clearly demonstrate the variations in load vs. displacement behavior in these zones with respect to change in loading rate.

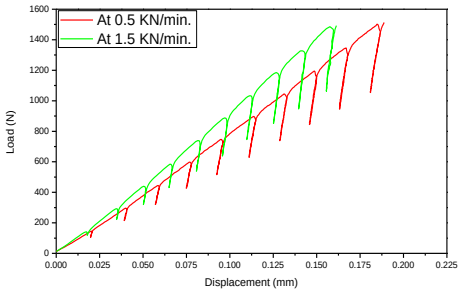

Fig. 5.7: Variation in load vs. displacement curve at SS 304 (Base Metal) zone with respect to loading rate

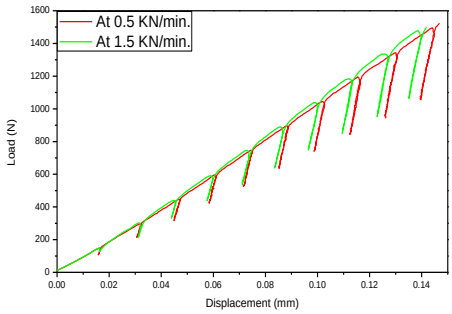

Fig. 5.8: Variation in load vs. displacement curve at HAZ of SS 304 with respect to loading rate

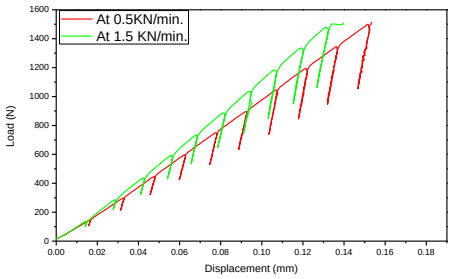

Fig. 5.9: Variation in load vs. displacement curve at weld zone with respect to loading rate

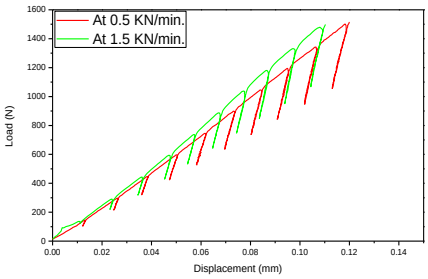

Fig. 5.10: Variation in load vs. displacement curve at HAZ of SA 508 with respect to loading rate

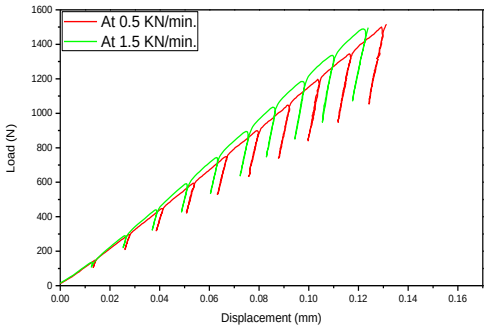

Fig.5.11: Variation in Load vs. displacement curve at SA 508 (Base Metal) with respect to loading rate

5.1.3 Comparison of Different zones of Bimetallic Weld Joint

A. Comparison of Load vs. Displacement Curves

The comparison of load vs. displacement curves at each of the 5 zones of bimetallic weld joint (i.e. SS 304 LN, HAZ of SS 304 LN, Weld, HAZ of SA-508 Class 2, and SA-508 Class 2) is shown in Fig.5.12, which clearly demonstrate the variations in load vs. displacement behavior in these zones.

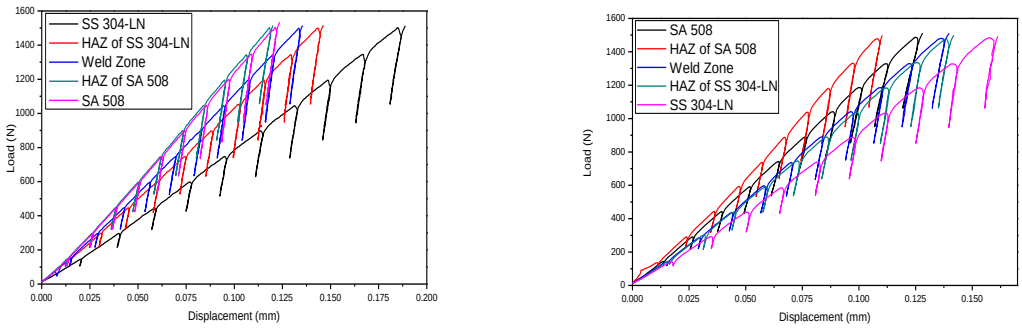

Fig.5.12: Comparison of Load vs. Displacement curves at 5 zones of Bimetallic Weld Joint at Loading rate 0.5 KN/min. (a) and 1.5 KN/min. (b)

B. Comparison of True Stress vs. True Strain Curves

The comparison of true stress vs. true strain curves at each of the 5 zones of bimetallic weld joint (i.e. SS 304 LN, HAZ of SS 304 LN, Weld, HAZ of SA-508 Class 2, and SA-508 Class 2) is shown in Fig.5.13, which clearly demonstrate the variations in mechanical behavior in these zones.

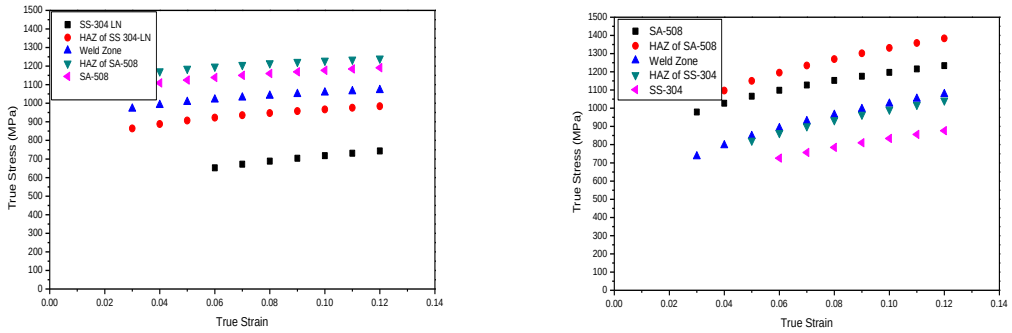

Fig. 5.13: Comparison of True Stress vs. True Strain curves at 5 zones of Bimetallic weld Joint at loading rate 0.5 KN/min. (a) and 1.5 KN/min. (b)

5.1.4 Comparison of Results

The comparison of mean values and standard deviation values of all the ABI experiments at different cold working conditions are shown in Table 5.1and Table 5.2.

A. Comparison of Mechanical Properties at Different Zones of Bimetallic Weld Joint at 0.5 KN/Min. Loading Rate

Table 5.1: Comparison of mean and Standard Deviation values of ABI generated Mechanical Properties at different zones of bimetallic weld at 0.5 KN/min. loading rate

Position	**SS 304 Base (10)***		**SS 304 HAZ (2)***		**Weld (7)***		**SA 508 HAZ (2)***		**SA 508 Base (7)***	
Mechanical Properties	**Mean**	**SD**	**Mean**	**SD**	**Mean**	**SD**	**Mean**	**SD**	**Mean**	**SD**
Strength Coefficient (MPa)	1064	82.23	1243	63.64	1166.5	79.01	1296	126.5	1453.4	80.5
Strain Hardening Exponent	0.126	0.033	0.109	0.023	0.072	0.027	0.043	0.013	0.086	0.021
Yield Strength (MPa)	303.6	22.06	777.2	21.89	633.90	27.68	902.5	71.79	613.65	26.26
UTS (MPa)	726.1	59.79	875.2	0.358	902.27	37.21	1086.	60.01	1082.4	7.29

* Number in brackets shows total number of experiments carried out at respective zone.

B. Comparison of Mechanical Properties of Bimetallic Weld Joint at Different Zones at 1.5 KN/Min. Loading Rate

Table 5.2: Comparison of mean and Standard Deviation values of ABI generated Mechanical Properties at different zones of bimetallic weld at 1.5 KN/min. loading rate

Position	**SS 304 Base (10)***		**SS 304 HAZ (2)***		**Weld (7)***		**SA 508 HAZ (1)***		**SA 508 Base (7)***	
Mechanical Properties	**Mean**	**SD**	**Mean**	**SD**	**Mean**	**SD**	**Mean**	**SD**	**Mean**	**SD**
Strength Coefficient (MPa)	1499.8	148.6	1868	21.92	1784	166	2164	1	1804.5	149.1
Strain Hardening Exponent	0.269	0.029	0.266	.007	0.243	0.04	0.211	1	0.187	0.044
Yield Strength (MPa)	314.5	34.55	846.9	37.93	665.5	23.8	1086.1	1	603.65	23.39
UTS (MPa)	806.6	77.49	1007	21.23	992.7	47.1	1262.8	1	1096.3	15.07

5.1.5 Local Variation of YS & UTS along Bimetallic Weld Joint

Local variation of yield strength and ultimate tensile strength throughout the five regions of bimetallic weld joint at loading rate of 0.5 KN/min. is shown in Fig. 5.14 and Fig. 5.15.

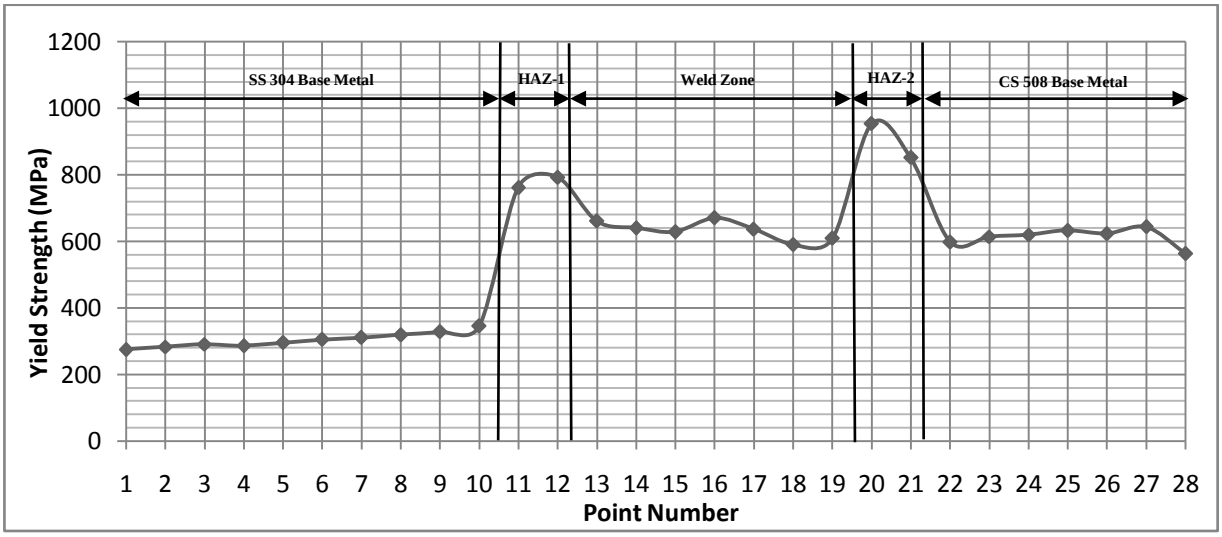

Fig.5.14: Variation of Yield Strength at different zones of Bimetallic weld Joint at 0.5 KN/min. loading rate

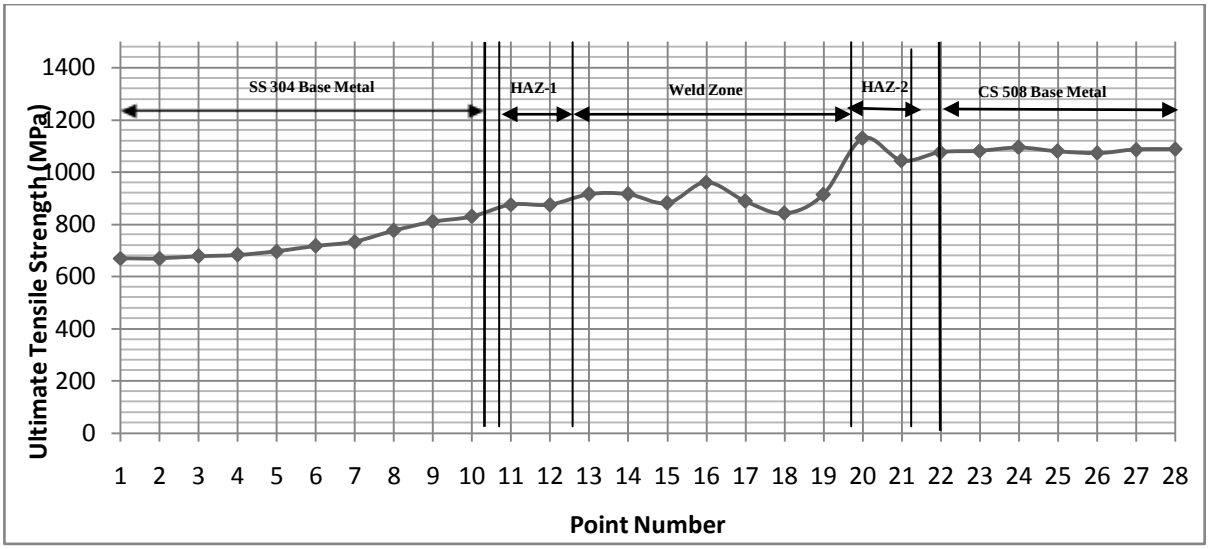

Fig.5.15: Variation of ABI generated Ultimate Tensile Strength at different zones of Bimetallic weld Joint at 0.5 KN/min. loading rate

Local variation of yield strength and ultimate tensile strength throughout the five regions of bimetallic weld joint at loading rate of 1.5 KN/min. is shown in Fig. 5.16 and Fig. 5.17.

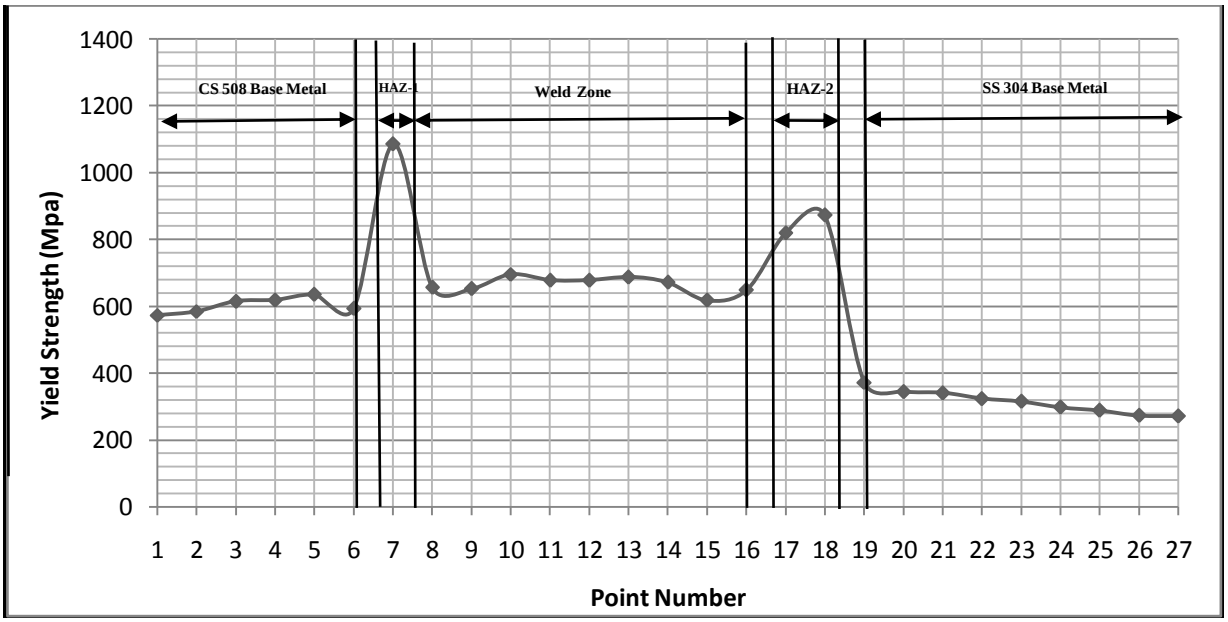

Fig. 5.16: Variation of Yield Strength at different zones of Bimetallic weld Joint at 1.5 KN/min. loading rate

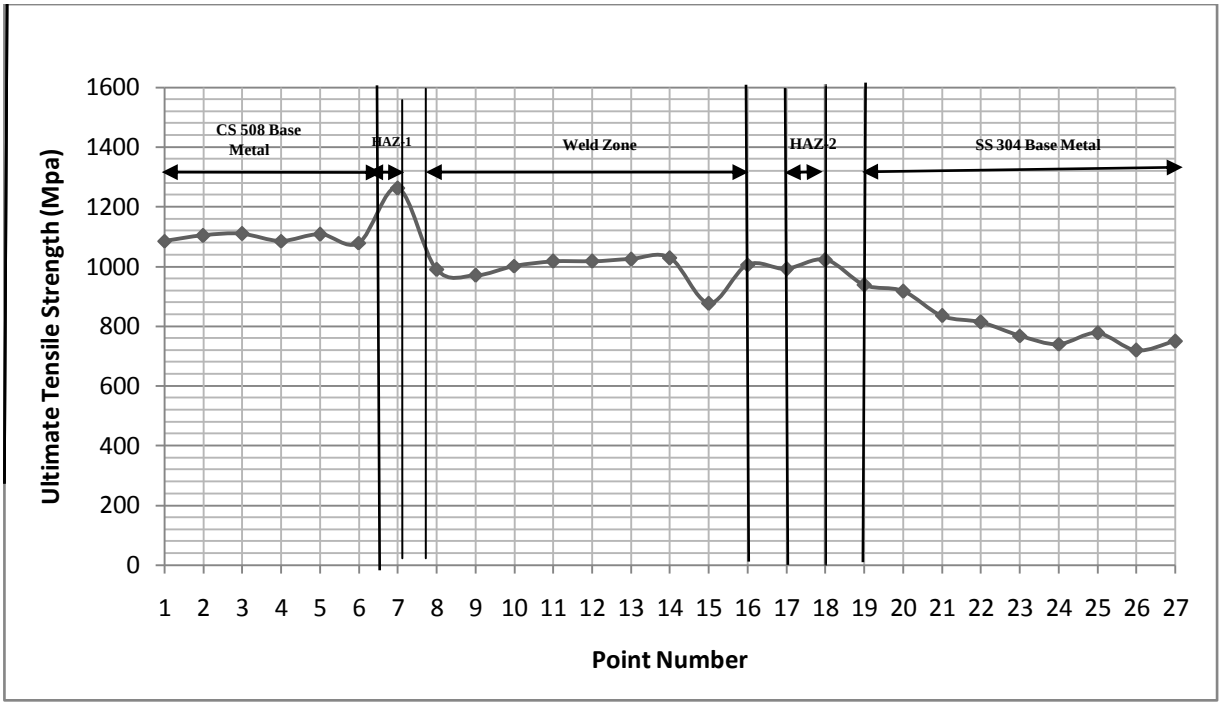

Fig. 5.17: Variation of ABI generated Ultimate Tensile Strength at different zones of Bimetallic weld Joint at 1.5 KN/min. loading rate

5.1.6 Validation through Finite Element Method (FEM) Simulation

FEM model was prepared in order to validate ABI experimental results. The FEM validation analysis was performed at each of 3 main zones of bimetallic weld joint. In order to perform the FEM analysis, power law was fitted on ABI derived True Stress vs. True Strain curve. And corresponding true stress and true strain values were took as input in the model. During its post processing phase, load vs. displacement curve were generated at each of 3 zones. The results found after FEM validation analysis at different zones are shown in Fig. 5.18 to Fig. 5.23.

FEM Validation at 0.5 KN/min rate

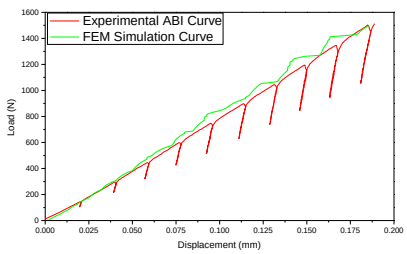

Fig. 5.18: FEM Validation of Load vs. Displacement Curves at SS 304 Base Metal

FEM Validation at 1.5 KN/min rate

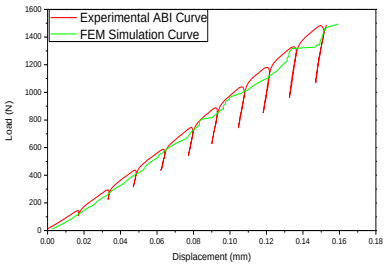

Fig. 5.19: FEM Validation of Load vs. Displacement Curves at SS 304 Base Metal

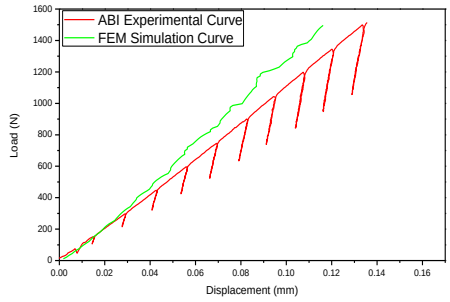

Fig. 5.20: FEM Validation of Load vs. Displacement Curves at weld Zone

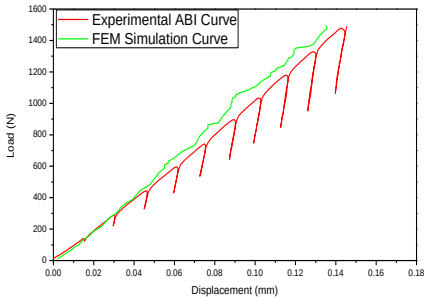

Fig. 5.21: FEM Validation of Load vs. Displacement Curves at weld Zone

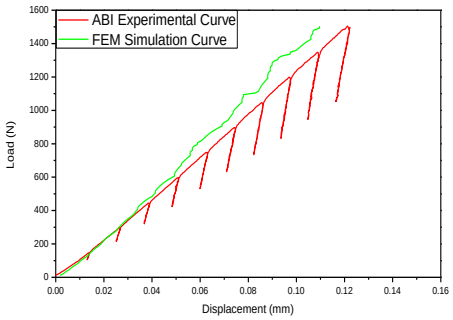

Fig. 5.22: FEM Validation of Load vs. Displacement Curves at SA 508 Base Metal

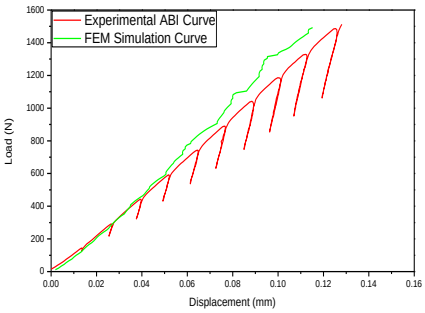

Fig. 5.23: FEM Validation of Load vs. Displacement Curves at SA 508 Base Metal

5.1.7 Discussion

The local variation of yield strength values and ultimate tensile strength values (as in Fig.5.14, Fig. 5.15, Fig. 5.16 and Fig. 5.17) shows the higher values at heat affected zone of SA 508 and of SS 304 regions in comparison to respective base metal zones. This sudden rise of yield strength values at both heat affected zones could be due to fine grain structure existed in their respective microstructure, which is due to recrystilization mechanism. A fine grain microstructure has higher number of grain boundaries as compared to a coarse grain microstructure. These grain boundaries have tendency to resist the motion of dislocations in the crystal structure.

Thus, a fine grain crystal structure has higher yield and ultimate tensile strength as compared to a coarse grain crystal structure. The recrystlization was not occurred on the base metal zones of both materials (SS 304 and SA 508). Due to this reason, coarse grain microstructures could exist on these zones. Thus, the base metal zones have lesser yield strength and ultimate tensile strength properties in comparison to respective heat affected zones.

5.2 Characterization of Similar Weld Joint through ABI Methodology

5.2.1 Reproducibility in ABI Load vs. Displacement Curve

In order to characterize the mechanical behavior variation in similar weld joint, ABI experiments were performed at different points of 3 main zones of similar weld joint (i.e. SS 304 LN Base Metal, Weld, and HAZ). Out of these experiments, the reproducibility in load vs. displacement curves on respective zones is shown in Fig 5.24, Fig. 5.25, and Fig. 5.26.

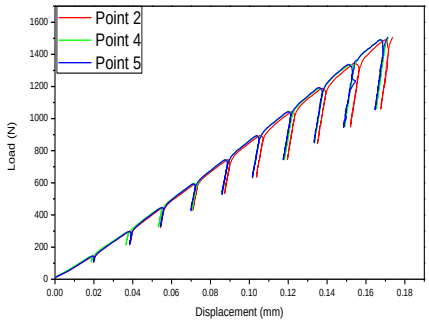

Fig. 5.24: Reproducibility of Load vs. Displacement Curves in weld zone

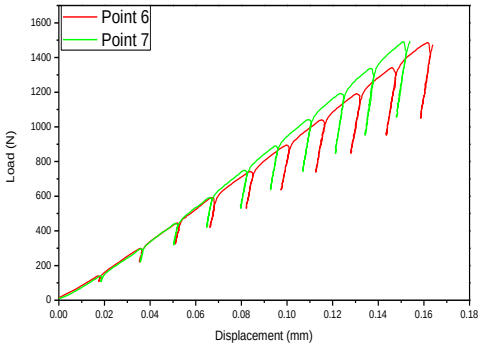

Fig. 5.25: Reproducibility of Load vs. Displacement Curves in HAZ (no reproducibility found)

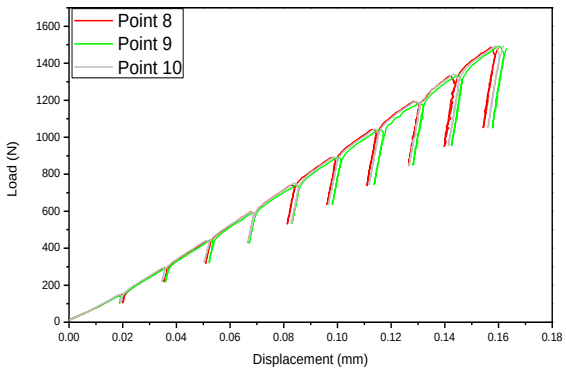

Fig. 5.26: Reproducibility of Load vs. Displacement Curves in base metal zone

5.2.2 Comparison of Different zones of Similar Weld Joint

A. Comparison of Load vs. Displacement Curves

The comparison of load vs. displacement curves at each of the 3 zones of similar weld joint (i.e. SS 304 LN, HAZ of SS 304 LN and Weld) is shown in Fig. 5.27, which clearly demonstrate the variations in load vs. displacement behavior in these zones.

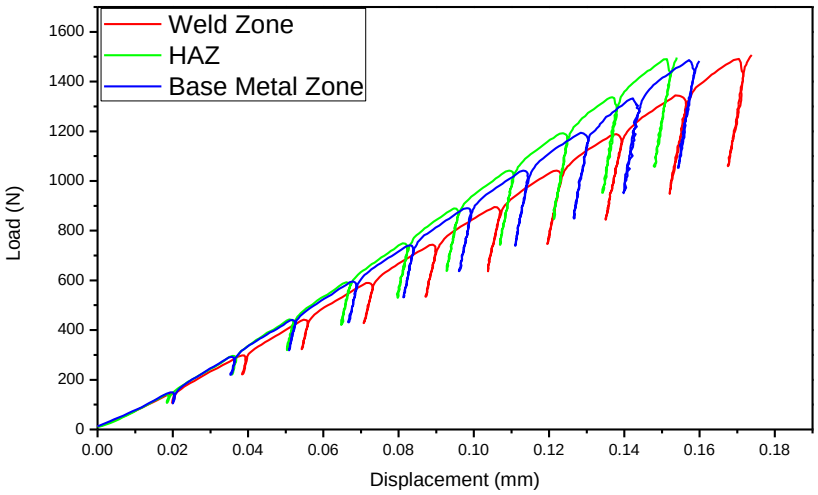

Fig. 5.27: Comparison of Load vs. Displacement curves at 3 zones of similar weld joint

B. Comparison of True Stress vs. True Strain Curves

The comparison of true stress vs. true strain curves at each of the 3 zones of similar weld joint (i.e. SS 304 LN, HAZ of SS 304 LN and Weld) is shown in Fig. 5.28, which clearly demonstrate the variations in mechanical behavior in these zones.

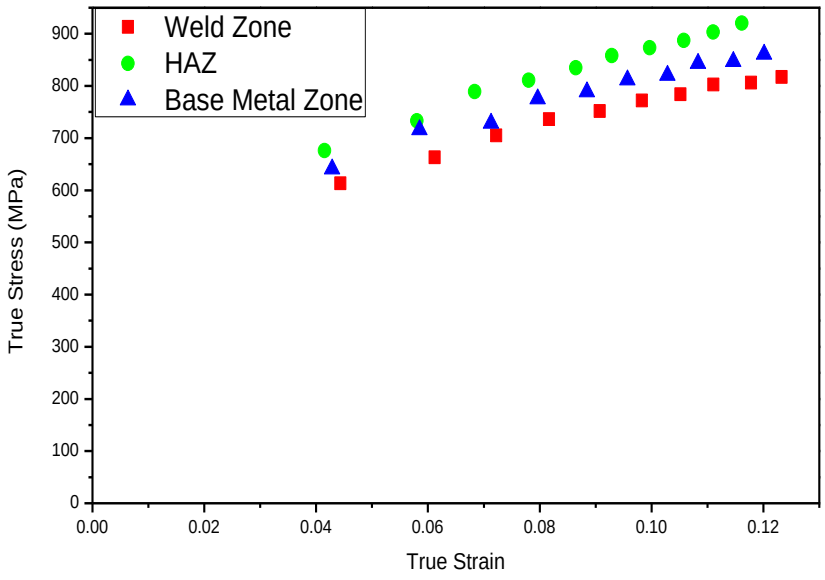

Fig. 5.28: Comparison of True Stress vs. True Strain curves at 3 zones of similar weld joint

5.2.3 Comparison of Results

The comparison of mean values and standard deviation values of all the ABI experiments at three zones of similar weld joint is shown in Table 5.3.

Table 5.3: Comparison of mean and Standard Deviation values of ABI generated Mechanical Properties at three zones of similar weld joint

Position	**SS 304 Weld (5)***		**SS 304 HAZ (2)***		**SS 304 Base (4)***	
Mechanical Properties	**Mean**	**SD**	**Mean**	**SD**	**Mean**	**SD**
Strength Coefficient (MPa)	1455.4	54.06	1529	306.8	1591.7	141.8
Strain Hardening Exponent	0.266	0.028	0.248	0.072	0.28	0.038
Yield Strength (MPa)	556.8	15.46	747.1	68.98	338.0	6.50
UTS (MPa)	785.08	9.68	843.0	85.2	842.7	35.34

5.2.4 Local Variation of ABI generated YS & UTS along Similar Weld Joint

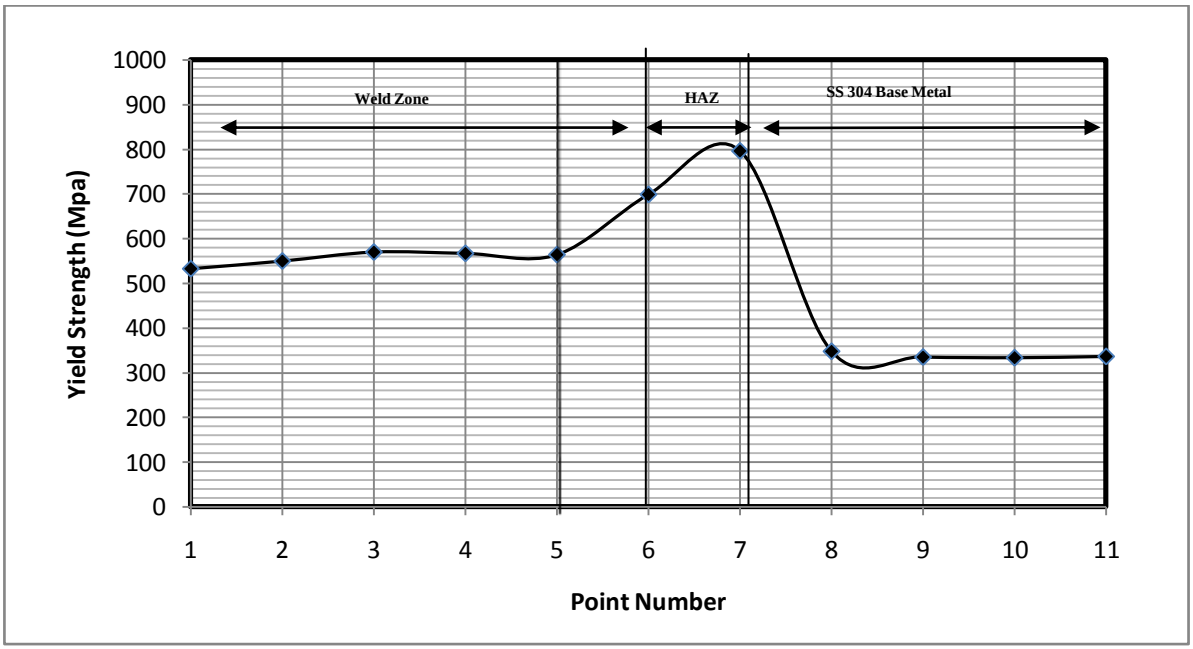

Fig. 5.29: Variation of Yield Strength at three zones of similar weld joint

* Number in brackets shows total number of experiments carried out at respective zone.

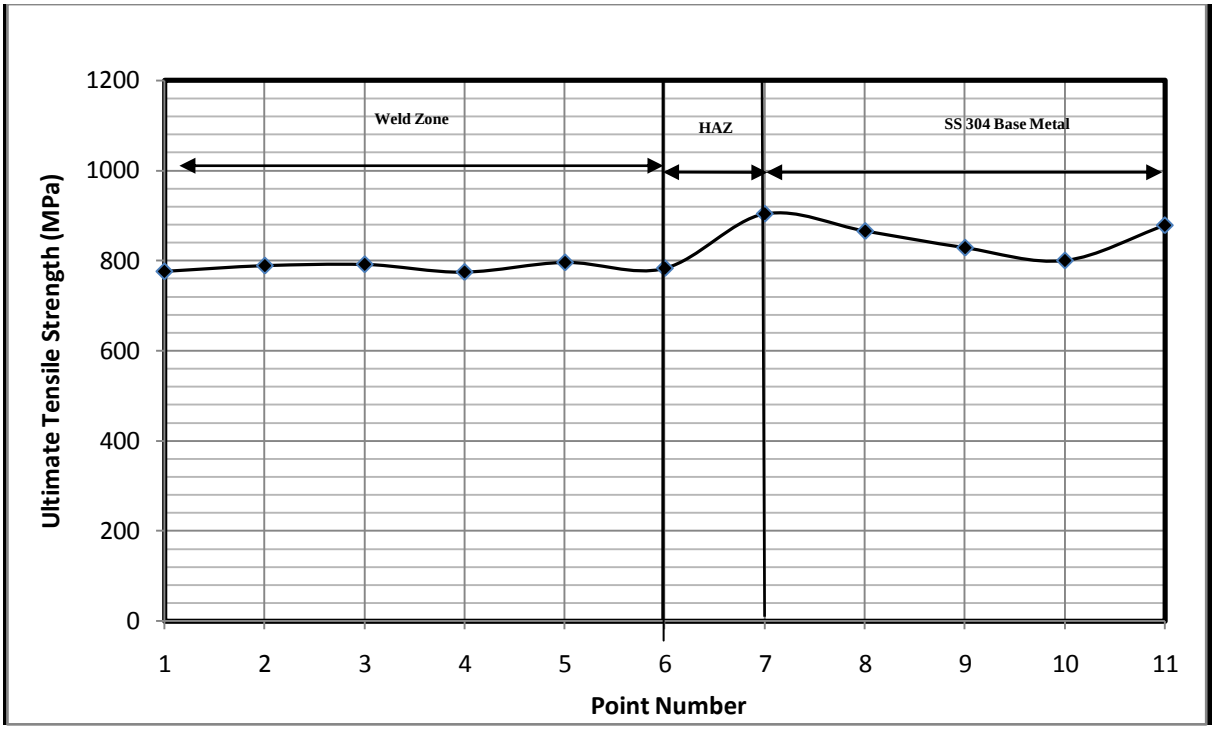

Fig. 5.30: Variation of ABI generated Ultimate Tensile Strength at different zones of similar weld joint

5.2.5 Validation through Finite Element Method (FEM) Simulation

FEM model was prepared in order to validate ABI experimental results. The FEM validation analysis was performed at each of 3 main zones of similar weld joint. In order to perform the FEM analysis, power law was fitted on ABI derived True Stress vs. True Strain curve. And corresponding true stress and true strain values were took as input in the model. During its post processing phase, load vs. displacement curve were generated at each of 3 zones. The results found after FEM validation analysis at different zones are shown in Fig. 5.31, Fig.5.32, and Fig.5.33.

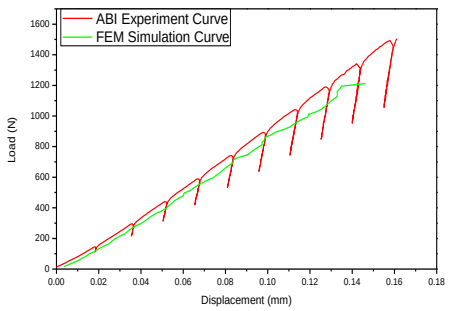

Fig. 5.31: FEM Validation of Load vs. Displacement Curves at base metal zone

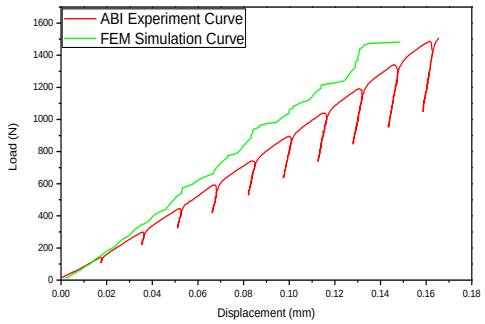

Fig. 5.32: FEM Validation of Load vs. Displacement Curves at HAZ

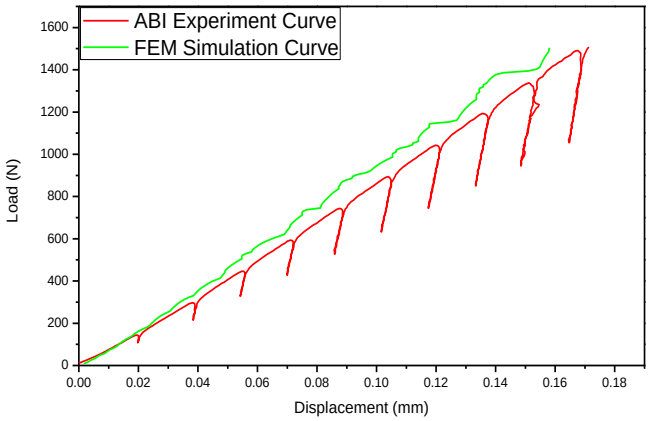

Fig. 5.33: FEM Validation of Load vs. Displacement Curves at weld zone

5.2.6 Discussion

During the characterization of similar weld joint using ABI approach, experimental results showed that the yield strength and ultimate tensile strength at heat affected zone of similar welded pipe was higher in comparison to base metal region, i.e. SS 304 region (Fig. 5.29 and Fig. 5.30). This rise in mechanical properties could be due to the finer grain microstructure exsisted in heat affected zone as compared to the microstructure of base metal zone. The fine grain microstructure is generated due to recrystilization at heat affected zone.

5.3. Mechanical Behavior Characterization of SA-508 Steel at Different Cold Working Conditions through ABI Methodology

5.3.1 Reproducibility in ABI Load vs. Displacement Curve

In order to predict the mechanical behavior of SA 508 at 0, 8, 10, 12, 14, and 15 % cold working conditions, ABI experiments were performed on respective specimens. The reproducibility of load vs. displacement curves in these ABI experiments at 0, 10, and 20% CW levels are shown in Fig. 5.34 to Fig. 5.39

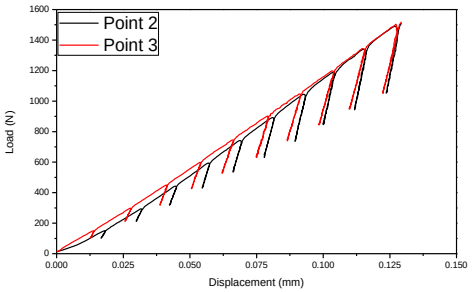

Fig. 5.34: Reproducibility of Load vs. Displacement Curves in 0% CW level

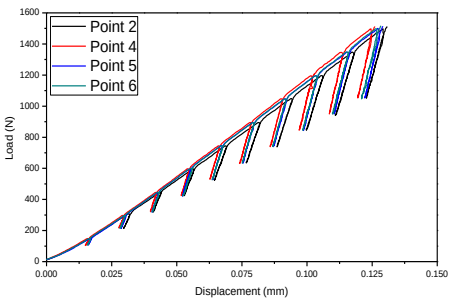

Fig. 5.35: Reproducibility of Load vs. Displacement Curves in 8% CW Level

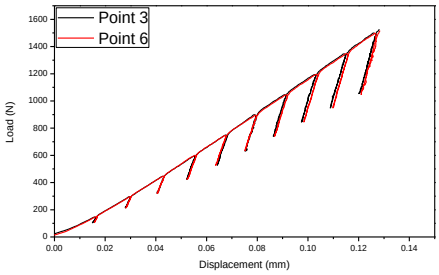

Fig. 5.36: Reproducibility of Load vs. Displacement Curves in 10% CW Level

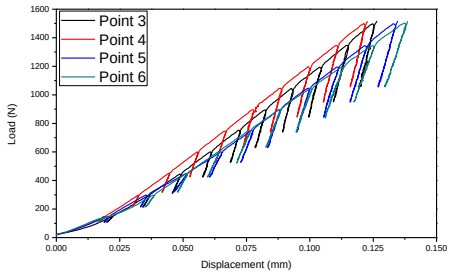

Fig. 5.37: Reproducibility of Load vs. Displacement Curves in 12% CW Level

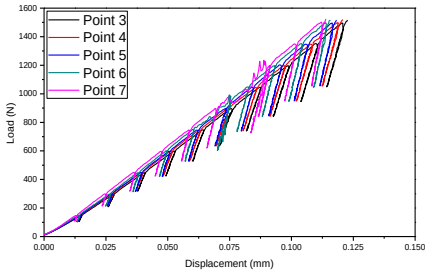

Fig. 5.38: Reproducibility of Load vs. Displacement Curves in 14% CW Level

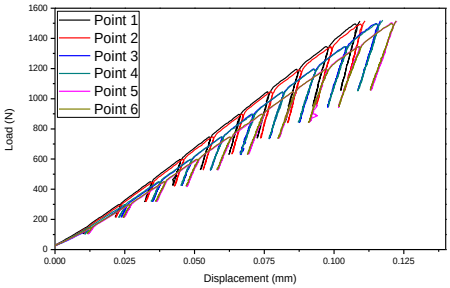

Fig. 5.39: Reproducibility of Load vs. Displacement Curves in 15% CW Level

5.3.2 Comparison of Different Cold working Conditions

A. Comparison of Load vs. Displacement Curves

The comparison of load vs. displacement curves at each of the 6 CW conditions is shown in Fig.5.40, which clearly demonstrate the change in slopes of ABI load vs. displacement curves corresponding to change in cold working levels.

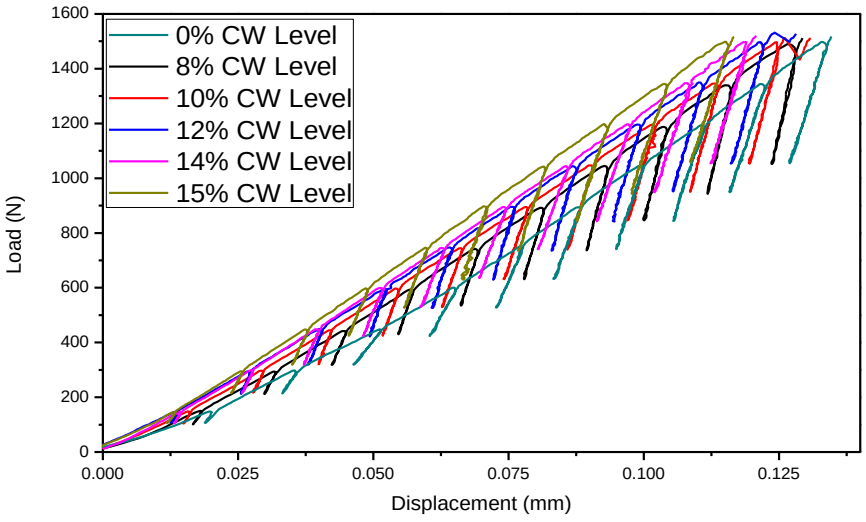

Fig. 5.40: Comparison of Load vs. Displacement curves at 6 CW Levels

B. Comparison of True Stress vs. True Strain Curves

The comparison of ABI generated true stress vs. true strain curves at 0, 8, 10, 12, 14 and 15% CW conditions is shown in Fig.5.11, which clearly demonstrate the change in slopes of ABI generated true stress vs. true strain curves corresponding to change in cold working levels.

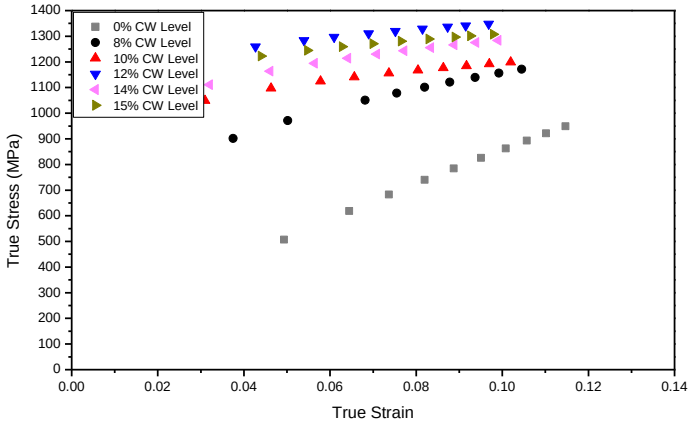

Fig. 5.41: Comparison of True Stress vs. True Strain curves at 6 CW Levels

5.3.3 Comparison of Results

The comparison of mean values and standard deviation values of all the ABI experiments at different cold working conditions are shown in Table 5.4.

Table 5.4: Comparison of mean and Standard Deviation values of ABI generated Mechanical Properties at different cold working levels

Level of Cold Work	**0% CW (3)***		**8% CW (6)***		**10% CW (6)***		**12% CW (6)***		**14% CW (7)***		**15% CW (6)***	
Mechanical Properties	**Mean**	**SD**	**Mean**	**SD**	**Mean**	**SD**	**Mean**	**SD**	**Mean**	**SD**	**Mean**	**SD**
Strength Coefficient (MPa)	1561	360.6	1752	117.4	1821	201.3	1826	182.9	1859	11.4	1914	207.2
Strain Hardening Exponent	0.26	0.012	0.21	0.109	0.198	0.050	0.19	0.118	0.192	0.06	0.191	0.09
Yield Strength (MPa)	310	164.9	475.1	20.14	532	42.1	536	82.5	563.7	27.3	584	30.01
UTS (MPa)	848.6	8.46	1076	75.4	1078	43.4	1054	10.9	1089.8	65.9	1093	55.6

*Numbers in brackets shows the number of experiments conducted on CW levels.

5.3.4 Validation through Finite Element Method (FEM) Simulation

FEM model was prepared in order to validate ABI experimental results. The FEM validation analysis was performed at each of 6 cold working levels. In order to perform the FEM analysis, power law was fitted on ABI derived True Stress vs. True Strain curve. Corresponding true stress and true strain values were took as input in the model. During its post processing phase, load vs. displacement curve were generated at each CW level. The results found after FEM validation analysis at different CW levels are shown in Fig. 5.42 to Fig. 5.47.

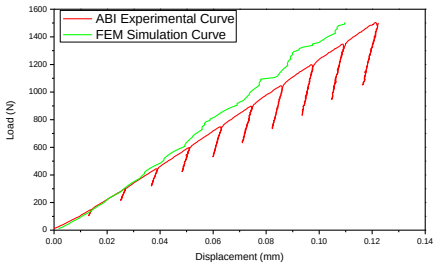

Fig. 5.42: FEM Validation of Load vs. Displacement Curves at 0% CW Condition

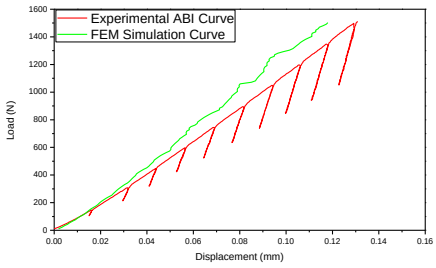

Fig.5.43: FEM Validation of Load vs. Displacement Curves at 8% CW Condition

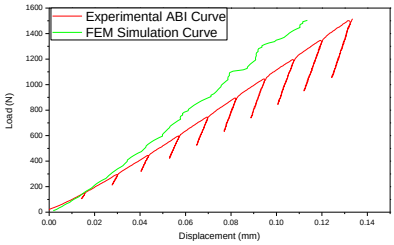

Fig. 5.44: FEM Validation of Load vs. Displacement Curves at 10% CW Condition

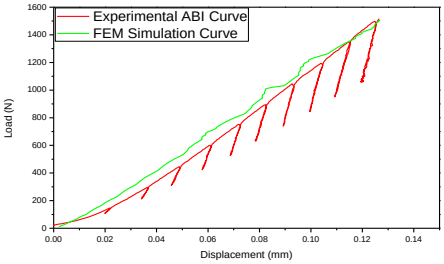

Fig.5.45: FEM Validation of Load vs. Displacement Curves at 12% CW Condition

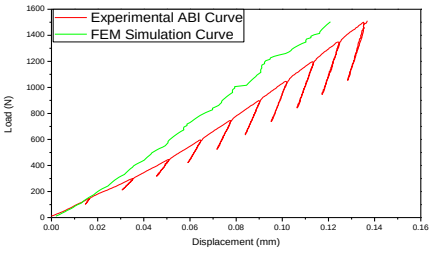

Fig. 5.46: FEM Validation of Load vs. Displacement Curves at 14% CW Condition

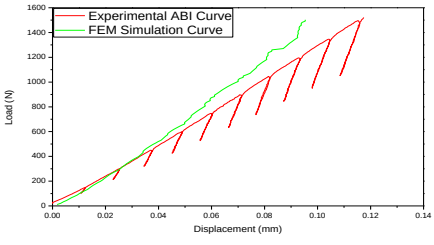

Fig.5.47: FEM Validation of Load vs. Displacement Curves at 15% CW Condition

5.3.5 Discussion

During characterization of mechanical properties of reactor pressure vessel steel (SA 508) at different cold worked conditions, it was found that yield strength, ultimate tensile strength and strength coefficient values was increasing with cold working levels (Table 5.4). This is due to the fact that during cold working, fine grain microstructure is generated in the material. More over due to the distortion of lattice structure, (which was caused due to cold work treatment), the strain accumulates in the material. This strain field causes resistance to further plastic deformation of material. Thus hardness, yield strength and ultimate tensile strength of material increase with cold working levels.

5.4 Mechanical Behavior Characterization of SS 304-LN Steel at Different Cold Working Conditions through ABI Methodology

5.4.1Reproducibility in ABI Load vs. Displacement Curve

In order to predict the mechanical behavior of SS 304 LN at 0, 10, and 20% CW conditions, ABI experiments were performed on points on respective specimens. The reproducibility of load vs. displacement curves in these ABI experiments at 0, 10, and 20% CW levels are shown in Fig. 5.48, Fig. 5.49, and Fig. 5.50.

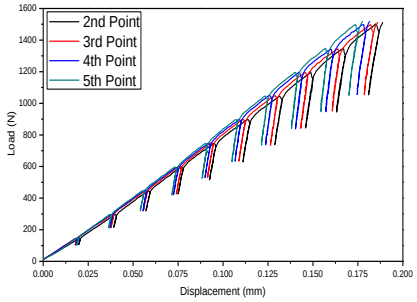

Fig. 5.48: Reproducibility of Load vs. Displacement Curves in 0% CW condition

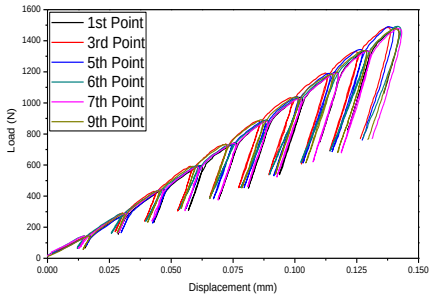

Fig. 5.49: Reproducibility of Load vs. Displacement Curves in 10% CW condition

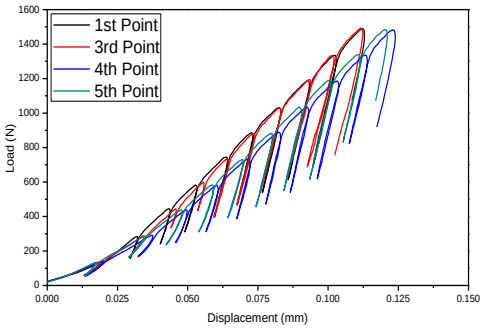

Fig. 5.50: Reproducibility of Load vs. Displacement Curves in 20% CW condition

5.4.2 Comparison of 0, 10, and 20% Cold working Conditions

A. Comparison of Load vs. Displacement Curves

The comparison of load vs. displacement curves at each of the 3 CW conditions is shown in Fig.5.51, which clearly demonstrate the change in slopes of ABI load vs. displacement curves corresponding to change in cold working levels.

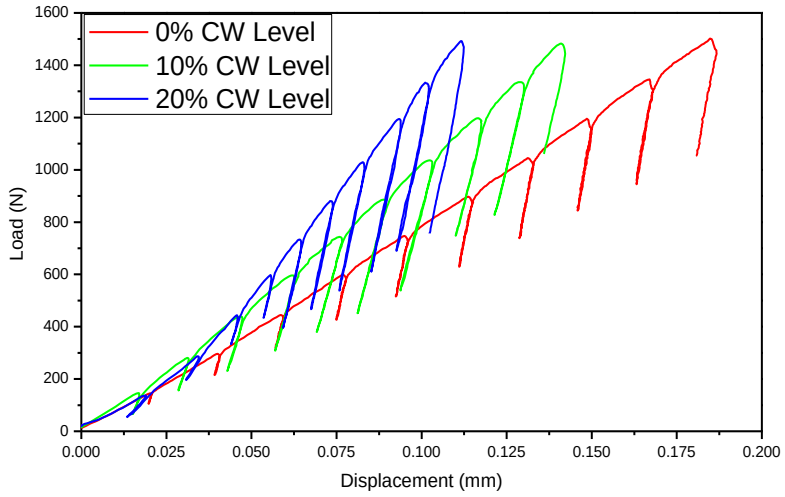

Fig. 5.51: Comparison of Load vs. Displacement curves at 3 CW Levels

B. Comparison of True Stress vs. True Strain Curves

The comparison of ABI generated true stress vs. true strain curves at 0, 10, and 20% CW conditions is shown in Fig.5.52, which clearly demonstrate the change in slopes of ABI generated true stress vs. true strain curves corresponding to change in cold working levels.

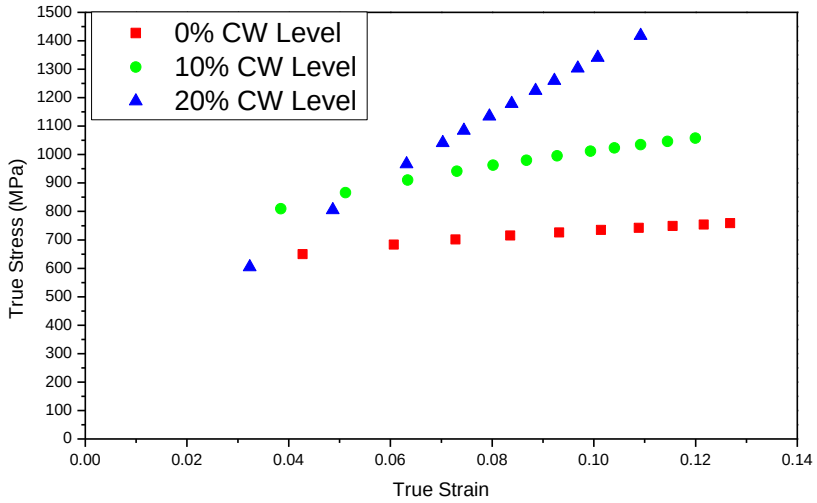

Fig. 5.52: Comparison of True Stress vs. True Strain curves at 3 CW Levels

5.4.3 Comparison of Results

The comparison of mean values and standard deviation values of all the ABI experiments at different cold working conditions are shown in Table 5.5.

Table 5.5: Comparison of mean and Standard Deviation values of ABI generated Mechanical Properties at different cold working levels

Level of Cold Work	**0% CW (5)***		**10% CW (8)***		**20% CW (5)***	
Mechanical Properties	**Mean**	**SD**	**Mean**	**SD**	**Mean**	**SD**
Strength Coefficient (MPa)	1015.96	60.49	1625.75	126.82	1995	197.30
Strain Hardening Exponent	0.221	0.037	0.20	0.048	0.179	0.139
Yield Strength (MPa)	285.95	7.79	783.77	6.42	1096.57	56.12
UTS (MPa)	567.018	10.98	965.3	38.34	1226.6	152.65

5.4.4 Validation through Finite Element Method (FEM) Simulation

FEM model was prepared in order to validate ABI experimental results. The FEM validation analysis was performed at each of 3 cold working levels. In order to perform the FEM analysis, power law was fitted on ABI derived True Stress vs. True Strain curve. And corresponding true stress and true strain values were took as input in the model. During its post processing phase, load vs. displacement curve were generated at each of 3 CW levels. The results found after FEM validation analysis at different CW levels are shown in Fig. 5.53, Fig. 5.54, and Fig. 5.55.

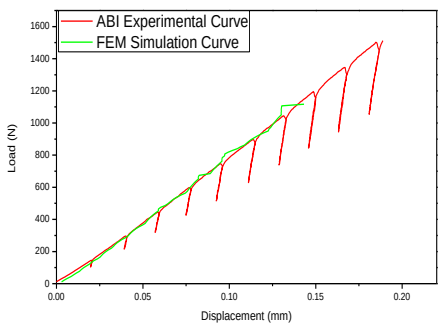

Fig. 5.53: FEM Validation of Load vs. Displacement Curves at 0% CW Condition

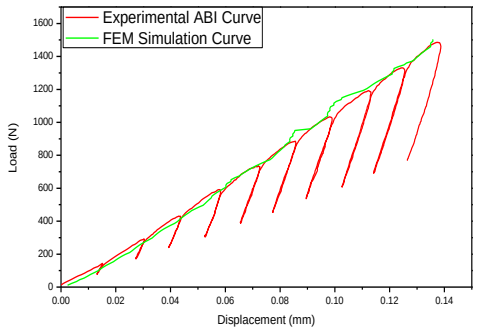

Fig. 5.54: FEM Validation of Load vs. Displacement Curves at 10% CW Condition

* Number in brackets shows total number of experiments carried out at respective stage.

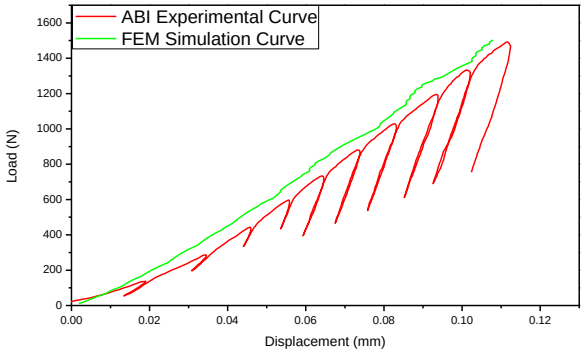

Fig. 5.55: FEM Validation of Load vs. Displacement Curves at 20% CW Condition

5.4.5 Discussion

Table 5.5, shows the increasing nature of yield strength, ultimate tensile strength and strength coefficient with increase in cold working levels. This is due to the fact that during cold working fine grain microstructure forms. Due to this microstructure, number of grain boundaries in the crystal structure increases. These grain boundaries cause resistance to further plastic deformation of material. Thus yield strength, ultimate tensile strength and strength coefficient with increase in cold working levels. More over accumulated strain caused due to cold working treatment in the crystal structure is another reason of increase in these mechanical properties.

5.5 Characterization of Zr-2.5-Nb alloy under Different Environmental Conditions

5.5.1Reproducibility in ABI Load vs. Displacement Curve

In order to predict the mechanical behavior of Zr 2.5 Nb at different working conditions (A, B, C, D, E, and, F) ABI experiments were performed on these specimens. The reproducibility of load vs. displacement curves in these ABI experiments at these levels are shown in Fig. 5.56 to Fig.5.61.

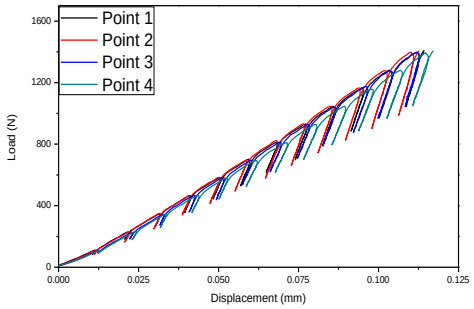

Fig. 5.56: Reproducibility of Load vs. Displacement Curves in A condition

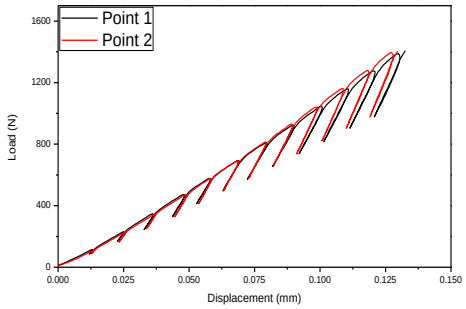

Fig. 5.57: Reproducibility of Load vs. Displacement Curves in B condition

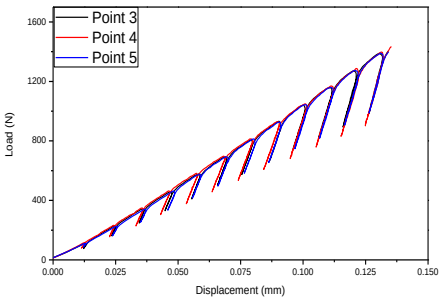

Fig. 5.58: Reproducibility of Load vs. Displacement Curves in C condition

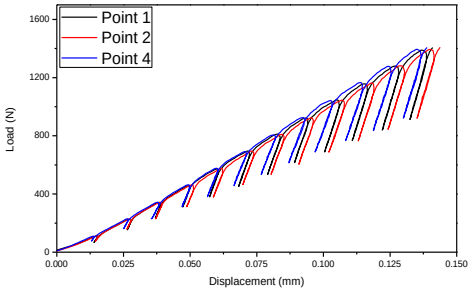

Fig. 5.59: Reproducibility of Load vs. Displacement Curves in D condition

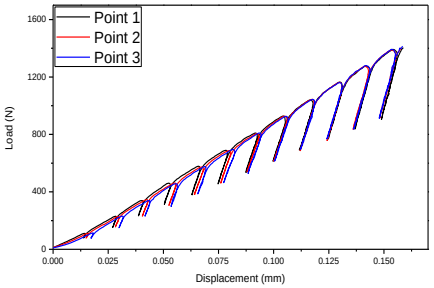

Fig. 5.60: Reproducibility of Load vs. Displacement Curves in E Condition

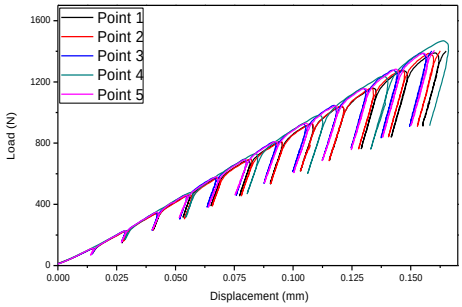

Fig. 5.61: Reproducibility of Load vs. Displacement Curves in F Condition

5.5.2 Comparison of Different Working Conditions

A. Comparison of Load vs. Displacement Curves

The comparison of load vs. displacement curves at each of the 6 conditions is shown in Fig.5.62, which clearly demonstrate the change in slopes of ABI load vs. displacement curves corresponding to change in working conditions.

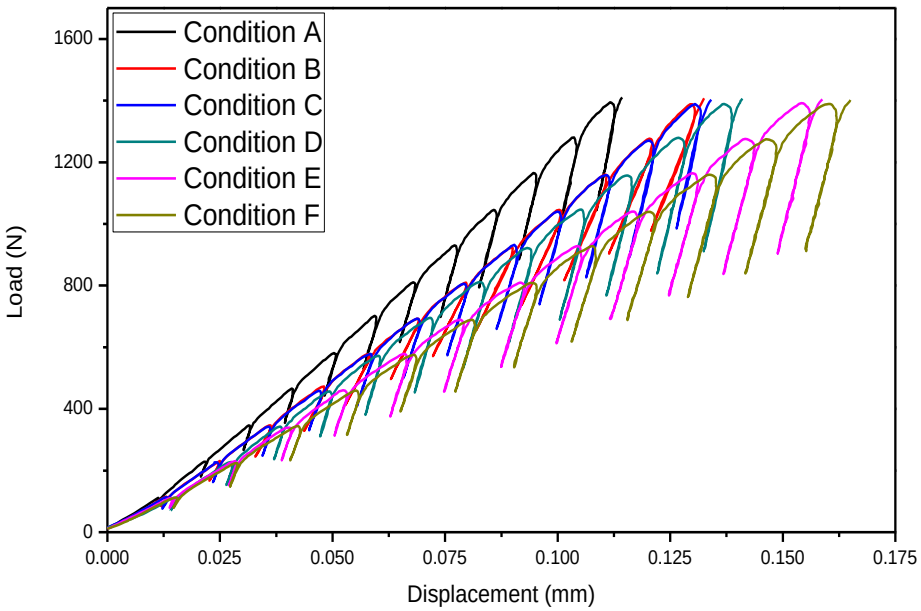

Fig. 5.62: Comparison of Load vs. Displacement curves at 6 working conditions

B. Comparison of True Stress vs. True Strain Curves

The comparison of ABI generated true stress vs. true strain curves at different conditions is shown in Fig.5.63, which clearly demonstrate the change in slopes of ABI generated true stress vs. true strain curves corresponding to change in working conditions.

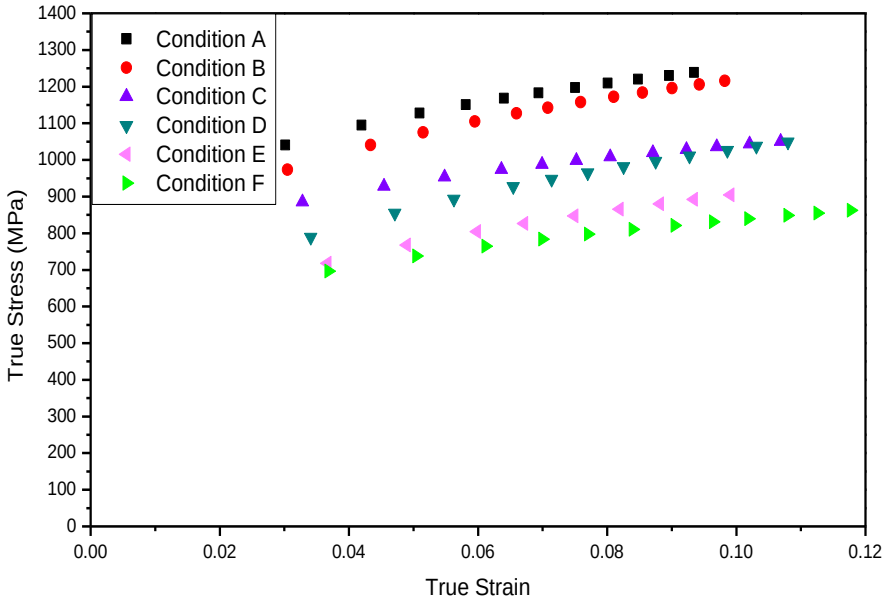

Fig. 5.63: Comparison of True Stress vs. True Strain curves at 6 working conditions

5.5.6 Comparison of Results

The comparison of mean values and standard deviation values of all the ABI experiments at different environmental conditions are shown in Table 5.6.

Table 5.6: Comparison of mean and Standard Deviation values of ABI generated Mechanical Properties at different environment conditions

Working Conditions	**Condition A (4)***		**Condition B (5)***		**Condition C (5)***		**Condition D (4)***		**Condition E (5)***		**Condition F (5)***	
Mechanical Properties	**Mean**	**SD**	**Mean**	**SD**	**Mean**	**SD**	**Mean**	**SD**	**Mean**	**SD**	**Mean**	**SD**
Strength Coefficient (MPa)	2209.3	640.8	1690	200.1	1612	227.5	1544	222.3	1488	283.2	1269.6	47.52
Strain Hardening Exponent	0.127	0.124	0.180	0.048	0.230	0.079	0.235	0.047	0.239	0.081	0.261	0.018
Yield Strength (MPa)	802.97	29.00	678.9	5.59	634.6	17.30	633.36	32.04	561.5	25.23	534.86	13.25
UTS (MPa)	1245.1	143.1	1103	38.34	953.3	13.11	943.17	68.85	868.9	63.34	784.59	14.82

* Number in brackets shows total number of experiments carried out at respective condition.

5.5.7 Validation through Finite Element Method (FEM) Simulation

FEM model was prepared in order to validate ABI experimental results. The FEM validation analysis was performed at each of 6 working conditions. In order to perform the FEM analysis, power law was fitted on ABI derived strength coefficient and strain hardening exponent values, and corresponding True Stress vs. True Strain curve has been inputted in the model. During its post processing phase, load vs. displacement curve were generated at each of 6 working conditions. The results found after FEM validation analysis at different working conditions are shown in Fig. 5.64 to Fig 5.69.

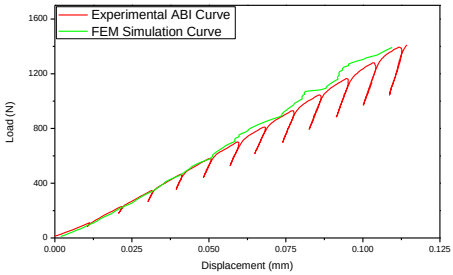

Fig. 5.64: FEM Validation of Load vs. Displacement Curves at A Condition

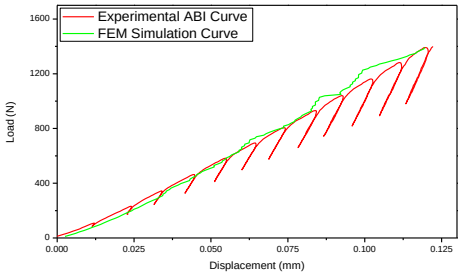

Fig.5.65: FEM Validation of Load vs. Displacement Curves at B Condition

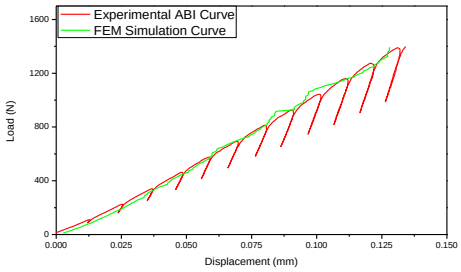

Fig. 5.66: FEM Validation of Load vs. Displacement Curves at C Condition

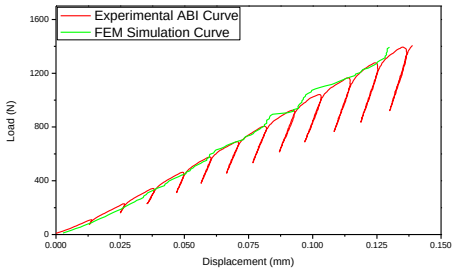

Fig. 5.67: FEM Validation of Load vs. Displacement Curves at D Condition

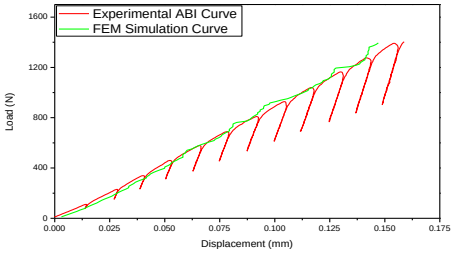

Fig. 5.68: FEM Validation of Load vs. Displacement Curves at E Condition

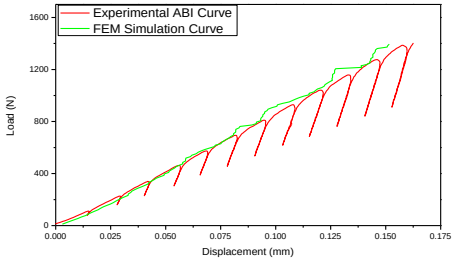

Fig. 5.69: FEM Validation of Load vs. Displacement Curves at F Condition

5.5.8 Discussion

During the comparison of results at different environmental conditions of pressure tube material Zr 2.5 Nb (Table 5.6), it was found that the highest yield strength, ultimate tensile strength, and strength coefficient properties is corresponding to annealing treatment at 550 ^{o}C temperature. It was observed that the elongated two-phase structure could be retained if the annealing temperature is kept 550^{o}C. Due to this reason annealing treatment at 550 ^{o}C shows higher mechanical properties as compared to other conditions.

CHAPTER 6

CONCLUSIONS

6.1. Characterization of Bimetallic Weld Joint using ABI Approach

After caring out the ABI experiments on the 5 zones of bimetallic weld joint (i.e. SS 304 LN, HAZ of SS 304 LN, Weld, HAZ of SA-508 Class 2, and SA-508 Class 2), following points are concluded:

i. The average yield strength at 5 zones of bimetallic weld joint (i.e. SS 304 LN, HAZ of SS 304 LN, Weld, HAZ of SA-508 Class 2, and SA-508 Class 2) corresponding to loading rate 0.5 KN/min. found to be 303.66 MPa, 777.24 MPa, 633.90MPa, 902.52MPa, & 613.65MPa and corresponding to loading rate 1.5 KN/min. found to be 314.49 MPa, 846.9 MPa, 665.55 MPa, 1086.1 MPa, and 603.65 MPa. The yield strength at each HAZ zone was found to be very higher than respective base metal zone. Thus, ABI methodology successfully predicts the variation in yield strength corresponding to change in zone in bimetallic weld joint. Moreover, ABI successfully predict the increase in yield strength at each zone corresponding to increase in loading rate.

ii. The average ultimate tensile strength at 5 zones of bimetallic weld joint (i.e. SS 304 LN, HAZ of SS 304 LN, Weld, HAZ of SA-508 Class 2, and SA-508 Class 2) corresponding to loading rate 0.5 KN/min. found to be 726.08 MPa, 875.25 MPa, 902.27 MPa, 1086.02 MPa, and 1082.44 MPa and corresponding to loading rate 1.5 KN/min. found to be 806.59 MPa, 1007.8 MPa, 992.65 MPa, 1262.8 MPa, & 1096.37 MPa. Thus ABI methodology successfully predicts the variation in yield strength corresponding to change in zone in bimetallic weld joint. Moreover, ABI successfully predict the increase in ultimate tensile strength at each zone corresponding to increase in loading rate.

iii. The average strength coefficient at 5 zones of bimetallic weld joint (i.e. SS 304 LN, HAZ of SS 304 LN, Weld, HAZ of SA-508 Class 2, and SA-508 Class 2) corresponding to loading rate 0.5 KN/min. found to be 1064.0 MPa, 1243 MPa, 1166.57 MPa, 1296.5 MPa, 1453.43MPa and corresponding to loading rate 1.5 KN/min. found to be 1499.88 MPa, 1868.5 MPa, 1784.44 MPa, 2164, & 1804.5 MPa. Thus ABI methodology successfully predicts the variation in Strength Coefficient corresponding to change in zone in bimetallic weld joint. Moreover, ABI successfully predict the increase in strength coefficient at each zone corresponding to increase in loading rate.

iv. The average strain hardening exponent at 5 zones of bimetallic weld joint (i.e. SS 304 LN, HAZ of SS 304 LN, Weld, HAZ of SA-508 Class 2, and SA-508 Class 2) corresponding to loading rate 0.5 KN/min. found to be 0.126, 0.109, 0.072, 0.043, 0.086 and corresponding to loading rate 1.5 KN/min. found to be 0.269, 0.266, 0.243, 0.211 & 0.187. Thus ABI methodology successfully predicts the variation in strain hardening exponent corresponding to change in zone in bimetallic weld joint. Moreover, ABI successfully predict the increase in strain hardening exponent at each zone corresponding to increase in loading rate.

v. Fig. 5.14, Fig. 5.15, Fig. 5.16, and Fig. 5.17 show that ABI methodology successfully characterizes the local variation in mechanical properties (yield strength and ultimate tensile strength) at each of 5 zones in bimetallic weld joint in both loading rates.

vi. The load vs. displacement results of FEM model simulation in ANSYS software was also found to be close with that of ABI load vs. displacement curves at 3 main zones of bimetallic weld joint (SS 304 LN, Weld and SA-508 Class 2) during validation examination of ABI generated experimental results.

Thus, it is concluded that ABI methodology successfully characterized the variation in the mechanical properties from zone to zone (global gradient), and from point to point in each zone (local gradient) of bimetallic weld joint (weld joint of SA 508-Class 2 nuclear reactor pressure vessel nozzle with SS 304 LN pipeline using an Inconel weld).

6.2 Characterization of Similar Weld Joint using ABI Approach

After caring out the ABI experiments on 3 zones (i.e. Base Metal, HAZ of Base Metal, and weld), following points are concluded:

i. The average values of Yield Strength at 3 zones (i.e. Base Metal, HAZ of Base Metal, and weld) were found to be 338 MPa, 747.1 MPa, and 556.8 MPa. The yield strength at each HAZ zone was found to be very higher than respective base metal zone. Thus ABI methodology successfully predicts the variation in yield strength corresponding to change in zone in similar weld joint.

ii. The average values of Ultimate Tensile Strength at 3 zones (i.e. Base Metal, HAZ of Base Metal, and weld) were found to be 842.7 MPa, 843 MPa, and 785.08 MPa. Thus ABI methodology successfully predicts the variation in ultimate tensile strength corresponding to change in zone in similar weld joint.

iii. The average values of strength coefficient at 3 zones (i.e. Base Metal, HAZ of Base Metal, and weld) were found to be 1591.7 MPa, 1529 MPa, and1455.4 MPa. Thus ABI methodology successfully predicts the variation in strength coefficient corresponding to change in zone in similar weld joint.

iv. The average values of strain hardening exponent at 3 zones (i.e. Base Metal, HAZ of Base Metal, and weld) were found to be 0.28, 0.248, and 0.266. Thus ABI methodology successfully predicts the variation in strain hardening exponent corresponding to change in zone in similar weld joint.

v. Fig. 5.29 and Fig. 5.30 show that ABI methodology successfully characterizes the local variation in mechanical properties (yield strength and ultimate tensile strength) at each of 5 zones in bimetallic weld joint in both loading rates.

vi. The load vs. displacement results of FEM model simulation in ANSYS software was also found to be close with that of ABI load vs. displacement curves at 3 main zones of similar weld joint during validation examination of ABI generated experimental results.

Thus, it is concluded that ABI methodology successfully characterized the variation in the mechanical properties from zone to zone, and from point to point in each zone of similar weld joint (weld joint of two SS 304 LN pipelines).

6.3 Mechanical Behavior Characterization of SA 508 Steel at Different Cold Working Conditions using ABI Approach

After caring out the ABI experiments on the specimens of SA 508 Class 2 material at different cold working levels (0, 8, 10, 12, 14, & 15%), following points are concluded:

i. The average yield strength of specimens was found to be 310 MPa, 475.1 MPa, 532 MPa, 536.8 MPa, 563.74 MPa, & 584 MPa at 0, 8, 10, 12, 14, & 15% cold working levels respectively. Thus ABI methodology successfully predicts the increasing nature of yield strength with increase in the cold working level.

ii. The average ultimate tensile strength of specimens was found to be 848.6 MPa, 1076 MPa, 1078 MPa,1054 MPa, 1089.8 MPa, & 1093 MPa at 0, 8, 10, 12, 14, & 15% cold working levels respectively. Thus ABI methodology successfully predicts the increasing nature of ultimate tensile strength with increase in the cold working level.

iii. The average strength coefficient of specimens was found to be 1561 MPa, 1752 MPa, 1821 MPa, 1826 MPa, 1859 MPa, & 1914 MPa at 0, 8, 10, 12, 14, & 15% cold working levels

respectively. Thus ABI methodology successfully predicts the increasing nature of strength coefficient with increase in the cold working level.

iv. The average strain hardening exponent of specimens was found to be 0.26, 0.21, 0.198, 0.197, 0.192, & 0.191 at 0, 8, 10, 12, 14, & 15% cold working levels respectively. Thus ABI methodology successfully predicts the increasing nature of strain hardening exponent with increase in the cold working level.

v. The load vs. displacement results of FEM simulation in ANSYS software was found to be close (only in some cases) with that of ABI load vs. displacement curves at 6 cold working levels (0, 8, 10, 12, 14, & 15%) during reverse checking of ABI generated experimental results.

Thus from above discussion, it is concluded that ABI methodology successfully predicted the effects of cold working on the mechanical properties of SA 508 Class 2 material.

6.4 Mechanical Behavior Characterization of SS 304-LN Steel at Different Cold Working Conditions using ABI Approach

After caring out the ABI experiments on the specimens of SS 304-LN material at different cold working levels (0, 10 and 20 %), following points are concluded:

i. The average yield strength of specimens was found to be 285.95 MPa, 783.77MPa, & 1096.57 MPa at 0, 10, 20 % cold working levels respectively. Thus ABI methodology successfully predicts the increasing nature of yield strength with increase in the cold working level.

ii. The average ultimate tensile strength of specimens was found to be 567.018 MPa, 965.3 MPa, & 1226.6 MPa at 0, 10, 20 % cold working levels respectively. Thus ABI methodology successfully predicts the increasing nature of ultimate tensile strength with increase in the cold working level.

iii. The average strength coefficient of specimens was found to be 1015.96 MPa, 1625.75 MPa, & 1995 MPa at 0, 10, 20 % cold working levels respectively. Thus ABI methodology successfully predicts the increasing nature of strength coefficient with increase in the cold working level.

iv. The average strain hardening exponent of specimens was found to be 0.221, 0.20, & 0.179 at 0, 10, 20 % cold working levels respectively. Thus ABI methodology successfully predicts the increasing nature of Strain Hardening Exponent with increase in the cold working level.

v. The load vs. displacement results of FEM simulation in ANSYS software was also found to be close with that of ABI load vs. displacement curves at 3 cold working levels (0%, 10%, and 20 %) during reverse checking of ABI generated experimental results.

Thus, it is concluded that ABI methodology successfully predicted the effects of cold working on the mechanical properties of SS 304-LN material.

6.5 Characterization of Zr-2.5-Nb alloy under Different Environmental Conditions using ABI Approach

After caring out the ABI experiments on the specimens of Zr 2.5 Nb material at different working conditions (A, B, C, D, E, and F) following points are concluded:

i. The average yield strength of specimens was found to be 802.97 MPa, 678.93 MPa, 634.62 MPa, 633.36 MPa, 561.51 MPa, and 534.86 MPa at A, B, C, D, E, and F working conditions respectively. Thus ABI methodology successfully predicts the decreasing nature of yield strength with corresponding change in working conditions.

ii. The average ultimate tensile strength of specimens was found to be 1245.05MPa, 1103.90 MPa, 953.33 MPa, 943.17 MPa, 868.99 MPa, and 784.59 MPa at A, B, C, D, E, and F working conditions respectively. Thus ABI methodology successfully predicts the decreasing nature of ultimate tensile strength with corresponding change in working conditions.

iii. The average strength coefficient of specimens was found to be 2209.25 Mpa, 1690.5 MPa, 1612 MPa, 1544 Mpa, 1488 MPa, and 1269.6. at A, B, C, D, E, & F working conditions respectively. Thus ABI methodology successfully predicts the decreasing nature of strength coefficient with corresponding change in working conditions.

iv. The average strain hardening exponent of specimens was found to be 0.127, 0.180, 0.230, 0.235, 0.239, and 0.261 at A, B, C, D, E, and F working conditions respectively. Thus ABI methodology successfully predicts the decreasing nature of strain hardening exponent with corresponding change in working conditions.

v. The loads vs. displacement results of FEM model simulation in ANSYS software were also found to be close (in all cases) with that of ABI load vs. displacement curves at different working conditions during validation of ABI generated experimental results.

Thus, it is concluded that ABI methodology successfully predicted the effects of different working conditions on the mechanical properties of Zr 2.5 Nb material.

6.6 Scope of Future Work

ABI approach is a promising approach of characterization of different materials. Mostly, it has wide scope for the in -situ investigation of degradation of different component, which are used for commercial purposes like; thermal power plants components, components used in typical corrosive environments, etc. In the nuclear field, ABI approach also has wide scope for the investigation of degradation of reactor core material, control rod material, etc.

REFERENCES

[1] D. Tabor, *The Hardness of Metals,* Oxford University Press, New York, 1951

[2] F.M. Haggag, K. Linga Murty, Investigation of the Applicability of Using a New Automated Ball Indentation (ABI) Test, to Measure the Flow Properties of Metallic Materials, *Journal of Nuclear Materials,* Volume 252, pp. 77-83, 1988

[3] F.M. Haggag, In-Situ Measurements of Mechanical Properties Using Novel Automated Ball Indentation System, *Small Specimen Test Techniques Applied to Nuclear Reactor Thermal Annealing and Plant Life Extension,* Volume ASTM STP 1204, pp. 27-44, 1993

[4] F.M. Haggag, Larry D. Phillips, Integrating Automated Ball Indentation with ASME B31G code to assess integrity of corroded pipelines**,** *International Pipeline Conference, Calgary, Alberta, Canada,* Code IPC04-0357**,** October 4 - 8, 2004

[5] F.M. Haggag, In situ examination of SS 347, *American Society for Testing and Materials,* Volume 76, pp. 170-176, 1986

[6] F.M. Haggag, Nondestructive Determination of Fracture Toughness of Alloy 718 Welded Structures using Novel Stress-Strain Microprobe Technology**,** *Final Report for Period September 3, 1997 - March 17, 1998,* 1998

[7] F.M. Haggag, R.K. Nanstad, Estimating Fracture Toughness Using Tension or Ball Indentation Tests**,** *Innovative Approaches to Irradiation Damage, and Fracture Analysis,* Volume 170, Book No. H 485, 1989

[8] F.M. Haggag, In-Service Nondestructive Measurements of Stress-Strain Curves and Fracture Toughness of Oil and Gas Pipelines: Examples of Fitness-for-Purpose Applications

[9] F.M. Haggag, Nondestructive Detection and Assessment of Damage in Aging Aircraft Using a Novel Stress-Strain Microprobe System

[10] F.M. Haggag, Application of Flow Properties Microprobe to Evaluate Gradients in Weldment Properties**,** *ASM 3rd International Conference on Trends in Welding Research, Gatlinburg, Tennessee, USA,* pp. 629-635, June 1-5, 1992

[11] F.M. Haggag and Glenn E. Lucas, *Determination of Lüders Strains and Flow Properties in Steels from Hardness / Microhardness Tests*, 16th International Symposium, Philadelphia, 1993

[12] F.M. Haggag, R.K. Nanstad, D.N. Braski, Structural Integrity Evaluation based on an innovative Field Indentation Microprobe**,** *Innovative Approaches to Irradiation Damage, and Fracture Analysis*, Volume 170, Book No. H 485, 1989

[13] F.M. Haggag, K.L. Murty, *Non-destructive Evaluation and Materials Properties* III, *Journal of Material Testing*, pp. 101, 1997

[14] Goutam Das, Sabita Ghosh, S.K. Sahay, Use of ball indentation technique to determine the change of tensile properties of SS 316L steel due to cold rolling, *Materials Latter*, Volume 59, pp. 2246-2251, 2005

[15] G.E.C. Bell, Measurement of Yield Strength and Flow Properties in Spot Welds and their HAZs at Various Strain Rates**,** *ASM 3rd International Conference on Trends in Welding Research, Gatlinburg, Tennessee, USA.*, 1992

[16] K.L. Murty, M.D. Mathewa, Y. Wanga, V.N. Shahb, F.M. Haggag, Nondestructive determination of tensile properties and fracture toughness of cold worked A316 steel, *International Journal of Pressure Vessels and Piping*, Volume 75, pp. 831–840, 1998

[17] K.L. Murty, P.Q. Miragliaa, M.D. Mathewa, V.N. Shahb, F.M. Haggag, Characterization of gradients in mechanical properties of SA-533B steel welds using ball indentation, *International Journal of Pressure Vessels and Piping*, Volume 76, pp. 361-369, 1999

[18] K.L. Murty, F.M. Haggag, Characterization of Strain-Rate Sensitivity of Sn-5%Sb Solder Using ABI Testing

[19] K.L. Murty, M.D. Mathew, P.Q. Miraglia1, V.N. Shah, F.M. Haggag, Non-Destructive Evaluation of deformation and fracture properties of materials using stress-Strain Microprobe**,** *Non-destructive Characterization of Materials in Aging Systems***,** Volume 154, pp. 120-124, 1998

[20] M.D. Mathew, K.L. Murty, K.B.S. Rao , S.L. Mannan, Ball indentation studies on the effect of aging on mechanical behavior of alloy 625, *Materials Science and Engineering*, Volume A264, pp. 159-166, 1998

[21] R.K. Pandey, S. Banerjee, Strain Induced Fracture in Low carbon Steels, *Engineering Fracture Mechanics*, Volume 10, pp. 817-829, 1978

[22] Randy K. Nanstad , F.M. Haggag, John T. Hutton, David L. Thomas, and Ronald L. Swain, Use of Automated Ball Indentation Testing to Measure Flow Properties and Estimate Fracture Toughness in Metallic Materials, *Applications of Automation Technology to Fatigue and Fracture Testing*, Volume ASTM 1092, pp. 188-208, 1990

[23] Samuel Glasstone, Alexander Sesonske, Nuclear Reactor Engineering-Reactor Design Basics, *CBS Publications & Distributors, New Delhi*, Volume 1 (4^{th} Edison), pp. 406-454, 2001

[24] Samuel Glasstone, Alexander Sesonske, Nuclear Reactor Engineering-Reactor Design Basics, *D. Van Nostrand Company, Princeton*, Volume 1 (5^{th} Edison), pp. 31- 31, 1955

[25] S.P. Timoshenko, J.N. Goodier, *Theory of Elasticity*, 3rd ed., McGraw-Hill, New York, pp. 409–414, 1970

[26] Thak Sang Byun, Jin Weon Kim, Jun Hwa Hong, A theoretical model for determination of fracture toughness of reactor pressure vessel steels in the transition region from automated ball indentation test, *Journal of Nuclear Materials*, Volume 252, pp. 187-194, 1998

[27] http://www.igcar.ernet.in/nuclear/neutron_interactions.htm

[28] http://www.visionlearning.com/library/module_viewer.php?mid=59

[29] http://www.blass.com.au/definitions/gas-cooled%20reactor

[30] http://www.world-nuclear.org/info/inf32.html

[31] http://powerelectrical.blogspot.com/2007/05/candu-reactor.html

[32] http://www.nucleartourist.com/type/pwr.htm

[33] http://www.euronuclear.org/info/encyclopedia/p/pressurized-water-reactor.htm

[34] http://www.euronuclear.org/info/encyclopedia/boilingwaterreactor.htm

[35] http://www.ecology.at/nni/index.php?p=type&t=fbr